FINAL REPORT

INFLUENCE OF HEAVY TRUCKS ON HIGHWAY BRIDGES

Ton-Lo Wang

Chunhua Liu

Department of Civil & Environmental Engineering

Florida International University

Miami, FL 33199

1. Report No. FL/DOT/RMC/6672-379	2. Government Accession No.	3. Recipient's Catalog No.
4. Title and Subtitle Influence of heavy trucks on highway bridges		5. Report Date October 2000
		6. Performing Organization Code
7. Author(s) Ton-Lo Wang and Chunhua Liu		8. Performing Organization Report No.
9. Performing Organization Name and Address Florida International University Department of Civil and Environmental Engineering University Park Miami, Florida 33199		10. Work Unit No.
		11. Contract or Grant No. WPI 406672, BC379
12. Sponsoring Agency Name and Address Florida Department of Transportation Research Center, MS30 605 Suwannee Street Tallahassee, Florida 32399-0450		13. Type of Report and Period Covered Final Report September 1999 – October 2000
		14. Sponsoring Agency Code 99700-3596-119

15. Supplementary Notes
Prepared in cooperation with the Federal Highway Administration

16. Abstract

   In the present study, truck traffic data collected by Florida Department of Transportation (FDOT) statistics office are grouped into according to their types and loading condition (loaded or empty). Mean values of truck axle weight and spacing are used to represent their average effects on bridge structures. The mathematical models of typical trucks with significant counts are established and the input data are derived from the synthesized results. These typical trucks include types 5, 8, 9, and 10. Road surface roughness is generated as multi-correlated random processes. According to the research by Honda et al., the coefficient of correlation is approximately taken as a constant.

   Static effects of the heavy trucks are compared with those of the standard design truck HS20-44. The tandem axle weights of the heavy trucks are found to be higher than that of HS20-44 and exceed the limit by AASHTO *Guide*. Dynamic impact factors of moment at midspan and shear at end are analyzed for I-girder steel and prestressed concrete bridges ranging from 9.14m (30ft) to 42.67m (140ft). Effects of correlation of road surface roughness on dynamic impact factors are investigated. Fatigue accumulation damage incurred by the normal traffic at sites with significant counts is performed.

17. Key Words Bridges, Highway Truck, Fatigue, Impact, Dynamic Response, Road Surface Roughness, Simply Supported Beam		18. Distribution Statement This document is available to the public through the National Technical Information Service, Springfield, Virginia, 22161		
19. Security Classif. (of this report) Unclassified		20. Security Classify. (of this page) Unclassified	21. No. of Pages 176	22. Price

Form DOT F 1700.7 (8-72)

Reproduction of Completed Page Authorized

METRIC CONVERSIONS

$$N \times 1{,}000 = kN$$

$$ft \times 0.3048 = m$$

$$inch \times 2.54 = cm$$

$$kip \ (force) \times 4.448 = kN$$

$$kip \ (mass) \times 454 = kg \ (mass)$$

$$mph \times 1.609 = km/h$$

$$psi \times 6.895 = kPa$$

$$ksi \times 6.895 = MPa$$

DISCLAIMER

The opinions, findings and conclusions expressed in this publication are those of the authors and not necessarily those of the Department of Transportation or the U.S. Department of Transportation.

Prepared in cooperation with the State of Florida Department of Transportation and the U.S. Department of Transportation.

ACKNOWLEDGEMENTS

TABLE OF CONTENTS

LIST OF TABLES

LIST OF FIGURES

1. INTRODUCTION

Previous studies show that a heavy truck's gross weight, axle weights, and axle configuration directly affect the service life of highway bridge superstructures. Damage typically occurs in the bridge deck and in the main superstructure elements including floor beams and girders, diaphragms, joints, and bearings. Nowadays, with the rapid development of highway transportation, the increasing frequency of passing heavy trucks attributes to fatigue damage and causes more difficulty and financial costs to bridge maintenance as the result of shorter periods between needed maintenance, rehabilitation, or replacement, etc. These heavy loads may severely shorten the life span in service of the existing bridges. Moreover, it is necessary to investigate the damage mechanisms of specific local members caused by heavy trucks. This investigation will greatly benefit the maintenance of existing highway bridges.

The need for reliable truck weight data has been recognized by many state departments of transportation. The knowledge of actual truck-load spectra may reduce the uncertainty involved in the detrimental influence of heavy trucks. It is useful in many aspects, such as evaluation of the load-carrying capacity, estimation of remaining life, and prediction of deterioration rate. To monitor gross vehicle weight (GVW) of passing heavy trucks, stationary weight scales have been established over major highways. However, this conventional scale measurement has several drawbacks, such as drivers' awareness (may avoid it on purpose) and delay of traffic. More recently, weigh-in-motion (WIM) measurements have been developed as an extensive device

throughout the nation. The use of WIM databases can achieve more accurate truck loading since it can overcome the shortcomings inherent in stationary weight scales. Nowak et al. (1993) employed the WIM measurement on I-94 and US-23 in Michigan to obtain average daily truck traffic (ADTT) and truck weight. Totally, there are five highway bridges selected as samples for data acquisition. It is found that the obtained truck traffic data are very site-specific.

It is estimated that there is a volume range of approximately 3,000 to 14,300 heavy trucks per day on I-75 between the Georgia State line and Florida's Turnpike. Since the state of Florida has thousands of small to middle span bridges, it is necessary to perform corresponding research to meet the need of rapid increase in highway transportation. However, accurate truck traffic data is not available on specific highway bridge sites. The objective of the research project is to establish a truck traffic database (including axle weight and spacing), which is useful for the maintenance of highway bridges in the state Florida. This database is essential in estimating histograms of heavy trucks in association with their gross weight, axle weights, and axle configurations, and providing the fatigue life of the existing bridges to ensure the operation safety of these structures.

Literature search indicates that similar studies have been recently accomplished by a few researchers in the field of detrimental influence of heavy-duty trucks on steel highway bridges. Wang et al. (1993) predicted fatigue life of composite and non-composite steel bridges under various roadway surface conditions and with an assumption of 100 HS20-44 trucks per day. Nowak et al. (1993) developed a statistical basis for the live load model for Michigan Bridges based on data of truck counts and WIM measurements carried out at stationary truck weigh

station. Accordingly, an accumulative fatigue damage percentage is calculated and a fatigue-load model is recommended. Based on the measured data, Hwang and Nowak (1991) performed numerical simulations of truck loading. Laman and Nowak (1996) developed three- and four-axle fatigue truck models to represent actual trucks with axle numbers ranging from three to eleven. Moreover, the live load model is an important issue in the study of policy and checking of heavy permit trucks (Dicleli and Bruneau 1995; Fu and Hag-Elsafi 2000). Dicleli and Bruneau (1995) analyzed several existing steel bridges located in North America based on five typical heavy truck configurations, which were provided by the Ministry of Transportation of Ontario (MTO) by their permit-issuing experience. It was found that bridge members are largely affected by such overloads. Policy for the issuance of permit to heavy trucks was recommended according to the cumulative impact damage of these overloads. In summary, these studies indicate that the collection of actual heavy truck traffic data at a specific bridge site is essential for the evaluation of potential structural damage caused by these trucks. Most of the previous analytical studies used relatively simplified bridge and/or truck models. To further study dynamic impacts of multigirder bridges, Wang et al. (1992) and Huang et al. (1993) developed a three-dimensional nonlinear truck model for the AASHTO standard design truck HS20-44 and used the grillage bridge model. Based on these studies, a more detailed scientific investigation of impact and loading of normal truck traffic on bridge structures is available.

Distinct from previous studies, the peculiar features of this research project include the following: (1) dynamic response due to passing single or multiple trucks will be calculated by the finite element model; (2) several types of existing trucks will be modeled as rigid bodies connected with dampers and springs; (3) road surface roughness is generated as correlated

random processes; and (4) passing speed of trucks will be involved in the calculation. As a result of these facts, two advantages are apparent in the present study: (1) no need for strain measurement on a specific bridge site, which will certainly reduce cost for fatigue analysis; and (2) structural dynamic response under passing trucks (including the excitation of road surface roughness) is taken into account.

The objective of this study includes the following aspects: (1) synthesize truck traffic data collected through WIM measurements; (2) establish live-load spectra; (3) perform fatigue damage analysis for typical bridges; (4) carry out static and dynamic analyses. Three-dimensional nonlinear mathematical models of typical trucks with significant counts are developed based on the measured axle weights and configurations. Road surface roughness is simulated as transversely correlated random processes. The multigirder bridges are treated as a grillage beam system. Several important findings and conclusions are summarized.

Chapter 2 presents the synthesization methodology of requested truck traffic data. Bridge and truck models are described in Chapter 3. Chapter 4 gives the simulation of correlated road surface roughness in the transverse direction. In Chapter 5, the static and dynamic effects under typical trucks are studied. In Chapter 6, fatigue damage accumulation is analyzed using normal traffic. In Chapter 7, the effects of correlation of road surface roughness on dynamic impact factors are investigated. Chapter 8 summarizes the findings and conclusions obtained in this research.

2. SYNTHESIZATION OF TRUCK TRAFFIC DATA

2.1 COLLECTION OF TRUCK TRAFFIC DATA

Truck traffic counts and axle weights have been monitored by the extensive WIM measurements in the state of Florida (see *Florida AADT Report* 1998). Figure 2-1 shows the locations of these weigh stations. In this study, truck traffic data are collected at twenty stations in a one-week period. Through truck traffic counts, it is found that stations #19 and #26, respectively, located on interstate highway I-95, approximately 3.5 miles south of SR514, Malabar, and I-75, approximately 3 miles south of I-4, Tampa, have heavy truck traffic. These two stations are used as truck traffic input data in this study. The ADTT is 2838 for station #19 and 3689 for station #26, respectively. Figures 2-2 through 2-9 show the truck counts and the histogram of GVW at the two stations.

2.2 SYNTHESIZATION OF TRUCK TRAFFIC DATA

Since there is a large diversity of truck weights and configurations, one classification method is developed hereby to simplify the analysis. According to FHWA classification scheme "F", there are a total of fifteen vehicle types as shown in Fig. 2-10. In each type, trucks are sub-categorized by loading condition - empty or loaded. The dividing line for empty or loading condition is

selected by judgement to ensure the acceptable coefficient of variation (COV), which is generally considered acceptable if it is less than 0.3. According to the established criteria, a computer program is written to synthesize the data.

In this study, multiple presence of trucks is neglected because the occurrence is small, less than 8% according to Nowak et al. (1993). Single-lane truck traffic is processed and used as input data. Two lanes are herein selected as input data - southbound direction lane #1 of station #19 and southbound lane #2 of station #26. The lane ADTT is 1999 for station #19 and 1065 for station #26, respectively. The trucks are classified into twenty-four categories for station #19 and twenty-three categories for station #26 in this analysis. The mean value (MV) and standard deviation (SD) of axle weights and configurations are calculated in each category. The MVs are used to obtain average loading effects in the following static and dynamic impact study. Tables 2-1 through 2-4 present the synthesized results for each empty and loaded truck type. From Tables 2-1 through 2-4, it can be seen that coefficients of variation in the two categories are generally less than 0.3.

3. TRUCK AND BRIDGE MODELS

3.1 TRUCK MODELS

Table 3-1 presents the GVW (the sum of the mean values of each axle weight) and passages of each category processed in Chapter 2. According to the traffic counts in Table 3-1, three types of trucks are predominant: types 5, 8, and 9. Mathematical models of the three types of trucks are established based on the data of nationwide-used truck types H20-44, HS20-44, and 3S2. The masses of tractor and trailer are derived according to their static equilibrium relationship with the measured axle weights. The three-dimensional mathematical models for types 5, 8(2S1), 9, and 10 are illustrated in Fig. 3-1. Truck type 10 (developed from type 3-3) is of interest because it is the heaviest truck with a single trailer. These models simplify the trucks into several rigid masses connected by springs and dampers. The total numbers of degrees of freedom are, respectively, seven, eleven, sixteen, and eighteen. The equations of motion of the vehicle systems were derived using Lagrange's formulation. Details of derivation refer to Wang and Huang (1993). Fig. 3-2 shows the configurations and axle weights of these typical trucks. Appendix A shows the derived data for these typical trucks.

3.2 BRIDGE MODELS

In order to study the effects of normal truck traffic, six simply supported steel I-girder bridges and four prestressed concrete I-girder bridges were designed according to AASHTO

Specifications (1996) and the Standard Plans for Highway Bridge Superstructures (1990) from the U.S. Department of Transportation. The design is based on HS20-44 loading.

For the steel bridges, the span lengths are 10.67m (35ft), 16.76m (55ft), 22.86m (75ft), 30.48m (100ft), 36.58m (120ft), and 42.67m (140ft), respectively. The bridges have a roadway width of 8.53m (28ft) and a concrete deck thickness of 0.19m (7.5in). All the bridges consist of five identical girders. The five girders are evenly spaced at 2.13m (7ft) for the first three spans and 2.44m (8ft) for the last three spans. Also, there are diaphragms transversely connecting these girders. The number of intermediate diaphragm(s) is 1, 2, 2, 3, 4 and 5, respectively, increasing with span length. Except for the shortest span length of 10.67m (35ft), all the bridges have composite sections. Typical cross section of the bridge with a span of 16.76m (55ft) is shown in Fig. 3-3. Table 3-2 presents the mass and girder properties of these bridges.

For the prestressed concrete bridges, the span lengths are 9.14m (30ft), 18.29m (60ft), 30.48m (100ft), and 42.67m (140ft), respectively. All the bridges are of I-beam sections with a cast-in-place deck. The bridges have a roadway width of 9.74m (32ft) and a concrete deck thickness of 0.19m (7.5in). Typical cross section of the bridges is shown in Fig. 3-4. All five girders have identical sections and are transversely connected to each other by diaphragms. The number of diaphragms is 0, 1, 2, and 2, respectively, for the shortest to the longest span length. Table 3-3 presents the mass and girder properties of these bridges.

3.2.1 Grillage Model

These multigirder bridges are modeled as grillage beam systems. The node parameters are

$$\delta^e = \left\{\delta_i \quad \delta_j\right\}^T \qquad (3\text{-}1)$$

where $\delta_i = \left\{w_{zi} \quad \theta_{xi} \quad \theta_{yi}\right\}^T$ = the displacement vector of the left joint; $\delta_j = \left\{w_{zj} \quad \theta_{xj} \quad \theta_{yj}\right\}^T$ = the displacement vector of the right joint; w = vertical displacement in the z-direction, and θ_x and θ_y = rotational displacements about x- and y-axes, respectively. Fig. 3-5 shows the plan of one bridge and the corresponding grillage model. More details refer to Wang et al. (1992) and Huang et al. (1993).

3.2.2 Governing Equation

The equation of motion of a specific bridge under a moving vehicle can be written as:

$$\mathbf{M}_b\ddot{\delta}_b + \mathbf{C}_b\dot{\delta}_b + \mathbf{K}_b\delta_b = \mathbf{F}_b \qquad (3\text{-}2)$$

where $\mathbf{M}_b$ = global mass matrix of bridge structure; $\mathbf{K}_b$ = global stiffness matrix of bridge structure; $\mathbf{C}_b$ = global damping matrix of bridge structure; $\delta_b, \dot{\delta}_b, \ddot{\delta}_b$ = global nodal displacement, velocity, and acceleration vectors; and $\mathbf{F}_b$ = global load vector due to the interaction between bridge and vehicle. One percent damping ratio is assumed for the first and second modes of steel bridges in this study. The consideration of damping matrix refers to Clough and Penzien (1996).

3.2.3 Interaction between Truck and Bridge

The interaction force between the ith wheel of a truck and a bridge is given as the following:

$$F_{bi}^i = K_{tzi}U_{tzi} + C_{tzi}\dot{U}_{tzi} \tag{3-3}$$

where K_{tzi} = tire stiffness of the ith wheel; C_{tzi} = tire damping coefficient of the ith wheel; U_{tzi} = $z_{wi} - (-u_{sri}) - (-z_{bi})$, the relative displacement between the ith wheel and bridge, and the superscript dot of U_{tzi} denotes differential with respect to time; z_{wi} = vertical displacement of the ith wheel; u_{sri} = road surface roughness under the ith wheel (positive upwards); and z_{bi} = bridge vertical displacement under the ith wheel (positive upwards), which can be determined by the nodal displacement δ^e and the displacement interpolation function of the element.

In the present study, the fourth-order Runge-Kutta integration algorithm is employed to solve the nonlinear equations of motion of a vehicle (Chu et al. 1986; Wang et al. 1993). The dynamic equations of the bridge are solved by the modal superposition procedure based on the subspace iteration method.

4. SIMULATION OF ROAD SURFACE ROUGHNESS

Road surface roughness is one of the most important factors in the vehicle-bridge interaction. Currently, there are two widely accepted power spectral density (PSD) functions describing road surface roughness: one by Dodds and Robson (1973) and the other by Honda et al. (1982). The PSD function proposed by Dodds and Robson (1973) for highway surface roughness is as follows:

$$S(\phi) = \begin{cases} A(\phi/\phi_0)^{-w_1} & \phi \le \phi_0 \\ A(\phi/\phi_0)^{-w_2} & \phi > \phi_0 \end{cases} \tag{4-1}$$

where $S(\phi)$ = PSD function (m^2/cycle/m); ϕ = wave number (cycle/m); ϕ_0 = discontinuity frequency = $1/2\pi$ (cycle/m); A = roughness coefficient (m^3/cycle); and w_1, w_2 = roughness exponent, herein taken as 2.050 and 1.440, respectively, for the principal road. The PSD function proposed by Honda et al. (1982) for surface roughness on bridge decks is as follows:

$$S(\phi) = a\phi^{-n} \tag{4-2}$$

where a = spectral roughness coefficient; and n = spectral roughness exponent (n is taken as 1.94).

A comparison between the two spectra is shown in Fig. 4-1 on a log-log scale. The midpoint in the good condition range is used for roughness coefficients A and a, i.e., $A = 20.0 \times 10^{-6}$ m^3/cycle and $a = 0.62 \times 10^{-6}$ m^2/(m·cycle^{-1}). From Fig. 4-1, it can be seen that Dodds and Robson's PSD has higher values for the frequencies above $1/2\pi$ cycle/m.

4.1 ARMA APPROACH

The PSD functions in Fig. 4-1 present the characteristics of road surface roughness along the longitudinal direction. In reality, these longitudinal random processes vary in the transverse direction (Fenves et al. 1962; Dodds and Robson 1973; Law et al. 1975; Honda et al. 1982). To reflect the reality in the transverse direction, an auto-regressive and moving average (ARMA) approach suggested by Samaras et al. (1985) is employed to simulate road roughness based on a given spatial correlation relationship:

$$\mathbf{Y}_r = \sum_{i=1}^{q} \mathbf{B}_i \mathbf{X}_{r-i} - \sum_{i=1}^{q} \mathbf{A}_i \mathbf{Y}_{r-i} + \mathbf{B}_0 \mathbf{X}_r \tag{4-3}$$

where $\mathbf{Y}_r$ = two random processes (r = 1, 2); $\mathbf{A}_i$ and $\mathbf{B}_i$ (i = 0, 1, ..., q) = 2×2 auto-regressive (AR) and moving-average (MA) coefficient matrices, respectively; p and q = orders of an ARMA model; and $\mathbf{X}_r$ = two-variate Gaussian white noise series with mean zero and satisfying:

$$E[\mathbf{X}_r \mathbf{X}_s^T] = \mathbf{I}\delta_{rs} \tag{4-4}$$

where $\mathbf{I}$ = 2×2 identity matrix; δ_{rs} = Kronecker's delta.

The target $(p+1)\times(p+1)$ correlation function matrix $\mathbf{C}$ can be expressed in the following:

$$\mathbf{C} = \begin{bmatrix} \mathbf{C}_{YY}(0) & \mathbf{C}_{YY}^T(1) & \cdots & \mathbf{C}_{YY}^T(p) \\ \mathbf{C}_{YY}(1) & \mathbf{C}_{YY}(0) & \cdots & \mathbf{C}_{YY}^T(p-1) \\ \vdots & \vdots & \ddots & \vdots \\ \mathbf{C}_{YY}(p) & \mathbf{C}_{YY}(p-1) & \cdots & \mathbf{C}_{YY}(0) \end{bmatrix} \tag{4-5}$$

where the elements of $\mathbf{C}_{YY}(k)$ $(k = 0, 1, \ldots, p)$ consist of the auto- and cross-correlation functions of the two random processes $\mathbf{Y}_1$ and $\mathbf{Y}_2$.

Once the coefficient matrices $\mathbf{A}_i$ and $\mathbf{B}_i$ are obtained, the random process $\mathbf{Y}_r$ $(r = 1, 2)$ can be generated recursively using Eq. (3). $\mathbf{A}_i$ and $\mathbf{B}_i$ are determined based on only the prescribed correlation function matrix $\mathbf{C}$ in Eq. (5). The detailed procedure is shown as follows:

1. $\mathbf{A}_0$ is assumed to be an identity matrix;

2. $\mathbf{B}_0$ is solved by the following formula:

$$\mathbf{B}_0\mathbf{B}_0^T = \sum_{i=0}^{p} \widetilde{\mathbf{A}}_i \mathbf{C}_{YY}(i) \tag{4-6}$$

where $\widetilde{\mathbf{A}}_0$ = the identity matrix and $\begin{bmatrix} \widetilde{\mathbf{A}}_1 & \ldots & \widetilde{\mathbf{A}}_p \end{bmatrix} = -\begin{bmatrix} \mathbf{C}_{YY}^T(1) & \ldots & \mathbf{C}_{YY}^T(p) \end{bmatrix}\mathbf{C}^{-1}$; and

3. $\mathbf{A}_i$ and $\mathbf{B}_i$ $(i = 1, \ldots, q)$ are obtained as follows:

$$\begin{bmatrix} \mathbf{B}_1 & \ldots & \mathbf{B}_q & \mathbf{A}_1 & \ldots & \mathbf{A}_q \end{bmatrix} = \begin{bmatrix} \mathbf{C}_{YX}(-1) & \ldots & \mathbf{C}_{YX}(-q) & -\mathbf{C}_{YY}^T(1) & \ldots & -\mathbf{C}_{YY}^T(q) \end{bmatrix}\mathbf{D}^{-1} \tag{4-7}$$

where

$$D = \begin{bmatrix} \mathbf{I} & \cdots & 0 & -\mathbf{C}_{YX}^{T}(0) & \cdots & 0 \\ \vdots & \ddots & \vdots & \vdots & \ddots & \vdots \\ 0 & \cdots & \mathbf{I} & -\mathbf{C}_{YX}^{T}(1-q) & \cdots & -\mathbf{C}_{YX}^{T}(0) \\ -\mathbf{C}_{YX}(0) & \cdots & -\mathbf{C}_{YX}(1-q) & \mathbf{C}_{YY}(0) & \cdots & \mathbf{C}_{YY}^{T}(q-1) \\ \vdots & \ddots & \vdots & \vdots & \ddots & \vdots \\ 0 & \cdots & -\mathbf{C}_{YX}(0) & \mathbf{C}_{YY}(q-1) & \cdots & \mathbf{C}_{YY}(0) \end{bmatrix} \qquad (4\text{-}8)$$

4.2 SIMULATED ROUGHNESS AND CORRELATION FUNCTIONS

In this study, the input parameters p and q are chosen as 49 and 40, respectively. The spatial coherence function in the transverse direction can be derived from available measured data. Based on Honda's study (1982), the value of correlation function $Coh^2(\xi,\phi)$ in the range of $\phi = 0.01$ to 1.0 cycle/m is roughly 0.4. Thus, the coefficient of correlation can be obtained as $c = Coh(\xi,\phi) = 0.63$. Fig. 4-2 shows the simulated correlated road surface roughness. In this simulation, Dodds and Robson's PSD function is adopted and the frequencies in use range from 0.01 to 6.0 cycle/m. Fig. 4-3 shows the simulated auto- and cross-correlation functions together with the targets. From Fig. 4-3, it can be seen that the simulated results are of good accuracy.

5. STATIC AND DYNAMIC EFFECTS ON I-GIRDER BRIDGES

From Table 3-1, it can be seen that the GVWs of trucks of the same type and loading condition are close for stations #19 and #26. Generally, the trucks with significant counts have more gross weight at station #26 than at station #19. Hence, the processed truck configurations and axle weights at station #26 are used in the static and dynamic analyses in this chapter.

5.1 STATIC EFFECTS

The static moments and shears are calculated for each synthesized truck category. The processed mean values of actual axle weights as shown in Tables 2-3 and 2-4 are utilized as moving loads. One truck loading position placed symmetrically along the axis of girder #2 is used, as shown in Fig. 5-1(a). Figures 5-2 and 5-3 show the histograms of flexural stress at midspan and shear at end due to the synthesized truck data and one-truck loading. The cumulative distribution function (CDF) of the static stresses at midspan and shears at entrance end for the six bridges are listed in Fig. 5-4. From Fig. 5-4, it is observed that the CDFs of these flexural stresses and shears for the six span lengths are different. Figure 5-5 demonstrates the static moment and shear due to moving loaded type 9 loading.

To investigate the effects of overloaded trucks, the heaviest GVW in each truck type is searched from the surveyed data at station #26, as shown in Fig. 5-6. It can be seen that the heaviest GVW (in truck type 13) is approximately twice that of the AASHTO standard design truck HS20-44

(0.32MN or 72kips). The comparison of the effects of these heaviest trucks with HS20-44 is shown in Fig. 5-7. In Fig. 5-7, the moment and shear of girder #2 are computed. It can be seen that the effects of several heaviest truck types, 6, 7, 8, 10, and 13, exceed those caused by HS20-44. The "overloading" can reach as high as 42%. Because these results are based on single truck loading, this "overloading" does not mean that the ultimate strength of the subject girder is violated. Two heaviest truck types, 11 and 12, produce smaller loading than the design truck. This indicates that in addition to GVW, the truck loading is closely related to axle configuration. To further examine local effects, all the single axle weights of these heaviest trucks are shown in Fig. 5-8(a). It is found that some of single axle weights may significantly exceed the limiting value by AASHTO *Guide* (1991) – 0.089MN (20kips). The distance between tandem or group axles is observed to be about 1.5m. Fig. 5-8(b) indicates the weights of the single, tandem, and group axles as well as those of HS20-44. It is seen that the tandem or group axle weights might significantly exceed that of HS20-44 and the limiting value by AASHTO *Guide* (1991) – 0.15MN (34kips) for tandem axles and 0.18MN (40kips) for group axles (Types 7 and 10). Therefore, it is worthwhile in future study to check whether such a heavy weight may cause severe local damage in the bridge deck and secondary members.

5.2 DYNAMIC IMPACT EFFECTS

The impact factor is defined as the following:

$$I_{mp}(\%) = \left(\frac{R_d}{R_s} - 1 \right) \times 100\% \qquad (5\text{-}1)$$

where R_d and R_s = the absolute maximum dynamic and static responses for individual histories, respectively.

5.2.1 I-Girder Steel Bridges

In the study of dynamic impact factors, the girder subject to the highest loading is of interest. Figure 5-9 shows the lateral distribution of maximum flexural stress at midspan and shear at entrance end of each girder due to moving loaded truck type 7 loading. The purpose of the use of stress instead of moment is to avoid significant difference in moment for various span lengths. From Fig. 5-9, it is seen that among the five girders the highest moment occurs at girder #2 for the spans of 10.67m, 16.76m, and 22.86m, and at girder #1 for the spans of 30.48m, 36.58m, and 42.67m. The highest shear always occurs at girder #2.

To study the dynamic effects of these realistic trucks, the variation of impact factors, I_{mp}, with span lengths is shown in Fig. 5-10. The truck loading position is shown in Fig. 5-1(a). Truck models include types 5, 8(2S1), 9, 10, and HS20-44. The actual truck models are established based on the MVs of measured axle weights as shown in Fig. 3-2. Traveling speed is taken as 88km/h (55MPH), close to the speed limit of most highways. To simulate the truck entering the bridge with nonzero initial displacements and velocities at every degree of freedom, the truck is started at a five-vehicle length distance, L_0, away from the entrance end of the bridge. Each impact factor is taken as the mean value of twenty-time simulations on good road roughness. Dodds and Robson's PSD function is used in this analysis. There are approximately 2000 simulations carried out in this analysis. From Fig. 5-10, it is observed that the impact factors, for

two loaded types 9 and 10 (with a GVW of 0.29MN and 0.36MN) as well as HS20-44 (with a GVW of 0.32MN), are in accordance with AASHTO *Specifications* (1996). The *commentary* of AASHTO *Guide Specifications* (1990) reports that an average of 10 percent of impact is observed in the field measurements. The computed average impact factor of loaded types 9 and 10 is 10%, coinciding with the field observations. The reason for the impact factors higher than the specified value by AASHTO *Specifications* (1996) is that the corresponding trucks have GVWs less than 0.16MN, which is half of HS20-44. For example, the impact factors for empty truck types 5 and 8 (2S1) is very high because they have rather low GVWs of 0.06MN and 0.10MN. This confirms the tendency that a lighter truck weight generally leads to a higher impact factor (Hwang and Nowak 1991; Huang et al. 1993).

5.2.2 I-Girder Prestressed Concrete Bridges

Since the chance of two heavy trucks passing a bridge at the same time is relatively low, the one-truck loading position (load case I) shown in Fig. 5-1(b) is used in the analysis. The truck is assumed to travel along the center of lane 1. To simulate the truck entering the bridge with nonzero initial displacements and velocities at every degree of freedom, the truck is started at a five-vehicle length distance, L_0, away from the entrance end of the bridge. Honda et al.'s PSD function is used to generate longitudinal road profiles. There are a total of twenty sets of good surface roughness generated in this study. The roughness coefficient a is taken as 0.62×10^{-6} $m^2/(m \cdot cycle^{-1})$ and the PSD function is shown in Fig. 4-1.

In the study of dynamic impact factors, the girder subject to the highest loading is of interest. Figure 5-11 shows the maximum static and dynamic moments at the midspan sections due to moving truck type 9 at 88km/h (55MPH) in the longitudinal direction. It can be seen that the highest moment occurs at girder #2 for the bridge of span length of 9.14m (30ft), while it occurs at girder #1 for all other bridges. The girder with the highest loading is used in this study.

Under various passing speeds ranging from 24 to 121km/h (15 to 75MPH), the dynamic impact factors of moment at midspan are shown in Fig. 5-12. These results are for various typical trucks and bridge span lengths. At each truck speed, the impact factor is taken as the average of twenty simulations. From Fig. 5-12, it can be seen that for heavy trucks (types 9 and 10 and the design truck HS20-44), the impact factors are generally well below the specified values of AASHTO *Standard* (1996) and AASHTO *LRFD* (1998). Occasional exceptions occur in the case of span length of 9.14m (30ft) and type 9 loading. For light trucks (types 5 and 8), the impact factors may be much higher than the specified values. This is because the two light trucks have very low GVWs compared with that of HS20-44 (the ratio is 0.30 and 0.47, respectively). Figure 5-13 gives the dynamic history of the moment at midspan of girder #2 ($L = 9.14$m or 30ft) due to type 9 truck at a traveling speed of 24km/h (15MPH).

5.3 LIVE LOAD LATERAL DISTRIBUTION

The wheel load distribution factor is defined as:

$$\eta = \frac{M_i \cdot n}{M_t} \tag{5-2}$$

where M_t = the sum of maximum moment/shear of all girders at the specific section; n = number of wheel loads in the transverse direction; and M_i = maximum moment/shear of the ith girder at the section. In this study, the dynamic moment/shear for M_t and M_i (including impact effect) is taken into account.

Figure 5-14 shows the wheel load distribution factor of dynamic moment at midspan when a single truck travels along the center of lane 1. The results are obtained based on one simulation and a traveling speed of 88km/h. From Fig. 5-14, it is observed that the five selected trucks cause similar lateral moment distribution among the five girders, regardless of the variation in their axle weights and configurations. To examine the distribution factors specified by AASHTO *Specifications* (1996) and AASHTO *LRFD* (1998), the simulation is performed twenty times and an average is taken for each case. A two-lane loading (using the same truck) is considered in the analysis, which is achieved by the superposition of one-lane loading results. This assumes the symmetry of distribution factors for loading on each lane. Figure 5-15 shows the maximum wheel load distribution factor of moment at midspan and shear at end along with the specified values for interior girders by AASHTO *Specifications* (transferred to wheel load case). Also, in Fig. 5-15 the distribution factors are calculated on the basis of static moments and shears. It can be seen that the maximum distribution factors are similar for different truck types. The computed maximum factors based on both static and dynamic moments/shears are similar. The calculated factors for interior girders are lower than the specified values. This is consistent with the measured results reported by Kim and Nowak (1997). However, it should be noted that in this study two-lane traffic is used, while the specified values are obtained based on the controlling

static moment/shear caused by any number of trucks that fit the bridge transversely (Zokaie 2000). Thus, the specified values may lead to higher distribution factors.

6. FATIGUE ACCUMULATION ANALYSIS

6.1 FATIGUE DAMAGE ACCUMULATION

To evaluate fatigue damage caused by the surveyed normal traffic, it is necessary to obtain the dynamic stress ranges of a specific girder. Based on the previously described impact study, the impact factors can be approximately taken as 1.15 for loaded trucks and 1.20 for empty trucks, as shown in Figs. 5-10(a) and 5-10(b). The two values are intentionally selected to cover most of the calculated impact factors caused by types 9 and 10. The purpose is to consider mainly the heavy trucks that cause significant flexural stresses. This consideration of dynamic impacts will not involve significant loss of accuracy in fatigue analysis since empty trucks cause only a low level of stress ranges. Combining the dynamic impacts with the aforementioned static results, the histogram of dynamic stress range of the most highly stressed girder at station #26 is shown in Fig. 6-1. The corresponding CDF of dynamic stress ranges is given in Fig. 6-2. It can be seen that the stress ranges due to the normal truck traffic are different for the six bridge spans. The stress ranges from 6.89 to 43.43Mpa (1.0 to 6.3ksi). The bridges with a span length less than 30.48m (100ft) are assumed to have rolled girders (Category A), while other bridges are assumed to have welded girders (Category B). According to AASHTO *Guide* (1990), the calculated stress ranges multiplied by the reliability factor R_S, (R_S = 0.95×1.35 = 1.28 for nonredundant members, *alternative* 3 for fatigue truck, F_{S2} = 0.95) are less than the limiting stress range of Categories A and B. Therefore, the fatigue life of these girders can be considered infinite.

The fatigue damage analysis is performed based on the Miner's linear damage rule and the stress-life approach (Miner 1945; Bannatine et al. 1990). According to this rule, the damage in just one stress range cycle is $1/N_i$ if N_i cycles of a specific stress range S_i are needed to cause a structural detail to fail. When the number of cycles, n_i, at stress range S_i is applied, the damage fraction D_i is n_i/N_i. Failure is assumed to occur when the summation of damage fraction, D_i, equals 1.0. Based on the passages in each truck category, the computed sum of damage accumulation for various categories in 75 years for the six bridge span lengths are shown in Fig. 6-3. It is observed that the truck traffic at station #26 may cause severe fatigue damage to category E', while the truck traffic at station #19 may cause severe damage to categories D, E, and E', when details of these categories are used. The histogram for station #26 (shown in Fig. 6-1) is used for station #19. Since the GVWs of the same truck type and loading condition for the two stations are close, this simplification will not lead to significant errors.

Figure 6-4 illustrates the damage accumulation in a period of one week for the WIM data and for two fatigue trucks specified in the AASHTO *Guide* (1990) and *LRFD* (1998). Based on the surveyed trucks, the equivalent GVW is 0.24MN (54kips), exactly the same as that of the standard fatigue design truck in the AASHTO *Guide* (1990). Based on the processed truck data, the equivalent GVW is 0.23MN (52.56kips), which is slightly different from that obtained from every truck passage. From Fig. 6-4, it can be seen that the fatigue design truck of AASHTO *Guide* (1990) causes damage close to that from the surveyed WIM data. In this analysis, Category A of AASHTO *Specifications* (1996) is used for rolled girders and Category B is used for welded built-up girders. The increase in future truck volume is not considered. The load factor of 0.75 is

not included in the effect of the *LRFD* truck. If this load factor is considered, the *LRFD* fatigue truck would be the same as that of AASHTO *Guide*. The stress cycles per truck passage are taken in accordance with AASHTO *Guide* (1990) and *LRFD* (1998), respectively. To study the role of various trucks, the fatigue damage accumulation is calculated for each category. The results for the six bridges are shown in Fig. 6-5. From Fig. 6-5, it can be seen that the loaded truck types 9, 8(2S2), 7, and 8(3S1) are of the most significance. These trucks are either 4- or 5-axle.

6.2 EQUIVALENT NUMBER OF CYCLES

According to NCHRP *Report 299*, the equivalent number of cycles for a complex cycle can be approximately expressed as:

$$N_e = 1 + \left(S_{r1} / S_{rp}\right)^3 + \left(S_{r2} / S_{rp}\right)^3 + \cdots + \left(S_{rm} / S_{rp}\right)^3 \qquad (6\text{-}1)$$

where S_{rp} = the stress range for the primary cycle, and S_{ri} = the stress range for a higher order cycle.

Figure 6-6 shows the equivalent number of cycles using the processed data at station #19. Figure 6-7 shows the equivalent number of cycles using the processed data at station #19. Figures 6-6 and 6-7 also give the specified cycles by AASHTO *Specifications* (1996) and *LRFD* (1998). It can be seen that truck type 9, the most important truck accounting for fatigue damage, induces a number of cycles higher than the specified value by AASHTO *Specifications* (1996) for short span lengths less than 10m.

7. EFFECTS OF CORRELATION OF ROAD ROUGHNESS

To study the effect of correlation between the road profiles in the transverse direction on the dynamic impact factor, five cases are investigated in this study: $c = 0.9, 0.63, 0.0, -0.63$, and -0.9. The case of $c = 0.9, 0, $ and -0.9 denotes, respectively, strongly correlated, independent, and strongly but negatively correlated longitudinal road profiles. It should be noted that (1) a strong correlation (c approaches 1.0) excites the pitch mode of trucks; and (2) a strong but negative correlation (c approaches -1.0) excites the roll mode of trucks. Figure 7-1 shows one set of the simulated left- and right-lines of roughness. Figure 7-2 gives the comparison between the simulated auto- and cross-correlation functions and the targets. Honda et al.'s PSD function is used in this analysis. The frequency range is from 0.1 to 6.0 cycle/m. The simulated functions are computed based on a total road length of 900m with an interval of $\Delta = 0.125$m. From Fig. 7-2, it can be seen that the simulated results are of good accuracy.

In the simulation of the road roughness profiles at various correlationship, the following two prerequisites are satisfied: (1) the white noise input is the same for all the five correlation coefficients; and (2) the truck is assumed to run the same distance, L_0, of five truck lengths on the road before entering the bridges. These two prerequisites are introduced to avoid the randomness caused by initial phases. To illustrate the latter, Fig. 7-3 shows the variation of impact factor of the moment at midspan with the distance L_0. It can be seen that (1) the variation is apparent, and (2) the light trucks (types 8 and 5) cause more fluctuation than the heavy ones (types 9 and 10

and HS20-44). Under these two prerequisites, it can be implied that the only difference in the simulation using Eq. (3) exists in the prescribed $(p+1)\times(p+1)$ correlation function matrix.

The comparison of the computed impact factors of moment at midspan under the five correlation coefficients is shown in Figs. 7-4 and 7-5. The traveling speed ranges from 24 to 121km/h (15 to 75MPH). Two loading cases (HS20-44 truck) in Fig. 5-1(b) are used in the analysis. In load case II, it is assumed that (1) the truck travels along the center of each lane; and (2) the road surface roughness of both lanes is the same. From Figs. 7-4 and 7-5, it can be seen that (1) the impact factors generally increase with the coefficient c; and (2) for span length of 42.67m (140ft) the impact factors are insensitive to c in the high-speed range of 72 to 121km/h (45 to 75MPH). The former implies that in the impact study of moment at midspan, the pitch mode of vehicles is more important than the roll mode. To find out the reason for the latter, the impact factors under smooth surface (no roughness) are also presented in Figs. 7-4 and 7-5. It is observed that in this case the impact factors are not very sensitive to road surface roughness.

Based on Figs. 7-4 and 7-5, the maximum impact factor for each span length is listed in Tables 7-1 and 7-2 and Fig. 7-6. From Tables 7-1 and 7-2 and Fig. 7-6, it is seen that the maximum impact factor generally increases with coefficient of correlation c. For load case II, all the difference between $c = 0.9$ and -0.9 is greater than 10% and the highest can reach 19%. The shorter the span length, the more difference in the maximum impact factor.

To check the variation at the midspan section, Figs. 7-7 and 7-8 give the impact factors for girders #1, #2, and #3 for load case I and for all the five girders for load case II. For load case I, girders #4 and #5 are not included because the maximum static moments of these two girders are relatively small. The truck speed is taken as 88km/h (55MPH), which is close to the speed limit of most highways. From Figs. 7-7 and 7-8, it can be seen that in most cases the dynamic impact factors increase with the coefficient of correlation c. Some exceptions occur because the roll mode of vehicles produces some effects on exterior girders.

The above-described comparison is based on a single simulation. To further investigate the difference, twenty simulations are performed for $c = 0.0$ (independent) and $c = 0.9$ (close to completely the same) and the span length of 18.29m (60ft). Load case I is used for the analysis. This case is selected because an apparent difference is observed in Fig. 7-7(b). The average is taken as shown in Fig. 7-9. A consistent difference still distinctly exists. Therefore, it is concluded that the coefficient of correlation between road surface roughness plays an important role in the dynamic analysis of the vehicle-bridge system.

8. SUMMARIES AND CONCLUSIONS

8.1 SUMMARIES

In this study, truck traffic data are requested from the FDOT transportation statistics office. These data have been collected on major highways throughout the state using the advanced WIM equipment. These data are synthesized based on truck types and loading condition (empty or loaded). According to the classification criteria, a large number of different trucks are classified into limited categories. In each category, the mean value is used for the representative truck. Utilizing the processed truck configurations and axle weights, three-dimensional nonlinear mathematical models for the typical trucks with significant counts are derived. The selected trucks include types 5, 8, 9, and 10. Bridge structures are represented as the grillage model. The bridge span ranges from 10.67m (35ft) to 42.67m (140ft). Road surface roughness is generated as transversely correlated random processes. Based on these analytical models, the following ·aspects have been studied:

- Static effects of heavy trucks on bridge structures;

- Dynamic impact factors due to typical trucks;

- Fatigue damage accumulation due to normal traffic;

- Live load lateral distribution of I-girder bridges; and

- Effects of correlation of road surface roughness on the dynamic impact factor.

8.2. CONCLUSIONS

1. For simply supported steel bridges, static analysis indicates that truck traffic-induced flexural stress at midspan and shear at entrance end vary with bridge span length. The gross weight of the heaviest trucks can be twice that of the AASHTO standard design truck HS20-44. Several heaviest truck types generate more loading on bridge structures than HS20-44. Based on single truck loading, the observed overloading can reach as high as 42%. Truck loading does not necessarily increase with GVW, therefore, it is closely related to axle configuration. All the axle weights of these heaviest trucks are found to be less than the heavy one of HS20-44. However, if the tandem axles spaced at about 1.5m are considered, the axle weight will significantly exceed that of HS20-44 and the limiting value by AASHTO *Guide* (1991). The overweight may severely deteriorate the bridge deck and secondary members. This needs further investigation.

2. For simply supported steel bridges, the average impact factors induced by heavy truck types (9 and 10 and HS20-44) are lower than the specified values of AASHTO *Specifications* (1996). Also, the total average of the computed impact factors of moment for loaded types 9 and 10 is 10%, which is in accordance with the *Commentary* of AASHTO *Guide Specifications* (1990). Dynamic impact factors under light truck loading (types 5 and 8) are higher than the specified values. These light trucks have very low GVWs compared to HS20-44.

3. For simply supported prestressed concrete bridges, the mean values of impact factors of moment at midspan induced by heavy trucks (types 9 and 10 and HS20-44) are generally well below the specified values by AASHTO *Specifications*. Occasional exceptions occur at the span length of 9.14m (30ft) with type 9 loading (GVW of 294kN or 66kips). For light trucks (types 5 and 8), the mean values of impact factors may significantly exceed the specified values.

4. Through the fatigue damage accumulation analysis at two stations with heavy truck traffic, it is found that the heavy traffic will not cause severe fatigue problems on steel girders of categories A, B, and C.

5. Through the damage accumulation analysis for six bridge span lengths, the fatigue design truck of AASHTO *Guide* (1990) induces damage close to that caused by the simulation of the actual truck-traffic flow based on the WIM measurements. The comparison of fatigue damage accumulation demonstrates that the loaded truck types 9, 8-1(2S2), 7, and 8(3S1), either 4- or 5-axle, contribute the most to the fatigue damage.

6. Truck type 9, the most important truck accounting for fatigue damage, induces a number of cycles higher than the specified value by AASHTO *Specifications* (1996) for short span lengths less than 10m.

7. When the coefficient of correlation c between longitudinal road surface roughness is assumed to be a constant, the impact factors of moment at midspan generally increase with c. In most cases, the use of $c = 0.9$ leads to the highest impact factors and that of $c = -0.9$ leads to the lowest impact factors. Since the strong positive and negative correlation excites, respectively, the pitch mode and the roll mode of trucks, the participation of the pitch mode causes more dynamic impacts on moment at midspan than the roll mode.

8. The maximum impact factor with respect to vehicle velocity generally increases with c. For two-truck loading, the shorter the bridge span length, the larger the difference of the maximum impact factor. For all bridge spans, the difference between the two cases of $c = 0.9$ and -0.9 is more than 10% and the highest can reach 19%. The difference between the two cases of $c = 0.9$ and 0.0 can be as high as 11.8% for short span length of 9.14m (30ft). For one-truck loading, similar results can also be observed. Compared with the highest specified values of AASHTO *Specifications* of 30% (*Standard*) and 33% (*LRFD*) for moment at midspan of girders, these differences presented in this study may be considered significant.

9. The extensive selection of this correlation appears to be important in the simulation of vehicle-bridge interaction. Based on Honda et al.'s study, the coefficient of correlation may be approximately taken as 0.63. From Tables 7-1 and 7-2, the difference between $c = 0.9$ and $c = 0.63$ is small. For two-truck loading, it falls within 3% and for one-truck loading it falls within 3.2%. Therefore, it is concluded that in practice the use of two completely the same profiles ($c = 1.0$) does not cause much deviation.

10. For other girders at the midspan section, the trends are similar to those of the girder subjected to the highest loading. Some exceptions occur because the roll mode of vehicles demonstrates its influence.

11. For the span length of 42.67m and a high traveling speed range of 72 to 121km/h (45 to 75MPH), it is observed that the impact factors are insensitive to good road roughness. In this case, the dynamic vibration mainly depends on the characteristics of the vehicle and the bridge.

12. The nonzero velocities and displacements in every degree of freedom of a truck before it enters the bridge cause fluctuation in the impact factors for the light trucks obviously more than for the heavy ones. Hence, this randomness has less effect on heavy trucks.

13. Despite the variation in axle weights and configurations, the five typical trucks cause close lateral distribution factors.

14. Calculated distribution factors based on both static and dynamic moments/shears are similar.

15. Calculated lateral distribution factors for interior girders based on loading of two lanes are lower than the values specified by AASHTO *Specifications*.

REFERENCES

AASHTO. (1990). *Guide for Maximum Dimensions and Weights of Motor Vehicles and for the Operation of the Non-divisible Load Oversize and Overweight Vehicles.* Am. Assoc. of State Hwy. and Transp. Officials, revised 1991, Washington, D. C.

AASHTO. (1990) *Guide Specifications for Fatigue Evaluation of Existing Steel Bridges.* Am. Assoc. of State Hwy. and Transp. Officials, Washington, D. C.

AASHTO. (1996). *Standard Specifications for Highway Bridges*, 16th Ed., American Association of State Highway and Transportation Officials, Washington, D. C.

AASHTO. (1998). *LRFD Bridge Design Specifications-Customary U.S. Units*, 2nd Edition, Am. Assoc. of State Hwy. and Transp. Officials (AASHTO), Washington, D.C.

Bannatine, J. A., Comer, J. J., and Handrock, J. L. (1990). *Fundamentals of Metal Fatigue Analysis*, Prentice-Hall, Inc., Englewood Cliffs, N. J.

Chu, K. H., Garg, V. K., and Wang, T.-L. (1986). "Impact in Railway Prestressed Concrete Bridges," *J. Struct. Engrg.*, ASCE, 116(7), 1036-1051.

Clough, R.W., and Penzien, J. (1996). *Dynamics of Structures*, McGraw-Hill Book Co., 2nd edition, New York, N.Y.

Dicleli, M. and Bruneau, M. (1995). "Fatigue-Based Methodology for Managing Impact of Heavy-Permit Trucks on Steel Highway Bridges," *Journal of Structural Engineering*, ASCE, Vol. 121, No.11, 1651-1659.

Dodds, C. J. and Robson, J. D. (1973) "The Description of Road Surface Roughness," *Journal of Sound and Vibration*, 31(2), November, 175-183.

Fenves, S. J., Veletsos, A.S., and Siess, C.P. (1962). "Dynamic Studies of Bridges on the AASHTO Test Road," *Report No. 71*, Nat. Academy of Sci.-Nat. Res. Council, Washington, D.C.

Florida Annual Average Daily Traffic Report (1998). Florida Dept. Of Transp., Tallahassee, FL.

Fu, G. and Hag-Elsafi, O. (2000). "Vehicular Overloads: Load Model, Bridge Safety, and Permit Checking," *J. Struct. Div.*, ASCE, 108(9), 1956-1966.

Honda, H., Kajikawa, Y., and Kobori, T. (1982) "Spectra of Road Surface Roughness on Bridges," *J. Struct. Div.*, ASCE, 108(9), 1956-1966.

Huang, D. Z., Wang, T. L., and Shahawy, M. (1993). "Impact Studies of Multigirder Concrete Bridges," *J. Struct. Engrg.*, ASCE, 119(8), 2387-2402.

Hwang, E.-S. and Nowok, A.S. (1991). "Simulation of Dynamic Load for Bridges," *J. Struct. Engrg.*, ASCE, 117(5), 1413-1434.

Kim, S. and Nowak, A.S. (1997). "Load Distribution and Impact Factors for I-girder Bridges," *J. of Bridge Engrg.*, ASCE, 2(3), 97-104.

Laman, J. A., Nowak A. S. (1996). "Fatigue Load Models for Girder Bridges," *J. Struct. Engrg.*, ASCE, 122(7), 726-733.

Law, D. B., Williamson, H. J., and Hudson, W. R. (1975). "The Characterization of Road Roughness on Bridge Decks and the Adjoining Pavement," *Research Report No. FHWA-RD-75-SO409*, Texas Highway Dept. Planning & Research Division, Austin, Texas.

Miner M.A. (1945). "Cumulative Damage in Fatigue," *Transactions of the ASME*, vol. 67.

Nowak, A. S., Nassif, H. and DeFrain L. (1993). "Effect of Truck Loads on Bridges," *Journal of Transportation Engineering*, ASCE, Vol. 119, No.6, 853-867.

Ruhl, J. (1974). "Stress Histories for Highway Bridges Subjected to Traffic Loading," *Ph.D. dissertation*, University of Illinois, Urbana, Ill.

Samaras, E., Shinozuka, M., and Tsurui, A. (1985). "ARMA Representation of Random Processes," *J. Engrg. Mech.*, ASCE, 111(3), 449-461.

Standard Plans for Highway Bridge Superstructures. (1990). U.S. Dept. Of Transp., Federal Highway Admin., Washington, D. C.

Wang, T.-L. (1990). "Ramp/Bridge Interface in Railway Prestressed Concrete Bridges," *J. Struct. Engrg.*, ASCE, 116(6), 1648-1659.

Wang, T.-L., Garg, V.K., and Chu, K.H. (1991). "Railway Bridge/Vehicle Interaction Studies with a New Vehicle Model," *J. Struct. Engrg.*, ASCE, 117(7), 2099-2116.

Wang, T. L., Huang, D. Z., and Shahaway, M. (1992). "Dynamic Response of Multigirder Bridges," *J. Struct. Engrg.*, ASCE, 118(8), 2222-2238.

Wang, T. L., and Huang, D. Z. (1993). "Computer Modeling Analysis in Bridge Evaluation – Phase III," *Final Report, Project No. FL/DOT/RMC/0542(3)-7851*, Florida Dept. of Transp.

Wang, T.-L., Huang D. Z., and Shahawy, M. (1993). "Vibration and Impact in Multigirder Steel Bridges," *Transp. Research Record*, Transp. Research Board (TRB), National Research Council, Washinton, D.C., No. 1393, Aug., 96-103.

Wang, T. L., Shahaway, M., and Huang, D. Z. (1993). "Probabilistic Fatigue Life Analysis of Highway Steel Bridges," *Computers and Structures*, Vol. 48, No.2, pp. 241-248

Zokaie, T. (2000). "AASHTO-LRFD Live Load Distribution Specifications," *J. of Bridge Engrg.*, ASCE, 5(2), 131-138.

Table 2-1.
Statistics of Axle Weight at Station #19 ($\times 10^{-1}$ kips)

Vehicle Type	Loading Condition	Statistics	Number of Axle							
			1	2	3	4	5	6	7	8
4	Empty	MV	91.7	137.7	45.8	-	-	-	-	-
		SD	16.2	20.1	14.0	-	-	-	-	-
		COV	0.2	0.2	0.3	-	-	-	-	-
	Loaded	MV	115.9	179.9	66.1	-	-	-	-	-
		SD	11.9	20.1	21.4	-	-	-	-	-
		COV	0.1	0.1	0.3	-	-	-	-	-
5	Empty	MV	56.2	77.6	-	-	-	-	-	-
		SD	12.9	15.0	-	-	-	-	-	-
		COV	0.2	0.2	-	-	-	-	-	-
	Loaded	MV	76.6	127.8	-	-	-	-	-	-
		SD	17.6	23.7	-	-	-	-	-	-
		COV	0.2	0.2	-	-	-	-	-	-
6	Empty	MV	107.0	70.3	64.4	-	-	-	-	-
		SD	30.7	20.3	19.7	-	-	-	-	-
		COV	0.3	0.3	0.3	-	-	-	-	-
	Loaded	MV	123.7	139.1	129.7	-	-	-	-	-
		SD	36.5	34.3	34.8	-	-	-	-	-
		COV	0.3	0.3	0.3	-	-	-	-	-
7	Loaded	MV	163.9	94.3	182.4	186.7	-	-	-	-
		SD	17.7	41.7	30.9	29.5	-	-	-	-
		COV	0.1	0.4	0.2	0.2	-	-	-	-
8	Empty type 8-1	MV	81.1	95.0	50.4	-	-	-	-	-
		SD	15.3	16.3	22.1	-	-	-	-	-
		COV	0.2	0.2	0.4	-	-	-	-	-
	Empty type 8-2	MV	79.1	94.3	52.8	52.8	-	-	-	-
		SD	16.0	16.4	11.4	12.3	-	-	-	-
		COV	0.2	0.2	0.2	0.2	-	-	-	-
	Empty type 8-3	MV	85.6	71.2	67.3	71.0	-	-	-	-
		SD	11.4	10.1	8.9	20.4	-	-	-	-
		COV	0.1	0.1	0.1	0.3	-	-	-	-
	Loaded type 8-1	MV	84.1	125.6	98.2	-	-	-	-	-
		SD	15.3	27.1	27.0	-	-	-	-	-
		COV	0.2	0.2	0.3	-	-	-	-	-
	Loaded type 8-2	MV	91.1	141.0	95.9	97.6	-	-	-	-
		SD	14.0	24.3	27.1	31.1	-	-	-	-
		COV	0.2	0.2	0.3	0.3	-	-	-	-
	Loaded type 8-3	MV	101.1	94.8	94.2	126.7	-	-	-	-
		SD	16.3	19.1	19.5	38.0	-	-	-	-
		COV	0.2	0.2	0.2	0.3	-	-	-	-

To be continued

Continued

9	Empty	MV	94.7	81.0	78.9	64.0	67.7	-	-	-
		SD	17.6	14.4	14.2	15.7	16.0	-	-	-
		COV	0.2	0.2	0.2	0.3	0.2	-	-	-
	Loaded	MV	103.9	132.1	130.4	129.9	136.0	-	-	-
		SD	16.3	26.5	26.3	31.0	32.1	-	-	-
		COV	0.2	0.2	0.2	0.2	0.2	-	-	-
10	Empty	MV	97.0	102.5	100.4	75.7	73.1	71.4	-	-
		SD	16.3	19.5	19.8	20.2	16.9	20.1	-	-
		COV	0.2	0.2	0.2	0.3	0.2	0.3	-	-
	Loaded	MV	115.7	162.4	160.4	134.5	131.7	125.7	-	-
		SD	19.4	28.1	28.1	29.4	28.5	35.0	-	-
		COV	0.2	0.2	0.2	0.2	0.2	0.3	-	-
11	Empty	MV	85.8	111.4	92.3	84.4	79.4	-	-	-
		SD	12.9	17.7	16.0	15.9	13.8	-	-	-
		COV	0.2	0.2	0.2	0.2	0.2	-	-	-
	Loaded	MV	93.5	142.8	135.9	118.1	118.6	-	-	-
		SD	11.9	19.3	22.4	18.8	18.9	-	-	-
		COV	0.1	0.1	0.2	0.2	0.2	-	-	-
12	Empty	MV	89.3	80.6	77.0	95.8	88.5	82.8	-	-
		SD	13.6	12.7	12.1	21.0	15.8	19.1	-	-
		COV	0.2	0.2	0.2	0.2	0.2	0.2	-	-
	Loaded	MV	99.8	106.7	103.4	141.6	127.2	122.1	-	-
		SD	15.6	15.0	17.4	24.5	23.2	20.7	-	-
		COV	0.2	0.1	0.2	0.2	0.2	0.2	-	-
13	Empty 7-axle	MV	87.0	134.5	136.5	54.0	64.0	59.0	62.0	-
		SD	11.3	77.1	81.3	8.5	28.3	19.8	19.8	-
		COV	0.1	0.6	0.6	0.2	0.4	0.3	0.3	-
	Empty 8-axle	MV	103.0	99.0	98.0	87.0	40.0	46.0	48.0	48.0
		SD	0.0	0.0	0.0	0.0	0.0	0.0	0.0	0.0
		COV	0.0	0.0	0.0	0.0	0.0	0.0	0.0	0.0
	Loaded 7-axle	MV	87.8	117.8	184.0	181.8	179.8	170.8	177.2	-
		SD	9.9	10.0	39.0	39.3	37.9	34.0	34.6	-
		COV	0.1	0.1	0.2	0.2	0.2	0.2	0.2	-

Table 2-2.
Statistics of Axle Spacing at Station #19 (feet and tenths)

Vehicle Type	Loading Condition	Statistics	Number of Axle							
			1-2	2-3	3-4	4-5	5-6	6-7	7-8	8-9
4	Empty	MV	240.59	41.53	-	-	-	-	-	-
		SD	2.06	1.01	-	-	-	-	-	-
		COV	0.01	0.02	-	-	-	-	-	-
	Loaded	MV	245.57	12.64	-	-	-	-	-	-
		SD	41.70	0.96	-	-	-	-	-	-
		COV	0.05	0.02	-	-	-	-	-	-
5	Empty	MV	168.00	-	-	-	-	-	-	-
		SD	22.00	-	-	-	-	-	-	-
		COV	0.13	-	-	-	-	-	-	-
	Loaded	MV	180.49	-	-	-	-	-	-	-
		SD	18.98	-	-	-	-	-	-	-
		COV	0.11	-	-	-	-	-	-	-
6	Empty	MV	173.14	43.81	-	-	-	-	-	-
		SD	14.46	2.49	-	-	-	-	-	-
		COV	0.08	0.06	-	-	-	-	-	-
	Loaded	MV	190.15	44.38	-	-	-	-	-	-
		SD	20.97	2.25	-	-	-	-	-	-
		COV	0.11	0.05	-	-	-	-	-	-
7	Loaded	MV	115.70	43.20	45.20	-	-	-	-	-
		SD	3.23	2.04	0.79	-	-	-	-	-
		COV	0.03	0.05	0.02	-	-	-	-	-
8	Empty type 8-1	MV	150.42	236.84	-	-	-	-	-	-
		SD	40.02	64.32	-	-	-	-	-	-
		COV	0.27	0.27	-	-	-	-	-	-
	Empty type 8-2	MV	134.79	294.37	42.56	-	-	-	-	-
		SD	13.99	53.06	10.38	-	-	-	-	-
		COV	0.10	0.18	0.24	-	-	-	-	-
	Empty type 8-3	MV	148.61	43.61	250.00	-	-	-	-	-
		SD	33.74	1.12	67.60	-	-	-	-	-
		COV	0.23	0.03	0.27	-	-	-	-	-
	Loaded type 8-1	MV	131.79	265.08	-	-	-	-	-	-
		SD	17.86	61.10	-	-	-	-	-	-
		COV	0.14	0.23	-	-	-	-	-	-
	Loaded type 8-2	MV	133.86	312.75	41.85	-	-	-	-	-
		SD	14.44	47.55	5.82	-	-	-	-	-
		COV	0.11	0.15	0.14	-	-	-	-	-
	Loaded type 8-3	MV	149.59	44.00	299.27	-	-	-	-	-
		SD	30.73	1.72	81.87	-	-	-	-	-
		COV	0.21	0.04	0.27	-	-	-	-	-

To be continued

Continued

9	Empty	MV	153.93	43.97	320.03	44.62	-	-	-	-
		SD	29.44	1.01	31.26	13.27	-	-	-	-
		COV	0.19	0.02	0.10	0.30				-
	Loaded	MV	157.79	43.93	325.59	46.71				-
		SD	28.55	1.10	28.74	16.53				-
		COV	0.18	0.03	0.09	0.35				-
10	Empty	MV	163.20	44.15	310.59	43.76	43.80			-
		SD	24.76	0.70	62.95	2.91	2.79			-
		COV	0.15	0.02	0.20	0.07	0.06			-
	Loaded	MV	170.09	44.53	319.34	44.84	44.38			-
		SD	29.93	1.41	51.61	5.07	2.79			-
		COV	0.18	0.03	0.16	0.11	0.06			-
11	Empty	MV	132.42	216.86	97.30	225.04				-
		SD	14.58	6.82	4.13	4.76				-
		COV	0.11	0.03	0.04	0.02				-
	Loaded	MV	134.02	215.41	96.93	224.33				-
		SD	17.57	4.72	2.70	4.44				-
		COV	0.13	0.02	0.03	0.02				-
12	Empty	MV	133.46	44.11	203.89	97.79	225.82			-
		SD	27.36	0.42	5.84	4.10	3.70			-
		COV	0.21	0.01	0.03	0.04	0.02			-
	Loaded	MV	146.45	43.84	202.31	97.50	225.94			-
		SD	31.97	0.75	6.10	3.71	3.50			-
		COV	0.22	0.02	0.03	0.04	0.02			-
13	Empty 7-axle	MV	221.50	44.00	339.00	64.50	167.00	85.50		-
		SD	9.19	1.41	96.17	30.41	168.29	62.93		-
		COV	0.04	0.03	0.28	0.47	1.01	0.74		-
	Empty 8-axle	MV	161.00	42.00	152.00	42.00	344.00	43.00	43.00	-
		SD	0.00	0.00	0.00	0.00	0.00	0.00	0.00	-
		COV	0.00	0.00	0.00	0.00	0.00	0.00	0.00	-
	Loaded 7-axle	MV	165.60	42.60	45.00	370.20	43.80	81.60		-
		SD	21.79	1.95	2.00	28.64	1.64	54.27		-
		COV	0.13	0.05	0.04	0.08	0.04	0.67		-

Table 2-3.
Statistics of Axle Weight at Station #26 ($\times 10^{-1}$ kips)

Vehicle Type	Loading Condition	Statistics	Number of Axle							
			1	2	3	4	5	6	7	8
4	Empty	MV	97.4	147.9	37.3	-	-	-	-	-
		SD	9.4	17.2	12.9	-	-	-	-	-
		COV	0.1	0.1	0.3	-	-	-	-	-
	Loaded	MV	116.7	175.0	70.0	-	-	-	-	-
		SD	16.3	23.4	29.7	-	-	-	-	-
		COV	0.1	0.1	0.4	-	-	-	-	-
5	Empty	MV	54.5	73.7	-	-	-	-	-	-
		SD	16.7	16.5	-	-	-	-	-	-
		COV	0.3	0.2	-	-	-	-	-	-
	Loaded	MV	77.9	140.1	-	-	-	-	-	-
		SD	20.4	34.5	-	-	-	-	-	-
		COV	0.3	0.2	-	-	-	-	-	-
6	Empty	MV	109.1	76.5	64.3	-	-	-	-	-
		SD	27.3	25.3	20.1	-	-	-	-	-
		COV	0.3	0.3	0.3	-	-	-	-	-
	Loaded	MV	134.3	166.6	142.9	-	-	-	-	-
		SD	35.0	44.6	49.4	-	-	-	-	-
		COV	0.3	0.3	0.3	-	-	-	-	-
7	Loaded	MV	145.3	111.8	206.2	182.2	-	-	-	-
		SD	26.0	27.6	41.1	42.3	-	-	-	-
		COV	0.2	0.2	0.2	0.2	-	-	-	-
8	Empty type 8-1	MV	87.2	82.8	49.5	-	-	-	-	-
		SD	13.2	15.2	15.5	-	-	-	-	-
		COV	0.2	0.2	0.3	-	-	-	-	-
	Empty type 8-2	MV	82.1	86.6	44.2	41.4	-	-	-	-
		SD	11.7	17.6	11.4	9.8	-	-	-	-
		COV	0.1	0.2	0.3	0.2	-	-	-	-
	Empty type 8-3	MV	85.9	68.0	53.5	43.9	-	-	-	-
		SD	13.8	15.5	11.8	17.4	-	-	-	-
		COV	0.2	0.2	0.2	0.4	-	-	-	-
	Loaded type 8-1	MV	82.9	148.8	108.4	-	-	-	-	-
		SD	13.5	40.5	60.7	-	-	-	-	-
		COV	0.2	0.3	0.6	-	-	-	-	-
	Loaded type 8-2	MV	84.1	168.9	148.2	148.8	-	-	-	-
		SD	11.9	40.8	58.8	64.7	-	-	-	-
		COV	0.1	0.2	0.4	0.4	-	-	-	-
	Loaded type 8-3	MV	99.4	141.0	129.5	128.4	-	-	-	-
		SD	12.1	33.2	36.7	35.9	-	-	-	-
		COV	0.1	0.2	0.3	0.3	-	-	-	-

To be continued

Continued

9	Empty	MV	96.9	80.2	71.6	53.9	53.7	-	-	-
		SD	13.0	22.2	20.0	18.6	19.4	-	-	-
		COV	0.1	0.3	0.3	0.3	0.4	-	-	-
	Loaded	MV	100.0	146.7	137.6	139.7	137.8	-	-	-
		SD	12.3	27.8	30.7	34.3	35.8	-	-	-
		COV	0.1	0.2	0.2	0.2	0.3	-	-	-
10	Empty	MV	98.6	119.5	105.1	85.2	79.8	73.9	-	-
		SD	13.5	19.6	26.1	34.7	17.5	22.5	-	-
		COV	0.1	0.2	0.2	0.4	0.2	0.3	-	-
	Loaded	MV	101.7	155.6	147.6	131.1	136.0	144.3	-	-
		SD	18.4	39.0	39.0	41.6	28.7	47.0	-	-
		COV	0.2	0.3	0.3	0.3	0.2	0.3	-	-
11	Empty	MV	85.0	117.4	90.1	84.8	76.3	-	-	-
		SD	9.7	19.3	26.2	19.0	19.6	-	-	-
		COV	0.1	0.2	0.3	0.2	0.3	-	-	-
	Loaded	MV	89.2	160.4	146.0	119.8	114.7	-	-	-
		SD	11.1	27.1	22.2	24.9	23.7	-	-	-
		COV	0.1	0.2	0.2	0.2	0.2	-	-	-
12	Empty	MV	93.1	81.6	70.0	92.7	76.6	72.3	-	-
		SD	12.9	15.5	14.6	26.1	17.5	18.5	-	-
		COV	0.1	0.2	0.2	0.3	0.2	0.3	-	-
	Loaded	MV	95.3	102.1	80.3	142.6	115.6	117.7	-	-
		SD	18.3	24.1	19.1	29.5	30.8	32.2	-	-
		COV	0.2	0.2	0.2	0.2	0.3	0.3	-	-
13	Empty 7-axle	MV	109.5	113.5	152.0	158.5	155.0	142.5	159.5	-
		SD	17.7	31.8	0.0	20.5	2.8	13.4	0.7	-
		COV	0.2	0.3	0.0	0.1	0.0	0.1	0.0	-
	Empty 8-axle	MV	106.5	147.5	188.0	185.5	140.0	146.0	144.0	141.0
		SD	27.6	21.9	42.4	55.9	38.2	48.1	38.2	53.7
		COV	0.3	0.1	0.2	0.3	0.3	0.3	0.3	0.4

Table 2-4.
Statistics of Axle Spacing at Station #26 (feet and tenths)

Vehicle Type	Loading Condition	Statistics	Number of Axle							
			1-2	2-3	3-4	4-5	5-6	6-7	7-8	8-9
4	Empty	MV	239.42	41.83	-	-	-	-	-	-
		SD	5.70	3.21	-	-	-	-	-	-
		COV	0.02	0.08	-	-	-	-	-	-
	Loaded	MV	247.44	41.35	-	-	-	-	-	-
		SD	13.62	2.38	-	-	-	-	-	-
		COV	0.06	0.06	-	-	-	-	-	-
5	Empty	MV	165.05	-	-	-	-	-	-	-
		SD	22.37	-	-	-	-	-	-	-
		COV	0.14	-	-	-	-	-	-	-
	Loaded	MV	178.89	-	-	-	-	-	-	
		SD	21.15	-	-	-	-	-		-
		COV	0.12	-	-	-	-	-	-	-
6	Empty	MV	164.19	44.52	-	-	-	-	-	-
		SD	20.20	3.72	-	-	-	-	-	-
		COV	0.12	0.08	-	-	-	-	-	-
	Loaded	MV	176.33	44.37	-	-	-	-	-	-
		SD	25.40	3.94	-	-	-	-	-	-
		COV	0.14	0.09	-	-	-	-	-	-
7	Loaded	MV	116.03	43.97	46.51	-	-	-	-	-
		SD	10.88	3.95	8.71	-	-	-	-	-
		COV	0.09	0.09	0.19	-	-	-	-	-
8	Empty type 8-1	MV	136.30	244.80	-	-	-	-	-	-
		SD	28.47	64.42	-	-	-	-	-	-
		COV	0.21	0.26	-	-	-	-	-	-
	Empty type 8-2	MV	134.57	300.49	44.40	-	-	-	-	-
		SD	15.67	66.65	11.90	-	-	-	-	-
		COV	0.12	0.22	0.27	-	-	-	-	-
	Empty type 8-3	MV	138.71	44.91	289.16	-	-	-	-	-
		SD	24.24	4.20	60.63	-	-	-	-	-
		COV	0.18	0.09	0.21	-	-	-	-	-
	Loaded type 8-1	MV	145.17	251.63	-	-	-	-	-	-
		SD	31.35	64.52	-	-	-	-	-	-
		COV	0.22	0.26	-	-	-	-	-	-
	Loaded type 8-2	MV	135.46	269.91	42.61	-	-	-	-	-
		SD	15.19	71.46	6.19	-	-	-	-	-
		COV	0.11	0.27	0.15	-	-	-	-	-
	Loaded type 8-3	MV	144.83	45.01	318.93	-	-	-	-	-
		SD	30.54	4.04	37.78	-	-	-	-	-
		COV	0.21	0.09	0.12	-	-	-	-	-

To be continued

Continued

9	Empty	MV	155.53	44.96	319.66	45.41	-	-	-	-
		SD	32.14	3.42	39.42	13.85	-	-	-	-
		COV	0.21	0.08	0.12	0.31	-	-	-	-
	Loaded	MV	147.60	45.02	320.28	46.54	-	-	-	-
		SD	30.42	3.70	36.25	15.40	-	-	-	-
		COV	0.21	0.08	0.11	0.33	-	-	-	-
10	Empty	MV	154.43	44.81	314.24	43.05	41.52	-	-	-
		SD	30.55	3.03	51.19	2.69	3.23	-	-	-
		COV	0.20	0.07	0.16	0.06	0.08	-	-	-
	Loaded	MV	162.61	46.00	266.56	44.33	44.39	-	-	-
		SD	30.50	3.76	91.59	4.84	3.68	-	-	-
		COV	0.19	0.08	0.34	0.11	0.08	-	-	-
11	Empty	MV	127.74	214.89	96.42	220.26	-	-	-	-
		SD	11.07	8.66	5.33	8.13	-	-	-	-
		COV	0.09	0.04	0.06	0.04	-	-	-	-
	Loaded	MV	130.63	215.46	96.12	221.76	-	-	-	-
		SD	11.59	7.74	5.05	7.19	-	-	-	-
		COV	0.09	0.04	0.05	0.03	-	-	-	-
12	Empty	MV	147.06	45.35	201.91	99.91	222.91	-	-	-
		SD	33.44	3.36	9.66	6.05	9.82	-	-	-
		COV	0.23	0.07	0.05	0.06	0.04	-	-	-
	Loaded	MV	135.60	47.50	202.60	102.10	224.90	-	-	-
		SD	30.81	4.12	11.02	13.88	11.84	-	-	-
		COV	0.23	0.09	0.05	0.14	0.05	-	-	-
13	Empty 7-axle	MV	176.00	42.50	42.50	335.50	42.50	45.00	-	-
		SD	29.70	0.71	0.71	9.19	0.71	4.24	-	-
		COV	0.17	0.02	0.02	0.03	0.02	0.09	-	-
	Empty 8-axle	MV	161.00	44.50	47.00	381.00	50.00	49.00	131.00	-
		SD	9.90	2.12	5.66	8.49	9.90	2.83	39.60	-
		COV	0.06	0.05	0.12	0.02	0.20	0.06	0.30	-

Table 3-1.
Truck GVW and Passages in Each Classified Category

Category No.	Station #19 Southbound Lane #1			Station #26 Southbound Lane #2		
	Symbol [a]	GVW (kips)	One-week Passages	Symbol [a]	GVW (kips)	One-week Passages
1	4e	27.51	17	4e	28.26	12
2	4l	36.19	69	4l	36.17	48
3	5e	13.37	701	5e	12.82	789
4	5l	20.44	491	5l	21.80	493
5	6e	24.18	204	6e	24.99	271
6	6l	39.25	80	6l	44.38	164
7	7l	62.73	10	7l	64.55	93
8	8-1e	22.65	19	8-1e	21.95	10
9	8-2e	27.90	131	8-2e	25.43	114
10	8-3e	29.51	23	8-3e	25.13	55
11	8-1l	30.79	89	8-1l	34.01	287
12	8-2l	42.56	410	8-2l	55.00	680
13	8-3l	41.67	22	8-3l	49.83	430
14	9e	38.63	2949	9e	35.63	1227
15	9l	63.22	8032	9l	66.18	2595
16	10e	52.01	46	10e	56.21	21
17	10l	83.04	32	10l	81.63	18
18	11e	45.33	97	11e	45.36	57
19	11l	60.88	471	11l	63.01	41
20	12e	51.39	28	12e	48.63	34
21	12l	70.08	62	12l	65.36	10
22	13e(7-axle)	59.70	2	13l(7-axle)	99.05	2
23	13e(8-axle)	56.90	1	13l(8-axle)	119.85	2
24	13l(7-axle)	109.92	5	-	-	-

Note:

a. The number denotes the truck type by FHWA Classification Scheme "F" and "e" denotes empty and "l" denotes loaded.

Table 3-2.
Properties and Masses of Steel Bridges

Span Length (m)	Girder				Intermediate Diaphragm			Diaphragm at Ends		
	$I \times 10^{-2}$ (m⁴)	$J \times 10^{-4}$ (m⁴)	Mass (kN/m) Exterior	Mass (kN/m) Interior	$I \times 10^{-4}$ (m⁴)	$J \times 10^{-4}$ (m⁴)	Mass (kN/m)	$I \times 10^{-4}$ (m⁴)	$J \times 10^{-4}$ (m⁴)	Mass (kN/m)
10.67	0.19	2.08	16.44	11.79	1.31	0.004	0.49	0.13	0.004	0.49
16.76	0.99	3.98	17.06	12.40	12.03	1.723	0.62	0.85	1.723	0.49
22.86	1.58	4.11	18.67	14.01	12.03	1.723	0.62	0.85	1.723	0.49
30.48	4.00	4.53	18.98	14.32	40.83	2.789	1.00	7.71	2.789	0.54
36.58	6.74	4.55	19.84	15.18	50.86	3.351	1.12	11.66	3.351	0.67
42.67	10.26	4.56	20.61	15.95	73.47	3.908	1.12	16.50	3.908	0.67

Note:
a. The bridges with a span less than 30.48m have rolled girders, while the others have welded girders.

45

Table 3-3.
Mass and Girder Properties of Concrete Bridges

Span Length L (m)	Girder			Intermediate Diaphragm			Diaphragm at Ends		
	$I \times 10^{-2}$ (m^4)	$J_d \times 10^{-2}$ (m^4)	$\bar{m}$ (kN/m)	$I \times 10^{-2}$ (m^4)	$J_d \times 10^{-2}$ (m^4)	$\bar{m}$ (kN/m)	$I \times 10^{-2}$ (m^4)	$J_d \times 10^{-2}$ (m^4)	$\bar{m}$ (kN/m)
9.14	3.209	0.619	17.60[a] 13.27[b]	-	-	-	0.428	2.094	1.646
18.29	7.788	0.740	20.44[a] 15.78[b]	2.060	6.972	3.029	0.478	3.530	1.664
30.48	26.872	1.363	27.07[a] 22.43[b]	5.777	7.896	4.676	0.718	5.182	2.014
42.67	56.361	1.410	31.73[a] 27.09[b]	14.87	9.103	6.830	1.142	6.801	2.522

Note: a. for exterior girders; b. for interior girders; and c. I = inertial moment, J_d = torsional inertial moment, and $\bar{m}$ = mass per unit length.

Table 7-1.
Maximum Impact Factor (%) vs c
(Load Case I)

Coefficient of Correlation c	Span Length L			
	9.14m	18.29m	30.48m	42.67m
0.90	16.50	25.60	26.50	24.37
0.63	14.58	22.47	25.40	21.53
0.00	11.10	17.51	19.28	15.58
-0.63	4.78	16.55	10.47	8.42
-0.90	4.78	12.36	8.73	4.80

Table 7-2.
Maximum Impact Factor (%) vs *c*
(Load Case II)

Coefficient of Correlation *c*	Span Length *L*			
	9.14m	18.29m	30.48m	42.67m
0.90	34.19	21.84	16.75	12.54
0.63	31.30	20.03	15.11	13.21
0.00	22.39	15.13	11.43	10.52
-0.63	18.85	9.84	6.46	4.45
-0.90	15.07	8.46	5.91	0.23

Fig. 2-1. Locations of Weigh-in Motion Stations
(*from FDOT Website*)

Fig. 2.2 Truck Counts of Various Truck Types at Station #19

(a)

Station #19 - Southbound

Truck Type

Counts

Fig. 2.2 Truck Counts of Various Truck Types at Station #19

(b)

51

Station #19 - Northbound - Lane #1

Fig. 2.3 Truck Counts of Various Truck Types at Each Lane, Northbound, Station #19

(a)

Station # 19 - Northbound - Lane #2

Fig. 2.3 Truck Counts of Various Truck Types at Each Lane, Northbound, Station #19

(b)

Station # 19 - Southbound - Lane #1

Counts

Truck Type

(a)

Fig. 2.4 Truck Counts of Various Truck Types at Each Lane, Southbound, Station #19

Station # 19 - Southbound - Lane #2

Fig. 2.4 Truck Counts of Various Truck Types at Each Lane, Southbound, Station #19

(b)

Fig. 2.5 Histogram of Truck GVW at Station #19

(a)

Station #19 - Southbound

☐ Frequency

GVW (MN)

Frequency

(b)

Fig. 2.5 Histogram of Truck GVW at Station #19

Fig. 2.6 Truck Counts of Various Truck Types at Station #26

(a)

Station #26 - Southbound

Truck Type

Counts

(b)

Fig. 2.6 Truck Counts of Various Truck Types at Station #26

Fig. 2-7. Truck Counts of Various Truck Types at Each Lane, Northbound, Station #26

Fig. 2-7. Truck Counts of Various Truck Types at Each Lane, Northbound, Station #26

(b)
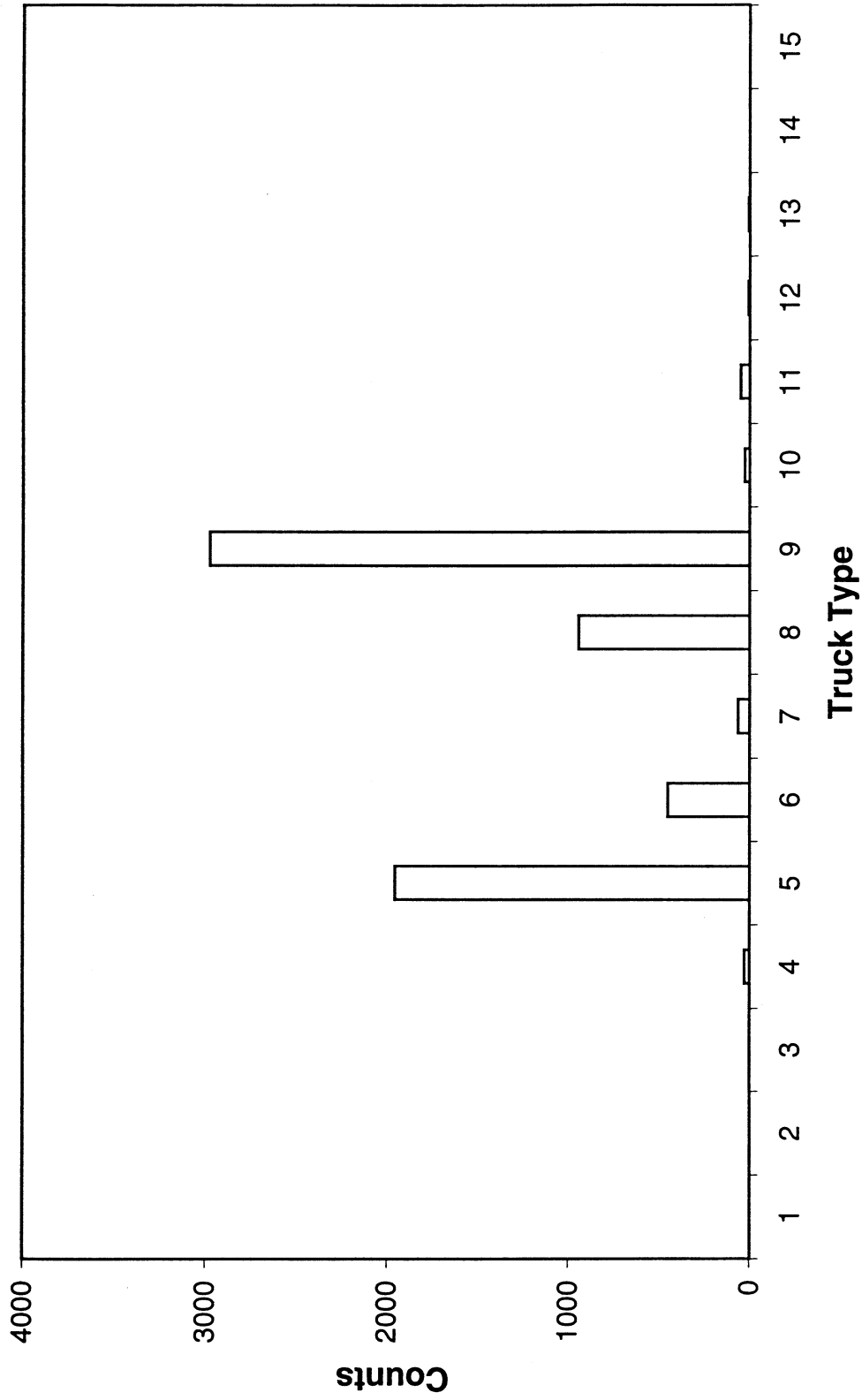
Fig. 2-8. Truck Counts of Various Truck Types at Each Lane, Southbound, Station #26

Station #26 - Southbound - Lane #2

Fig. 2-8. Truck Counts of Various Truck Types at Each Lane, Southbound, Station #26

(b)

Fig. 2.9 Histogram of Truck GVW at Station #26

(a)

Station #26 - Southbound

Fig. 2.9 Histogram of Truck GVW at Station #26

(b)
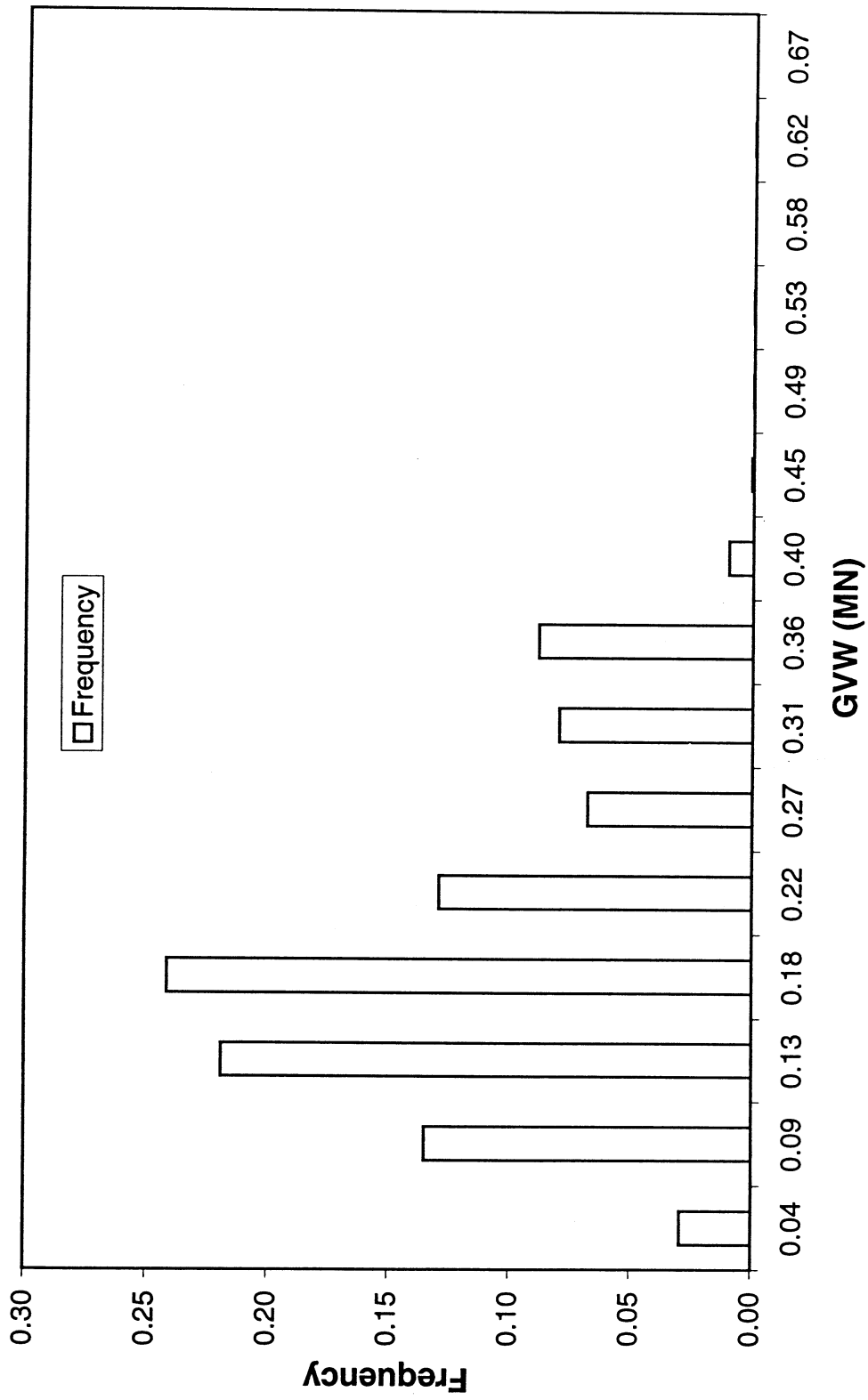
FHWA CLASSIFICATION SCHEME "F"

CLASS GROUP		DESCRIPTION	NO. OF AXLES
1		MOTORCYCLES	2
2		ALL CARS	2
		CARS W/ 1-AXLE TRAILER	3
		CARS W/ 2-AXLE TRAILER	4
3		PICK-UPS & VANS 1 & 2 AXLE TRAILERS	2, 3, & 4
4		BUSES	2 & 3
5		2-AXLE, SINGLE UNIT	2
6		3-AXLE, SINGLE UNIT	3
7		4-AXLE, SINGLE UNIT	4
8		2-AXLE, TRACTOR, 1-AXLE TRAILER (2S1)	3
		2-AXLE, TRACTOR, 2-AXLE TRAILER (2S2)	4
		3-AXLE, TRACTOR, 1-AXLE TRAILER (3S1)	4
9		3-AXLE, TRACTOR, 2-AXLE TRAILER (3S2)	5
		3-AXLE, TRUCK, W/ 2-AXLE TRAILER	5
10		TRACTOR W/ SINGLE TRAILER	6 & 7
11		5-AXLE MULTI-TRAILER	5
12		6-AXLE MULTI-TRAILER	6
13	ANY 7 OR MORE AXLE		7 or more
14	NOT USED		
15	UNKNOWN VEHICLE TYPE		

Fig. 2-10. FHWA Classification Scheme "F"
(Florida AADT Report 1998)

66
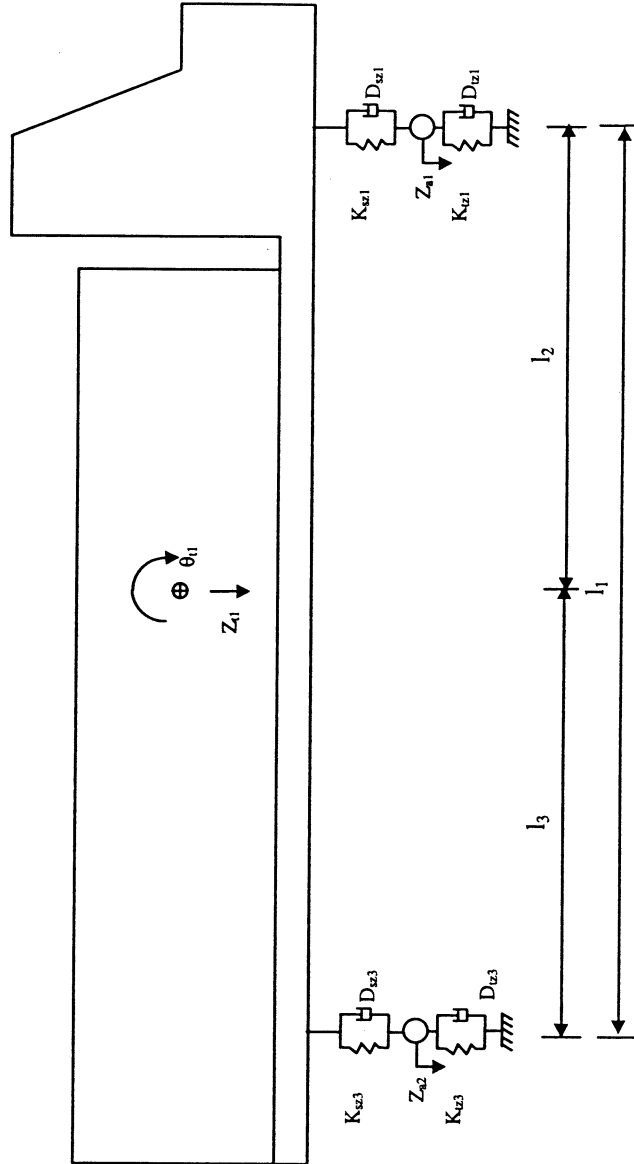
(a) Side View of Type 5

Fig. 3-1. 3D Models of Typical Trucks
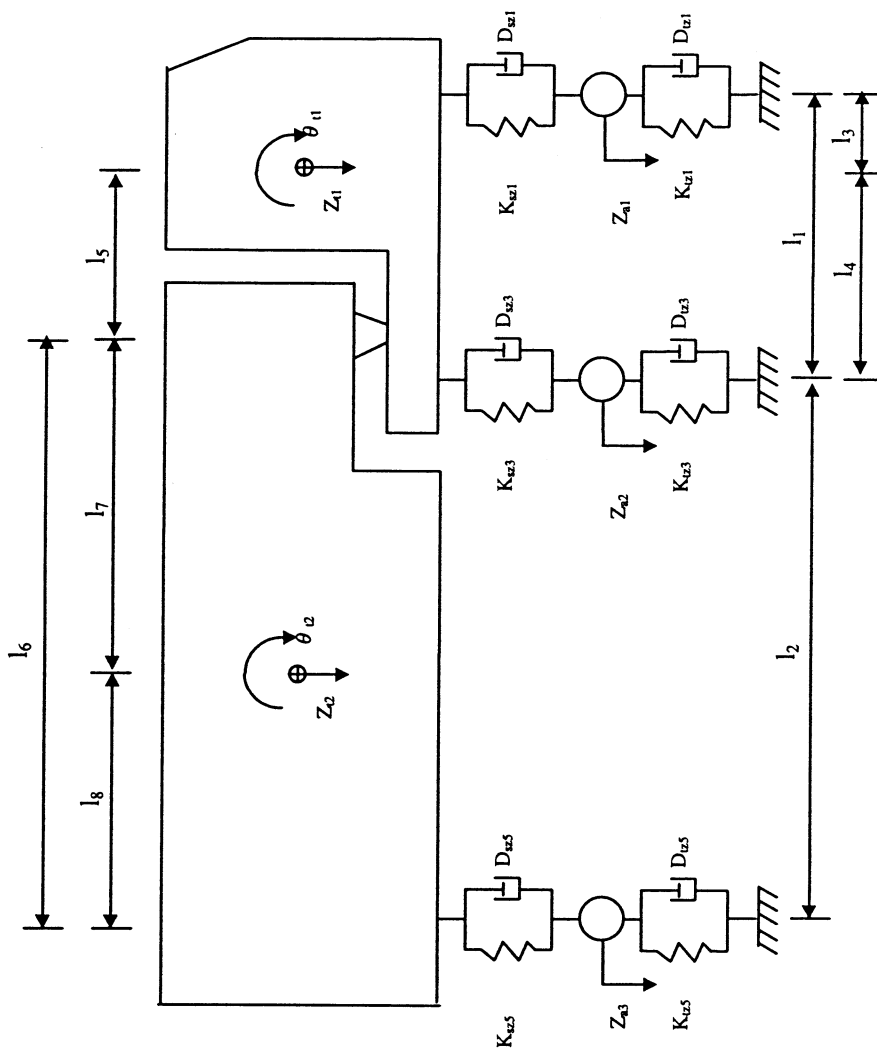
(b) Side View of Type 8(2S1)

Fig. 3-1. 3D Models of Typical Trucks

68
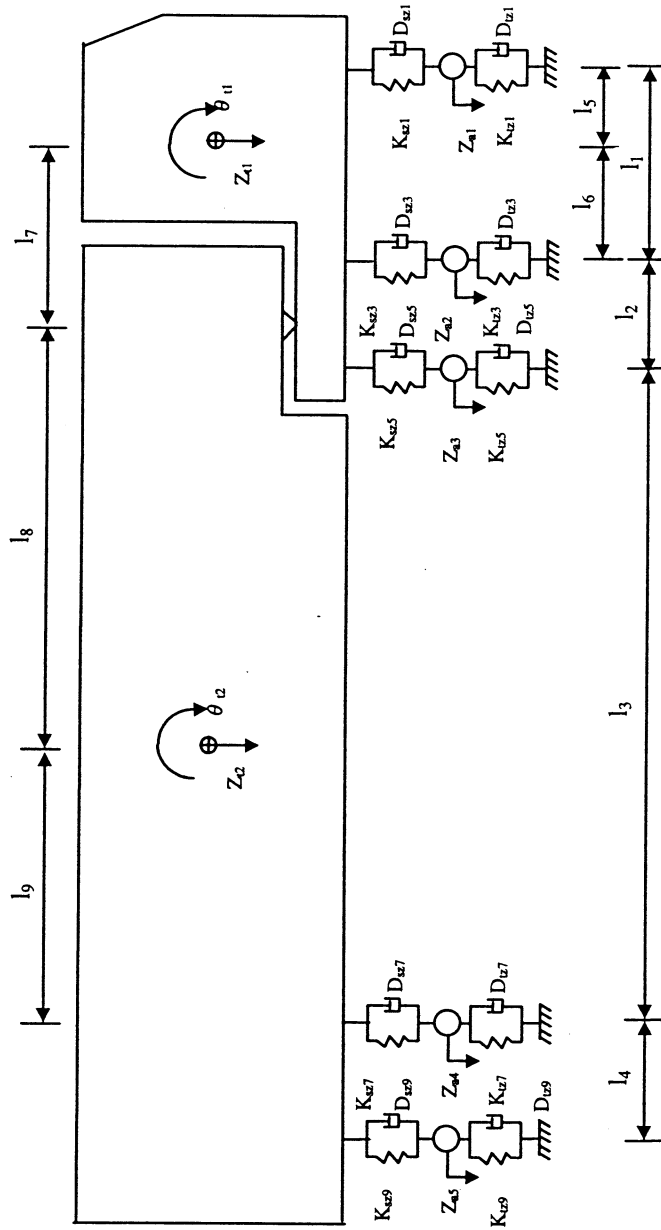
(c) Side View of Type 9(3S2)

Fig. 3-1. 3D Models of Typical Trucks
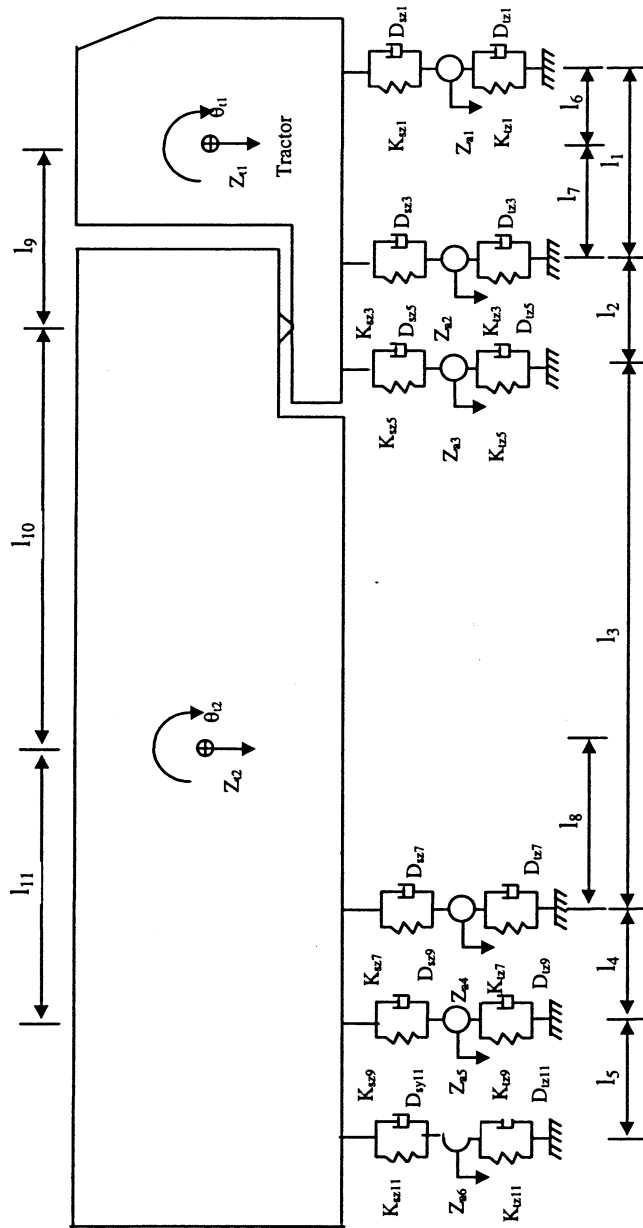
(d) Side View of Type 10

Fig. 3-1. 3D Models of Typical Trucks

70
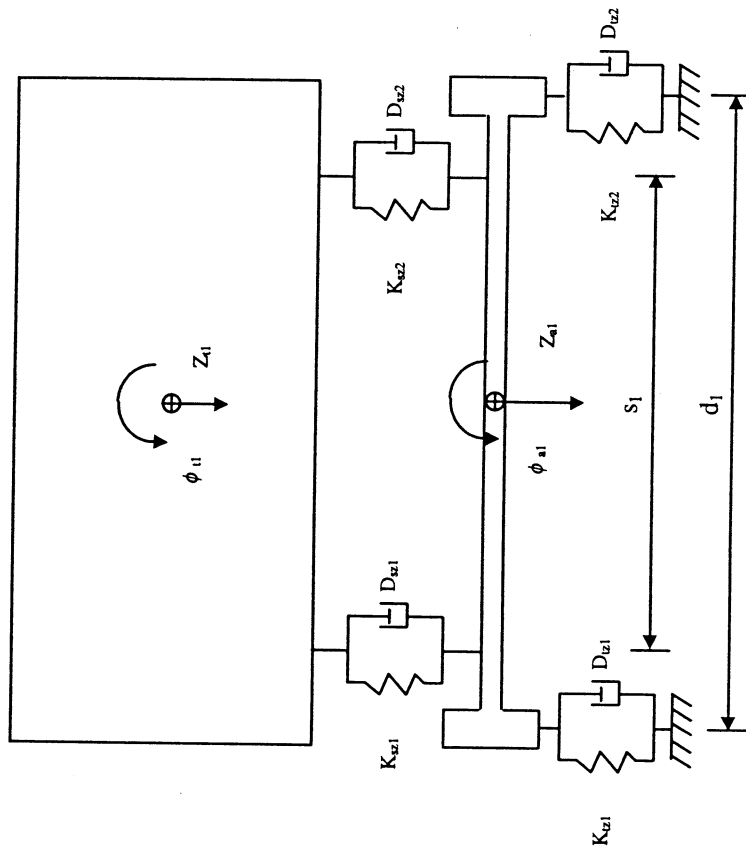
(e) Front View of Types 5 and 8(2S1)

Fig. 3-1. 3D Models of Typical Trucks

34.6kN   62.3kN

              5.45m

           GVW = 97kN

         (a) Loaded Type 5

36.1kN   67.9kN   47.2kN

        4.43m   7.67m

              GVW = 151kN

         (b) Loaded Type 8(2S1)

43.5kN 62.7kN/ea   62.7kN/ea
  4.50m   9.76m

      1.37m   1.42m

              GVW = 294kN

         (c) Loaded Type 9(3S2)

41.4kN 86.1kN/ea   49.8kN/ea
  4.96m   8.13m

      1.40m   1.35m 1.35m

              GVW = 363kN

         (d) Loaded Type 10
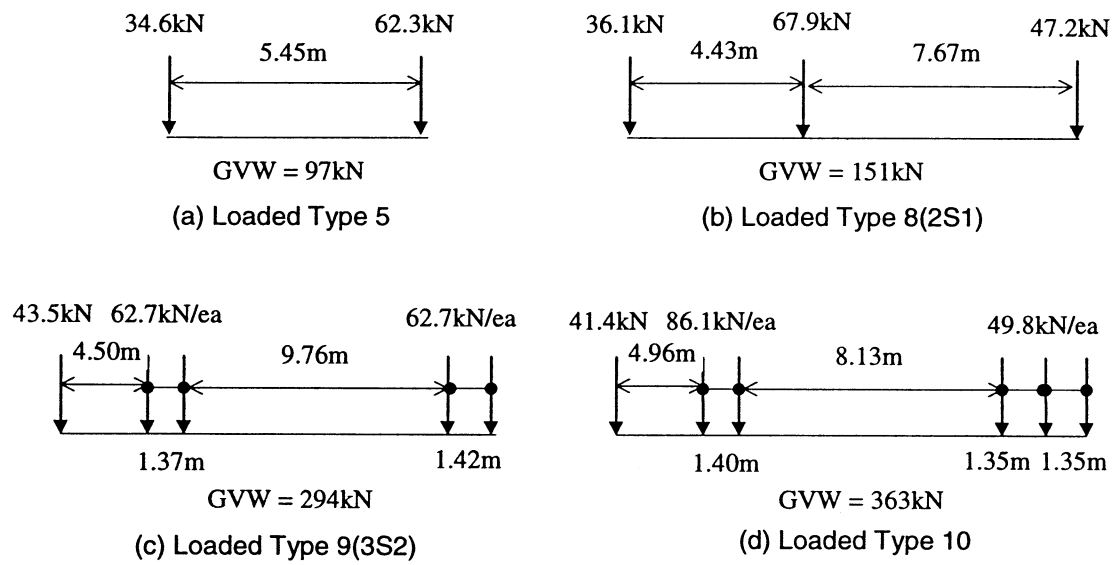
Fig. 3-2. Axle Weight and Configuration
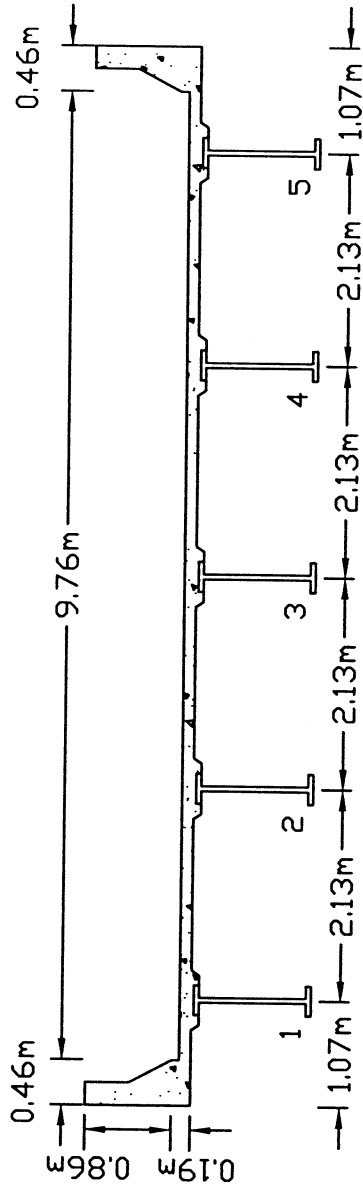
Fig. 3-3. Typical Cross Section of I-Girder Steel Bridges
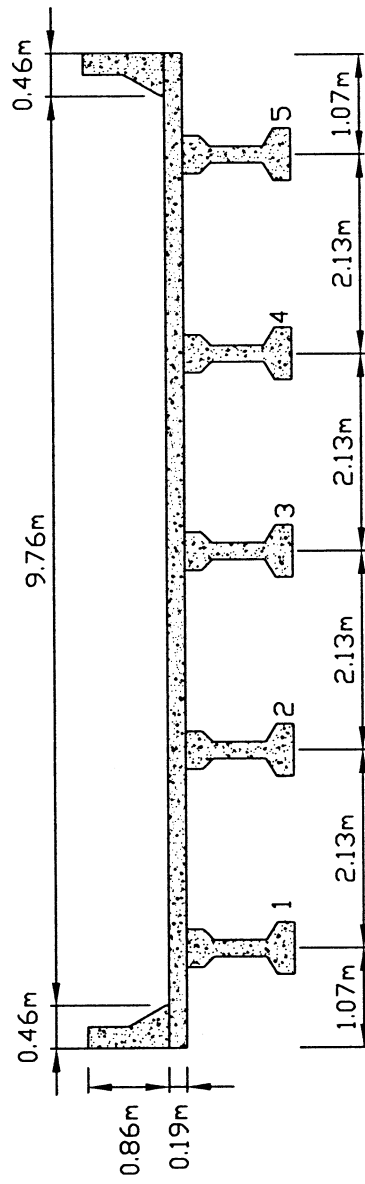
Fig. 3-4. Typical Cross Section of I-Girder Concrete Bridges
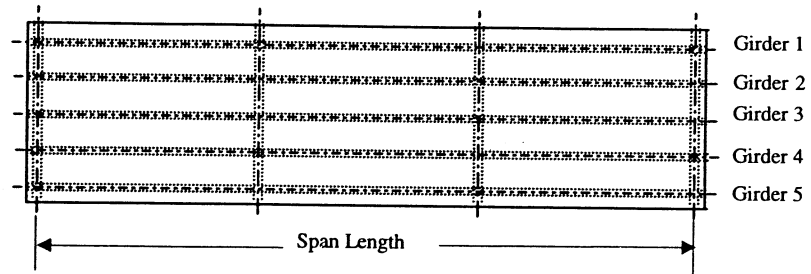
(a) Plan of bridges
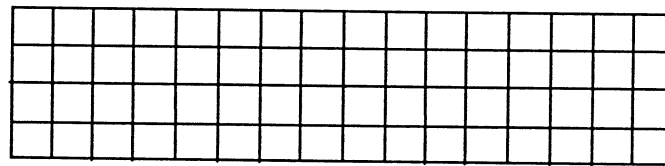
(b) Grillage model

Fig. 3-5. Typical Bridge Plan and Grillage Model
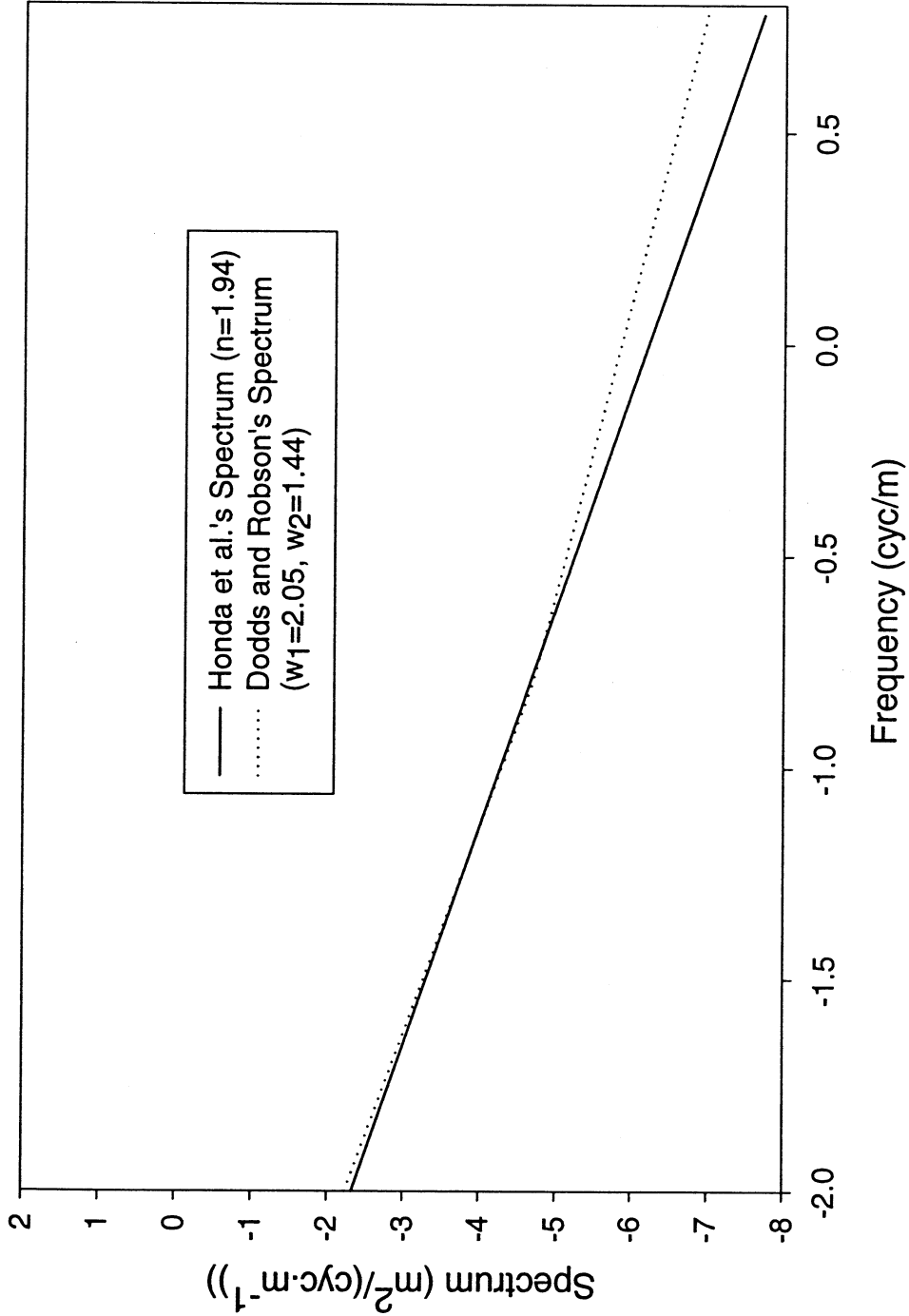
Fig. 4-1. Comparison of the PSD Functions

The figure legend reads:

Honda et al.'s Spectrum (n=1.94)

Dodds and Robson's Spectrum
(w$_1$=2.05, w$_2$=1.44)

X-axis: Frequency (cyc/m)

Y-axis: Spectrum (m^2/(cyc·m^{-1}))
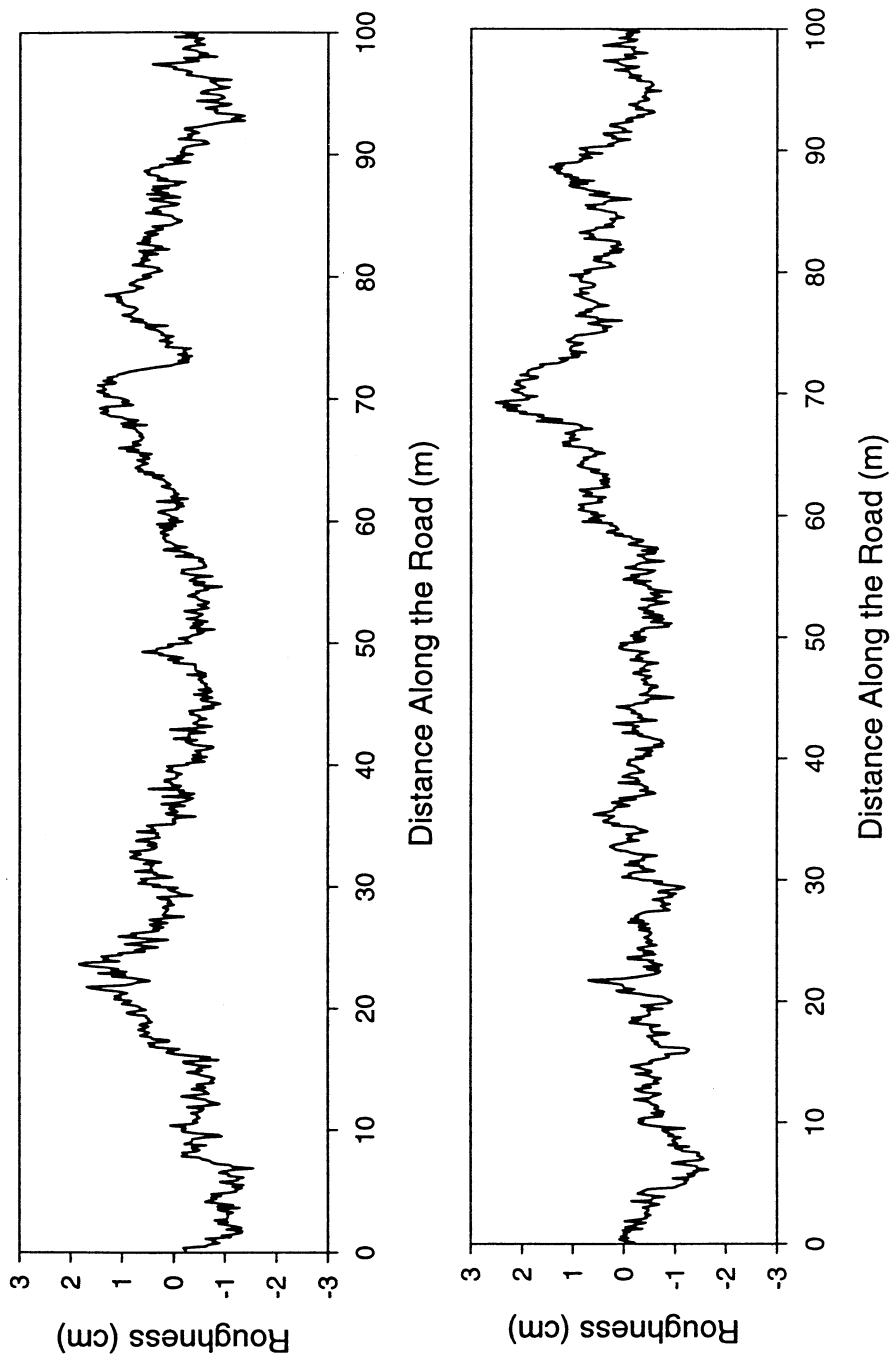
Fig. 4-2. Simulated Left- and Right-Lines

77
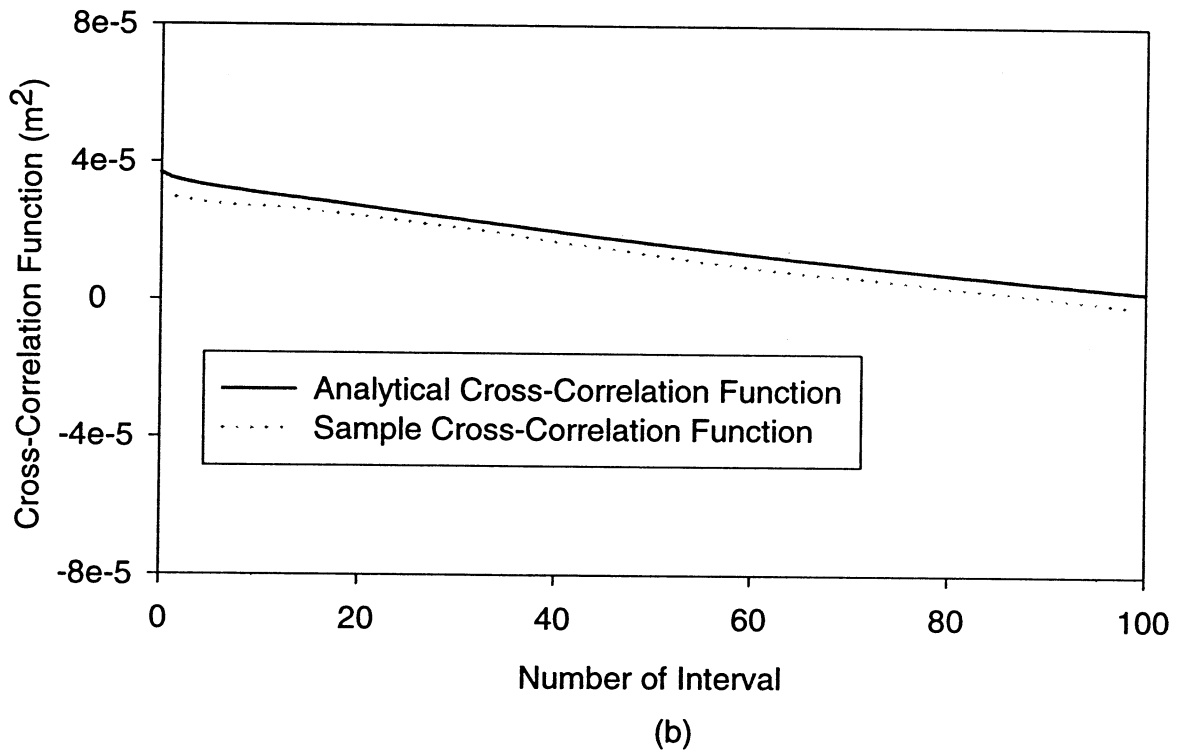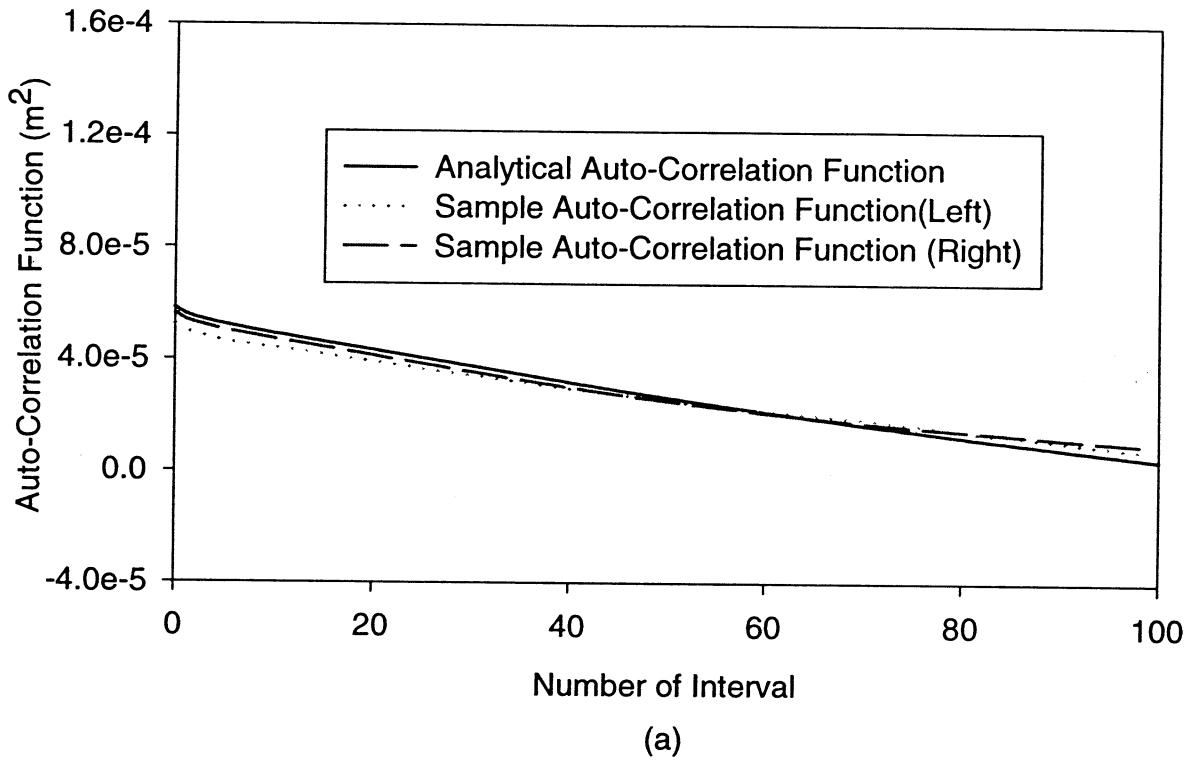
Fig. 4-3. Simulated Auto- and Cross-Correlation Functions and the Targets
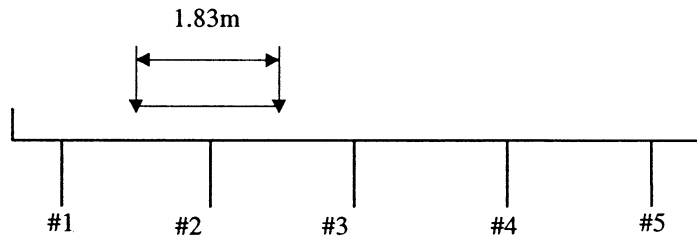
(a)
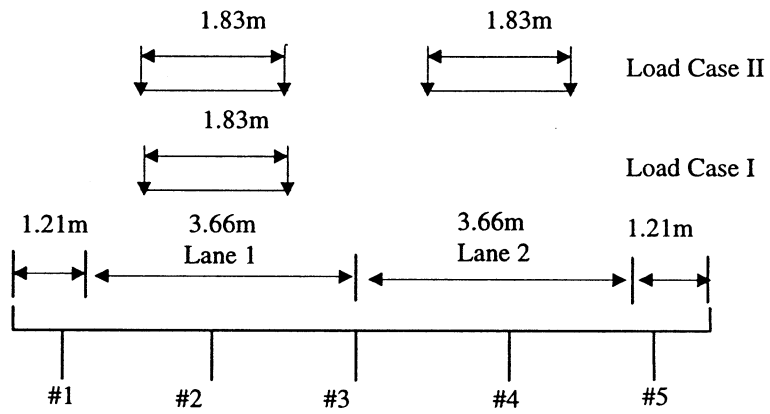
(b)

Fig. 5-1. Truck Loading Position

Fig. 5-2. Histogram of Static Flexural Stress

(a)

Fig. 5-2. Histogram of Static Flexural Stress

(b)

Span Length L = 22.86m

Frequency

Stress (ksi)

Frequency

(c)
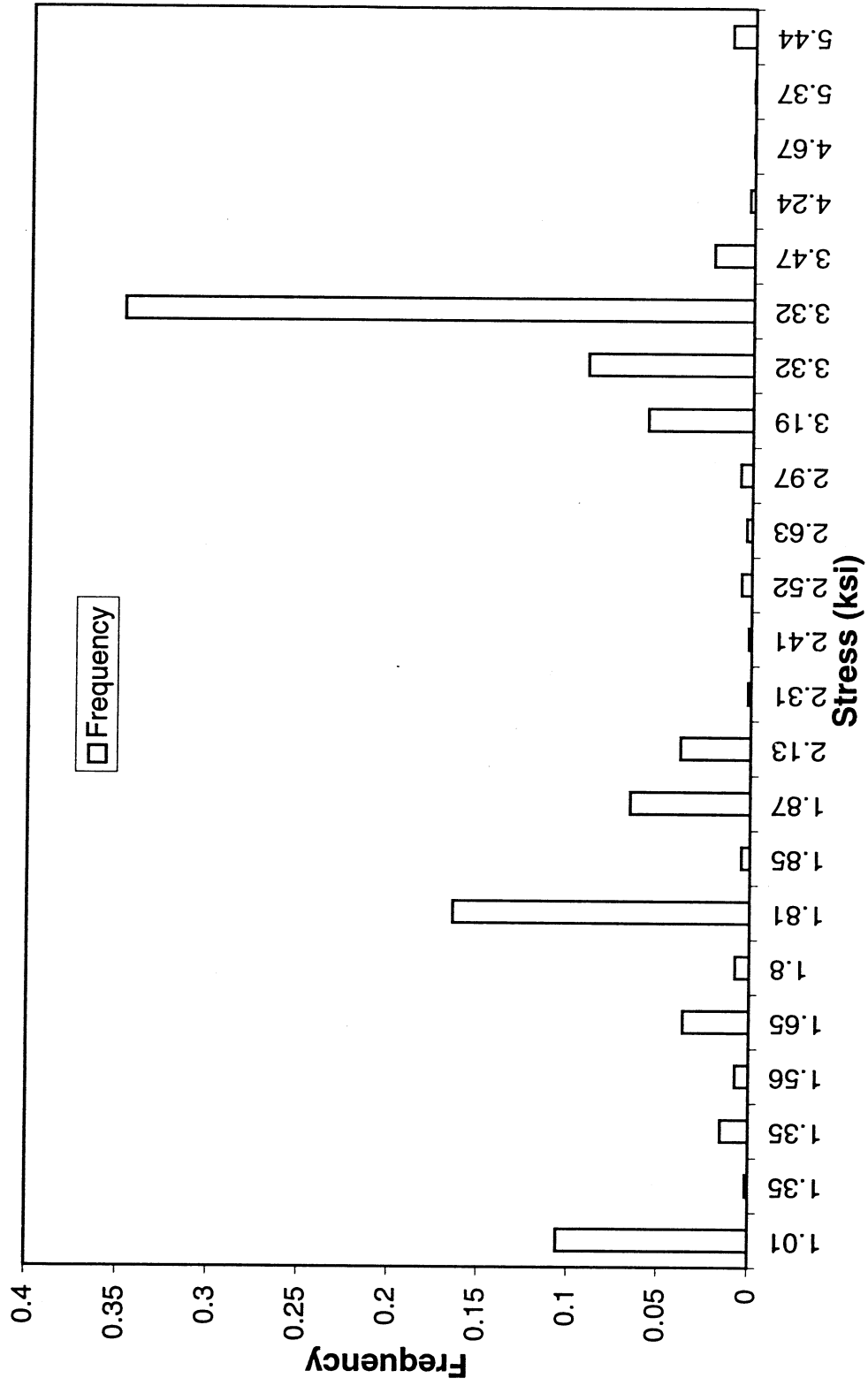
Fig. 5-2. Histogram of Static Flexural Stress

Span Length L = 30.48m
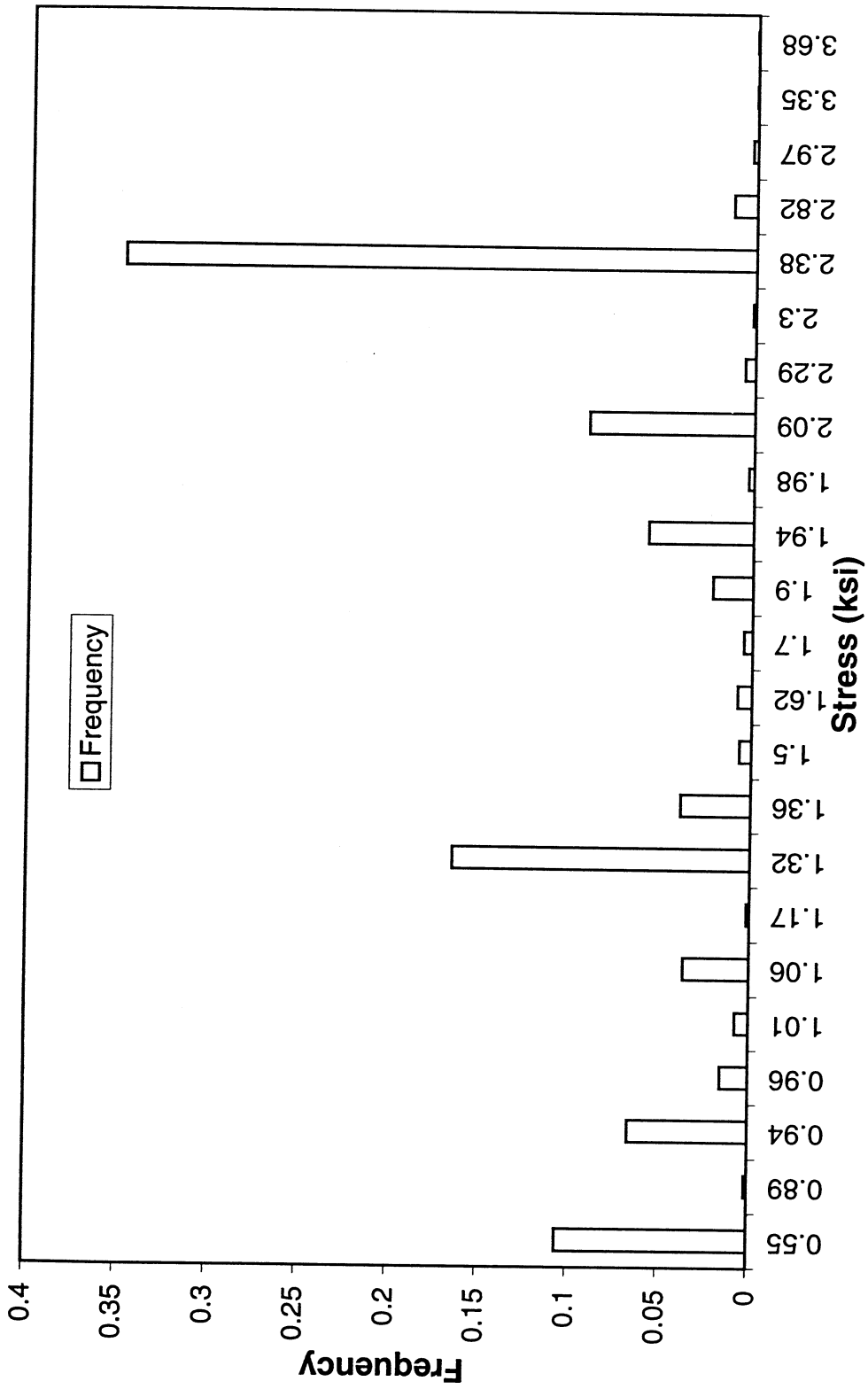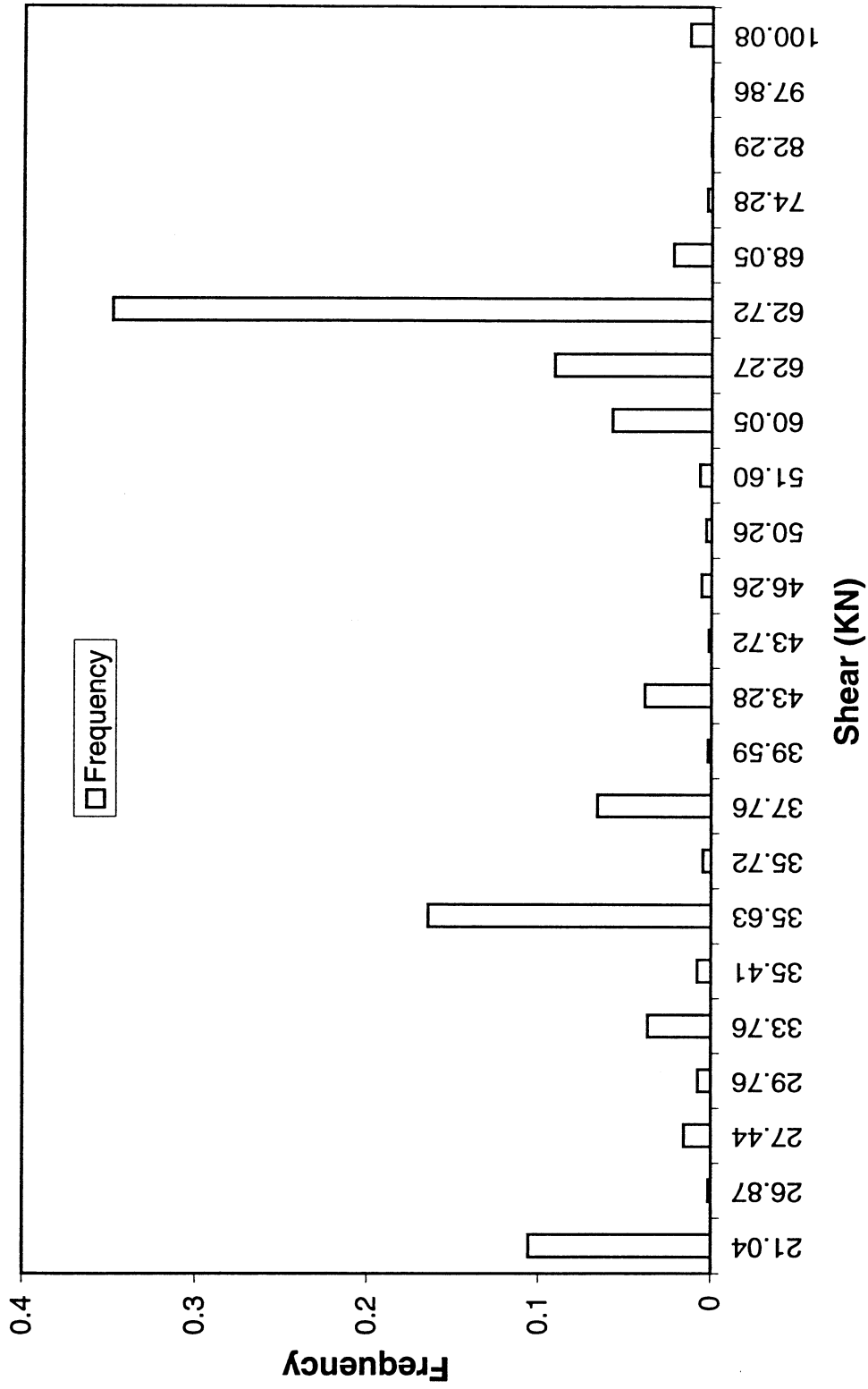
Fig. 5-2. Histogram of Static Flexural Stress

(d)

Span Length L = 36.58m

Fig. 5-2. Histogram of Static Flexural Stress

(e)

Fig. 5-2. Histogram of Static Flexural Stress

(f)

Fig. 5-3. Histogram of Static Shears

(a)

Span = 16.76m

Fig. 5-3. Histogram of Static Shears

(b)

Span = 22.86m

Fig. 5-3. Histogram of Static Shears

(c)
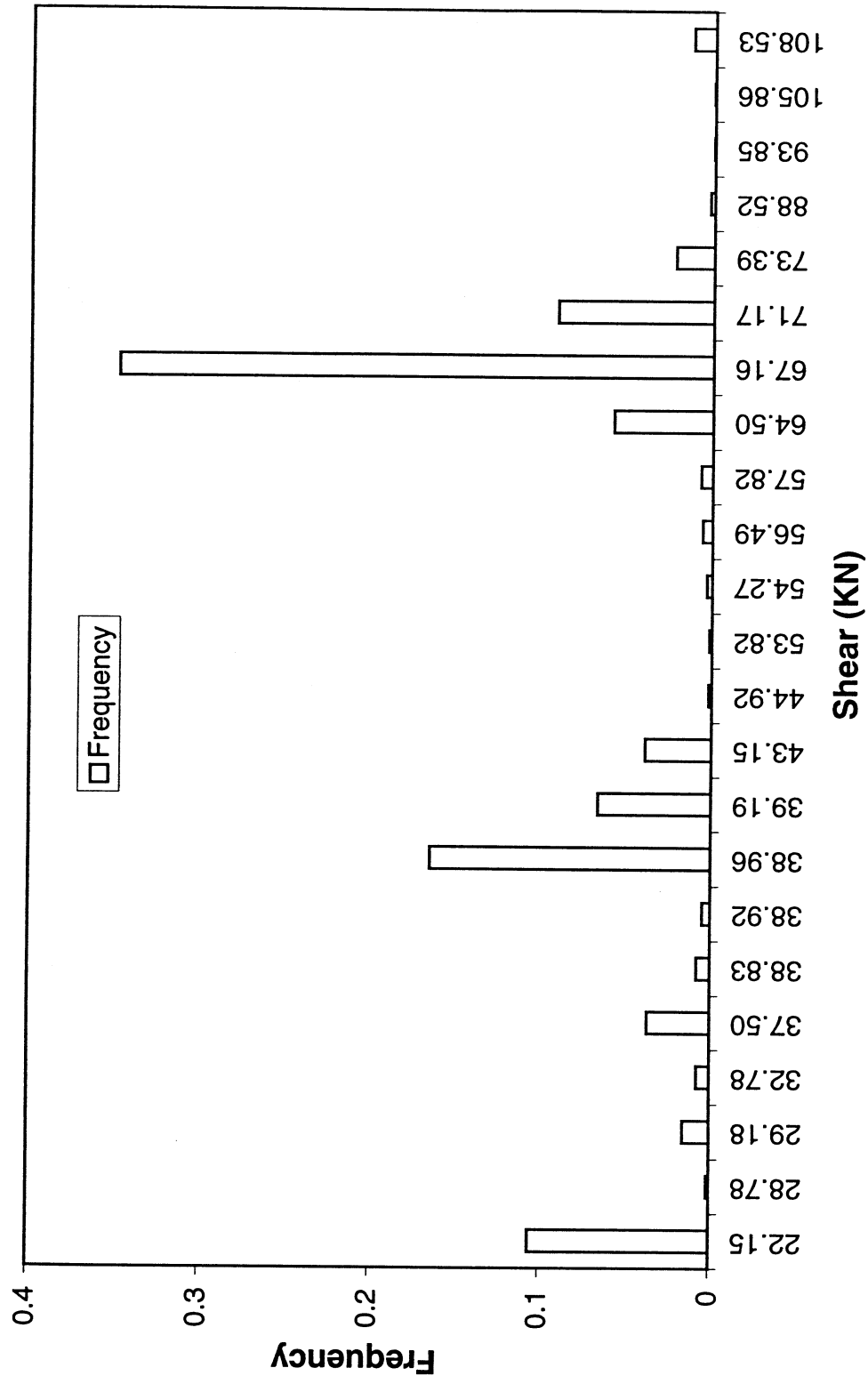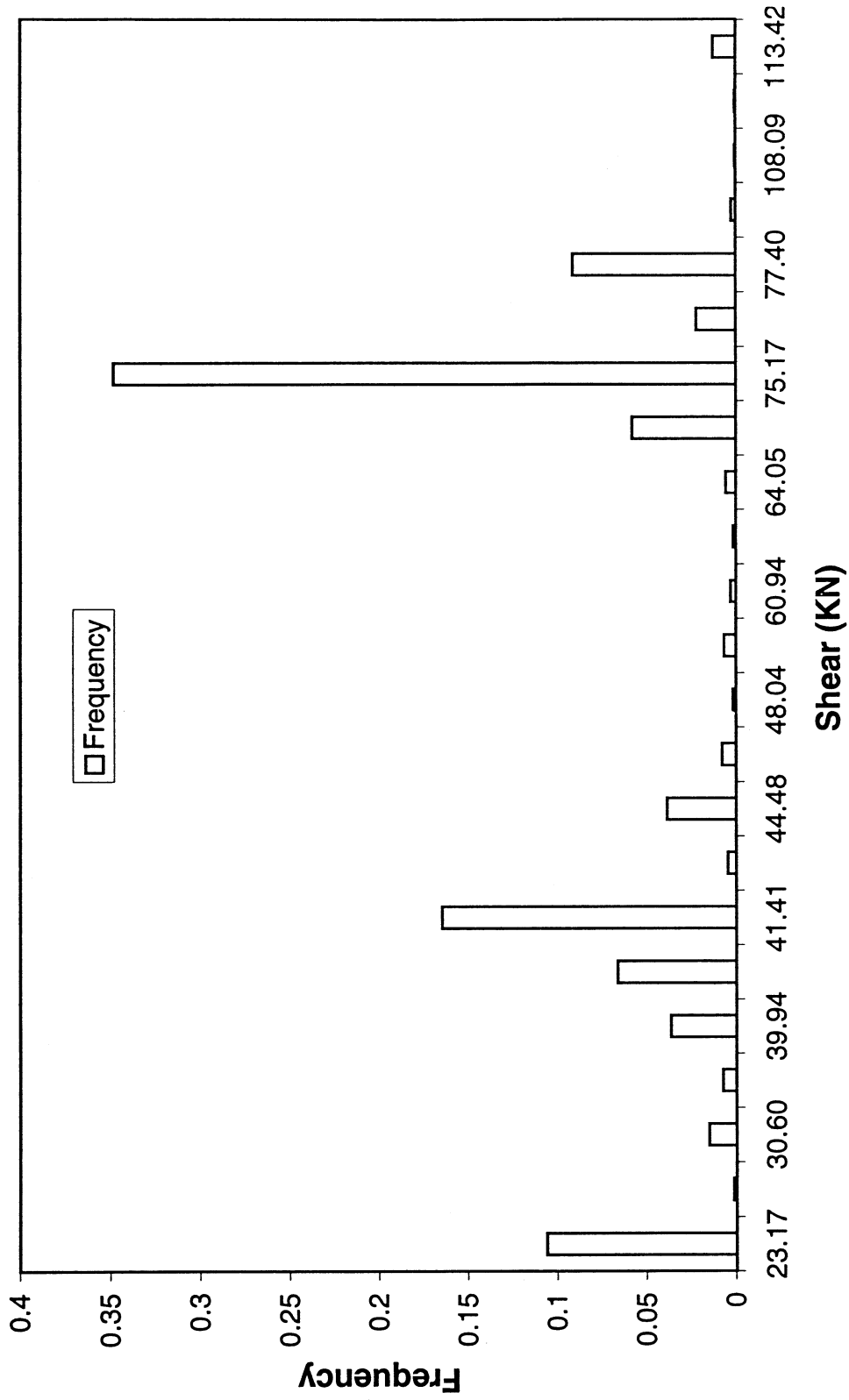
Span = 30.48m

Fig. 5-3. Histogram of Static Shears
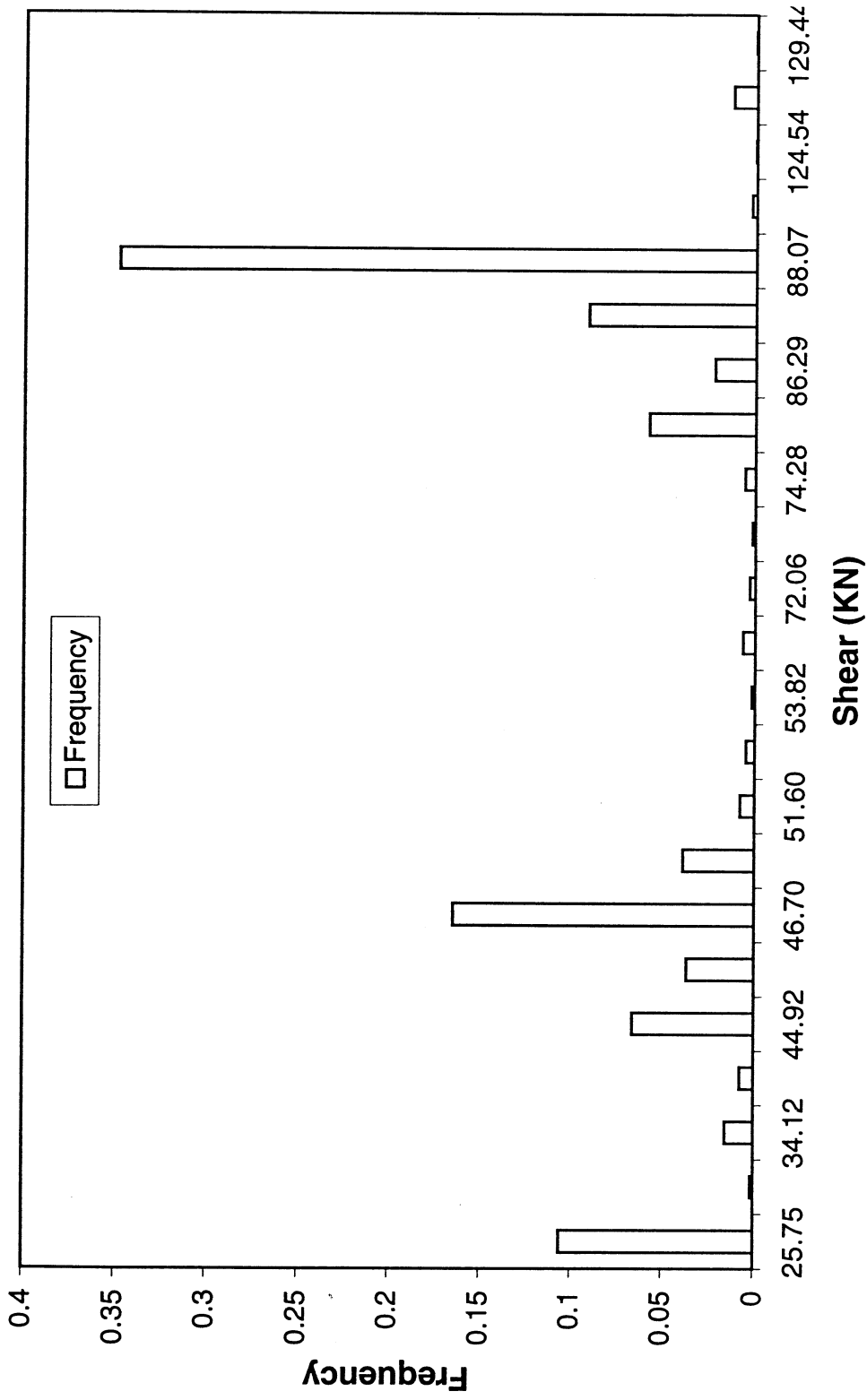
(d)

Fig. 5-3. Histogram of Static Shears
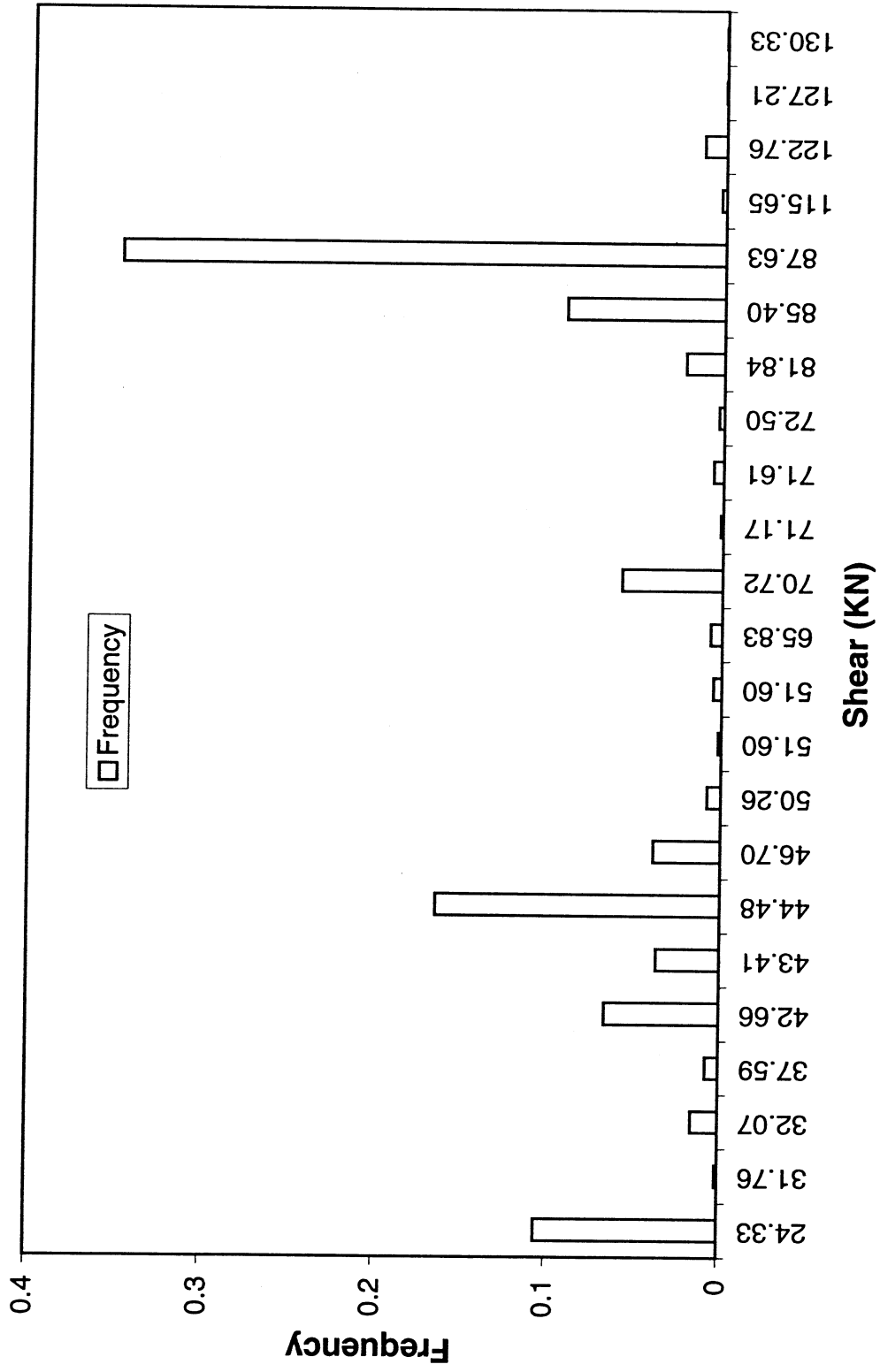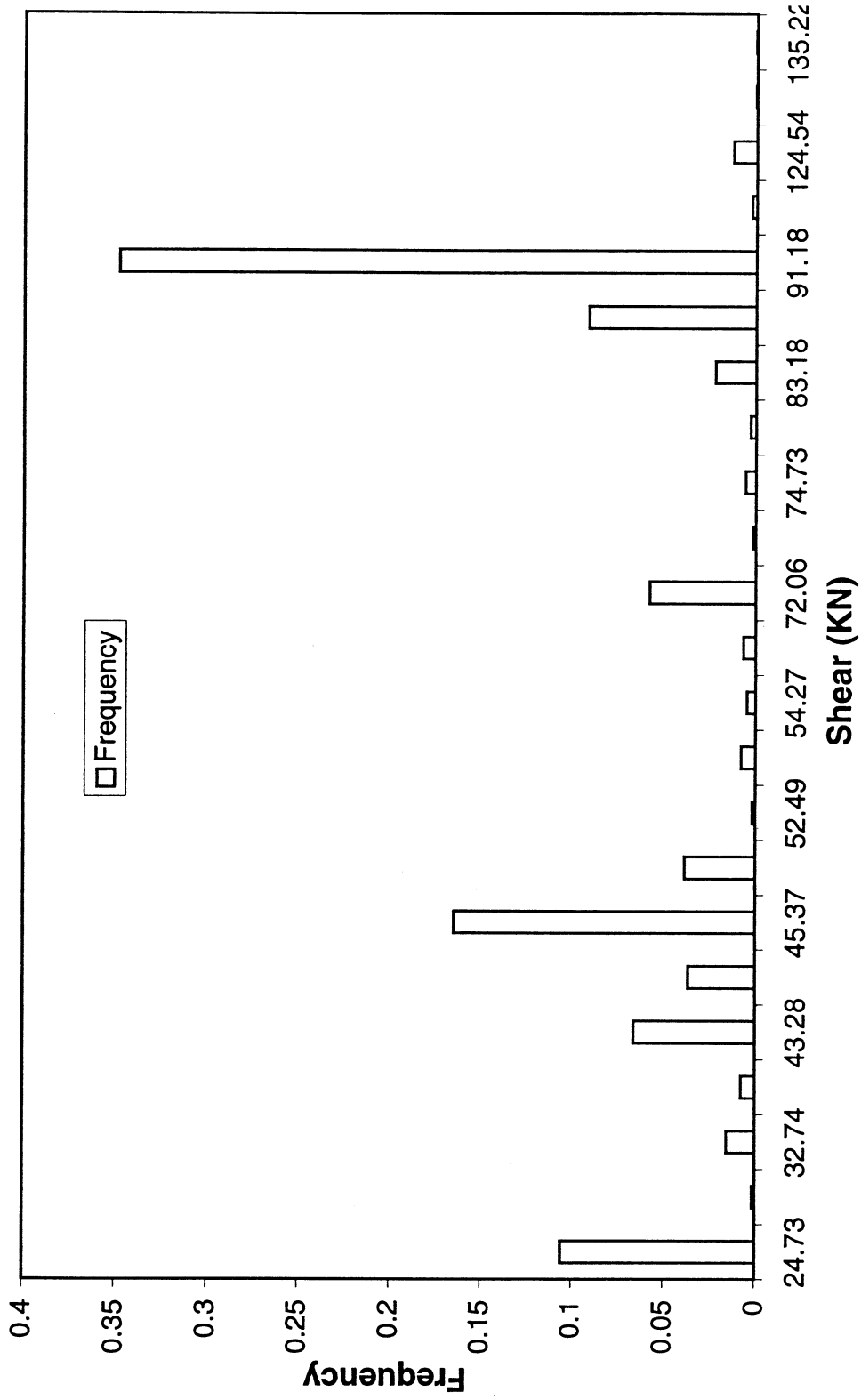
(e)

Span = 42.67m

Fig. 5-3. Histogram of Static Shears

(f)

91

Fig. 5-4. CDF of Static Flexural Stress and Shear

(a)

Fig. 5-4. CDF of Static Flexural Stress and Shear
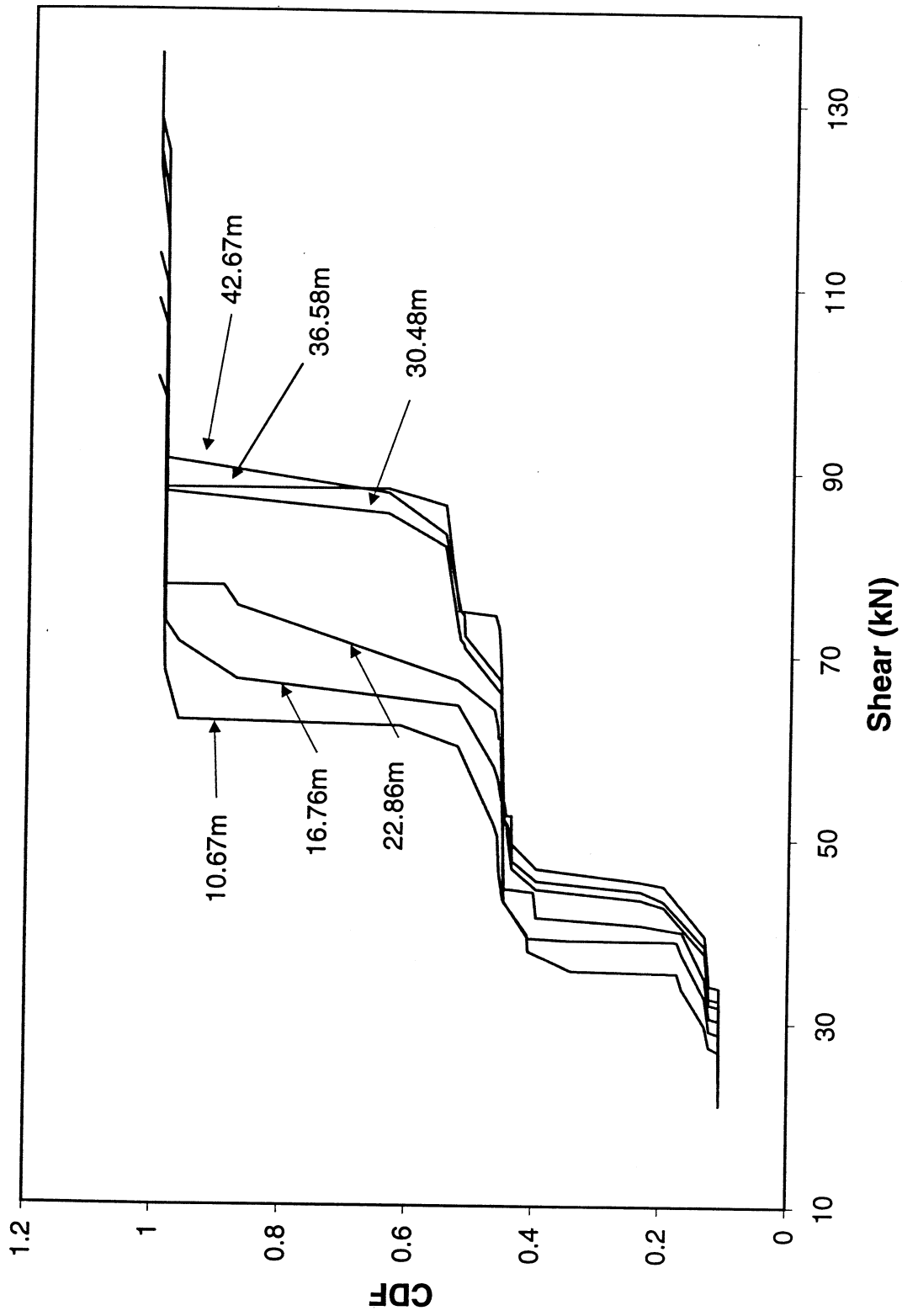
(b)

Fig. 5-5. Static Moment and Shear due to Moving Loaded Type 9
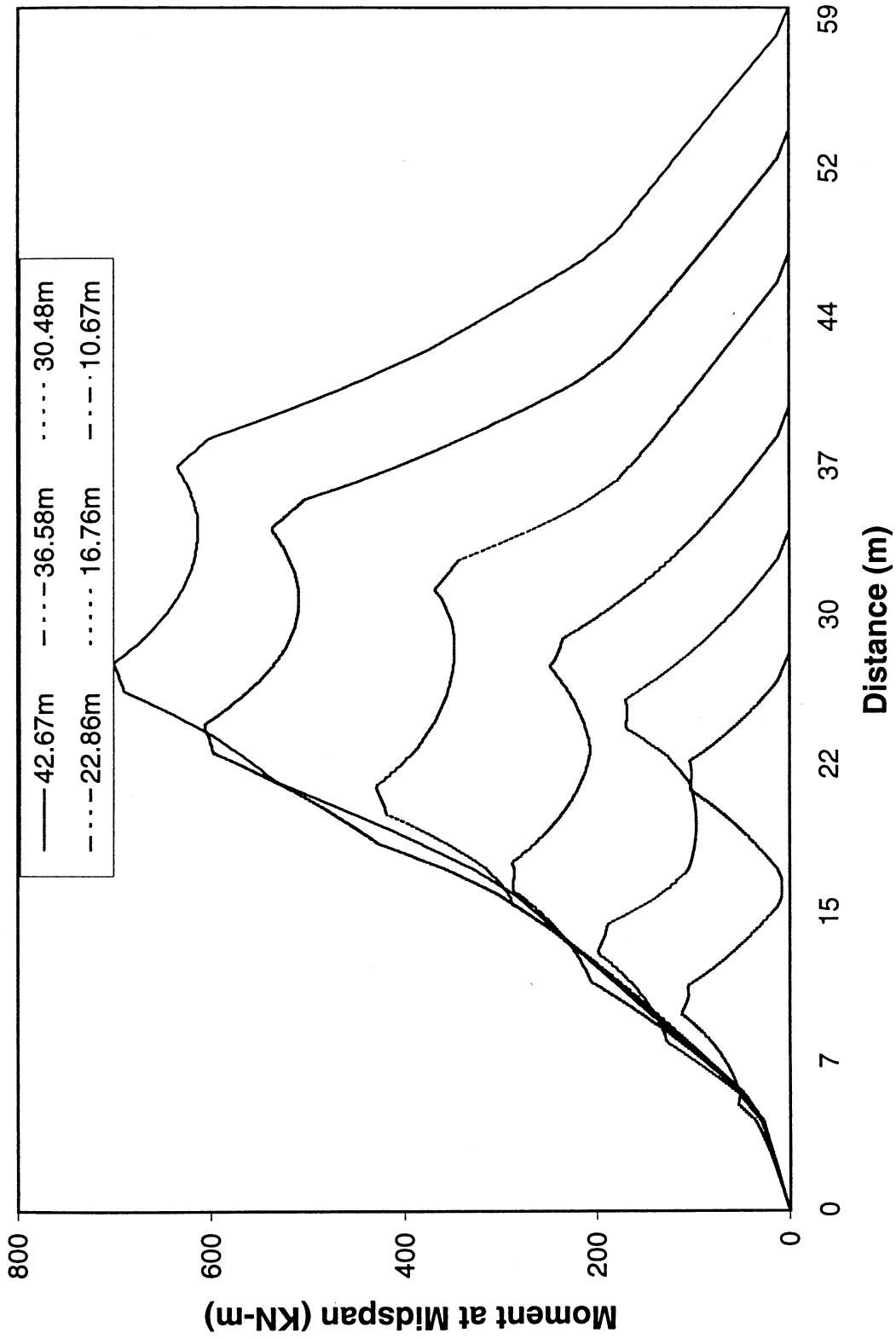
(a)

Legend:
— 42.67m   —·— 36.58m   ······ 30.48m
—··— 22.86m   ········ 16.76m   —·—· 10.67m

Y-axis: Moment at Midspan (KN-m)
X-axis: Distance (m)

Fig. 5-5. Static Moment and Shear due to Moving Loaded Type 9

(b)
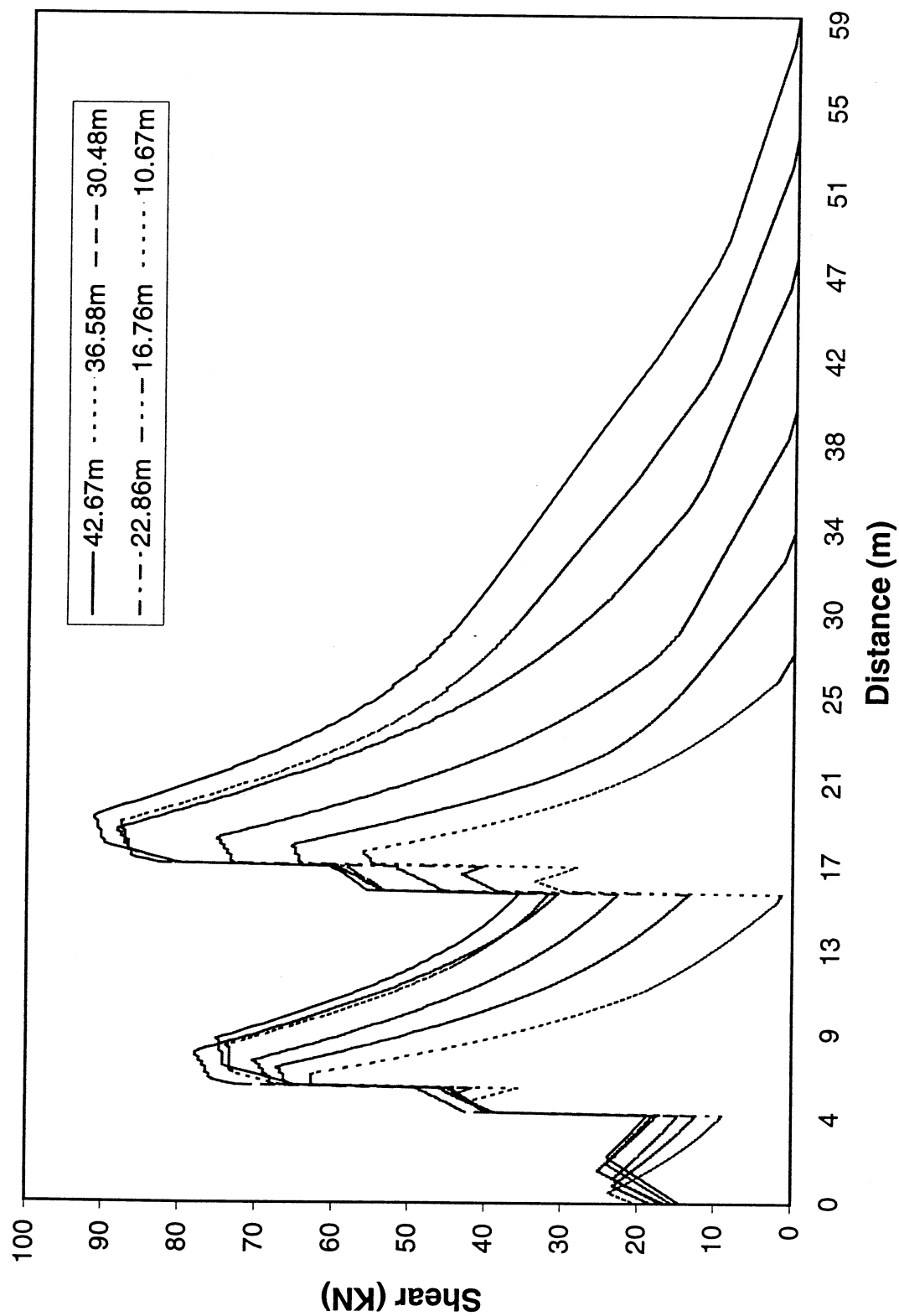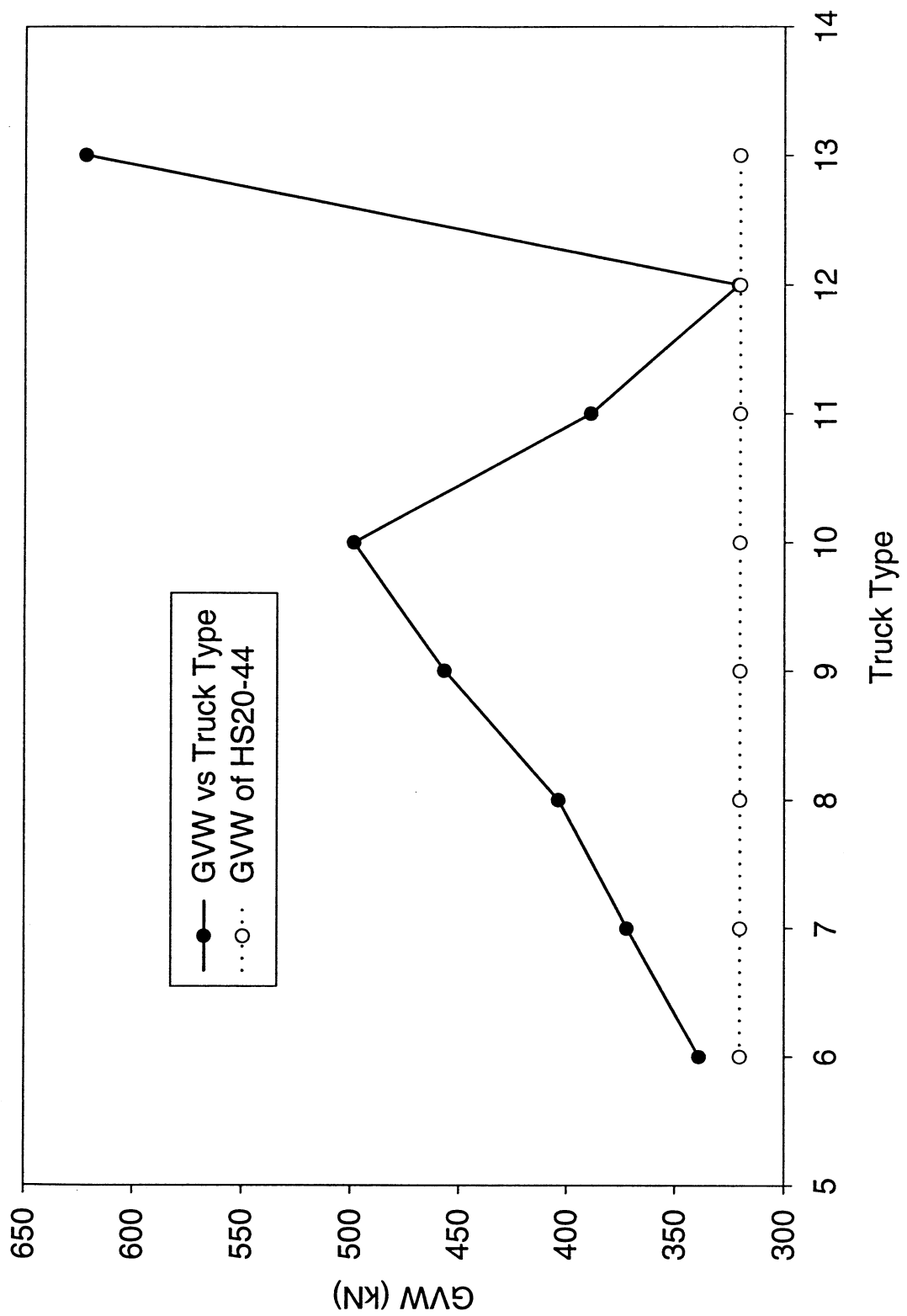
Fig. 5-6. The Heaviest GVW in Each Truck Type
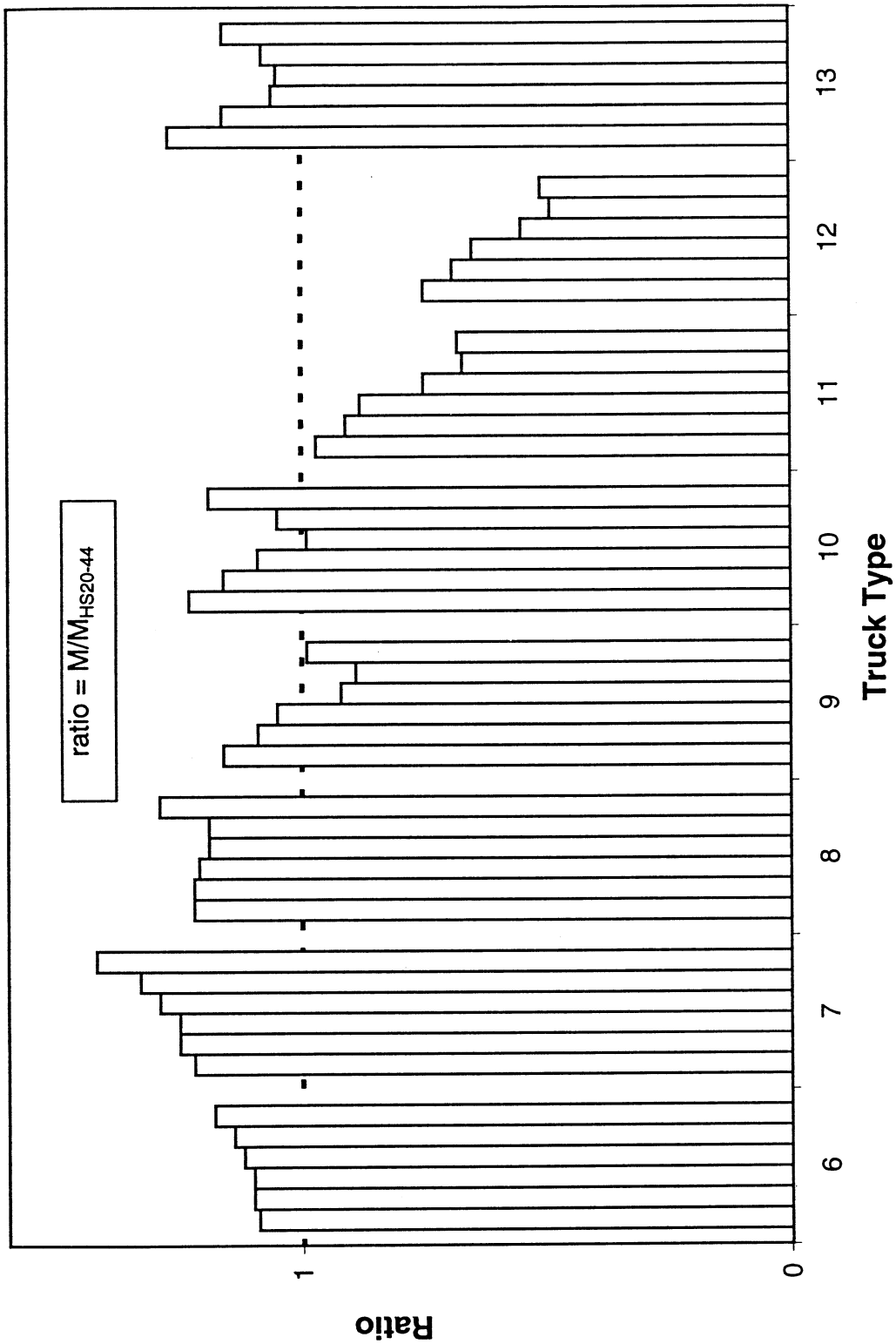
Note: Columns in each truck type denote the longest to the shortest span length.

(a) Moment

Fig. 5-7. Comparisons of Effects between the Heaviest Trucks and HS20-44

97
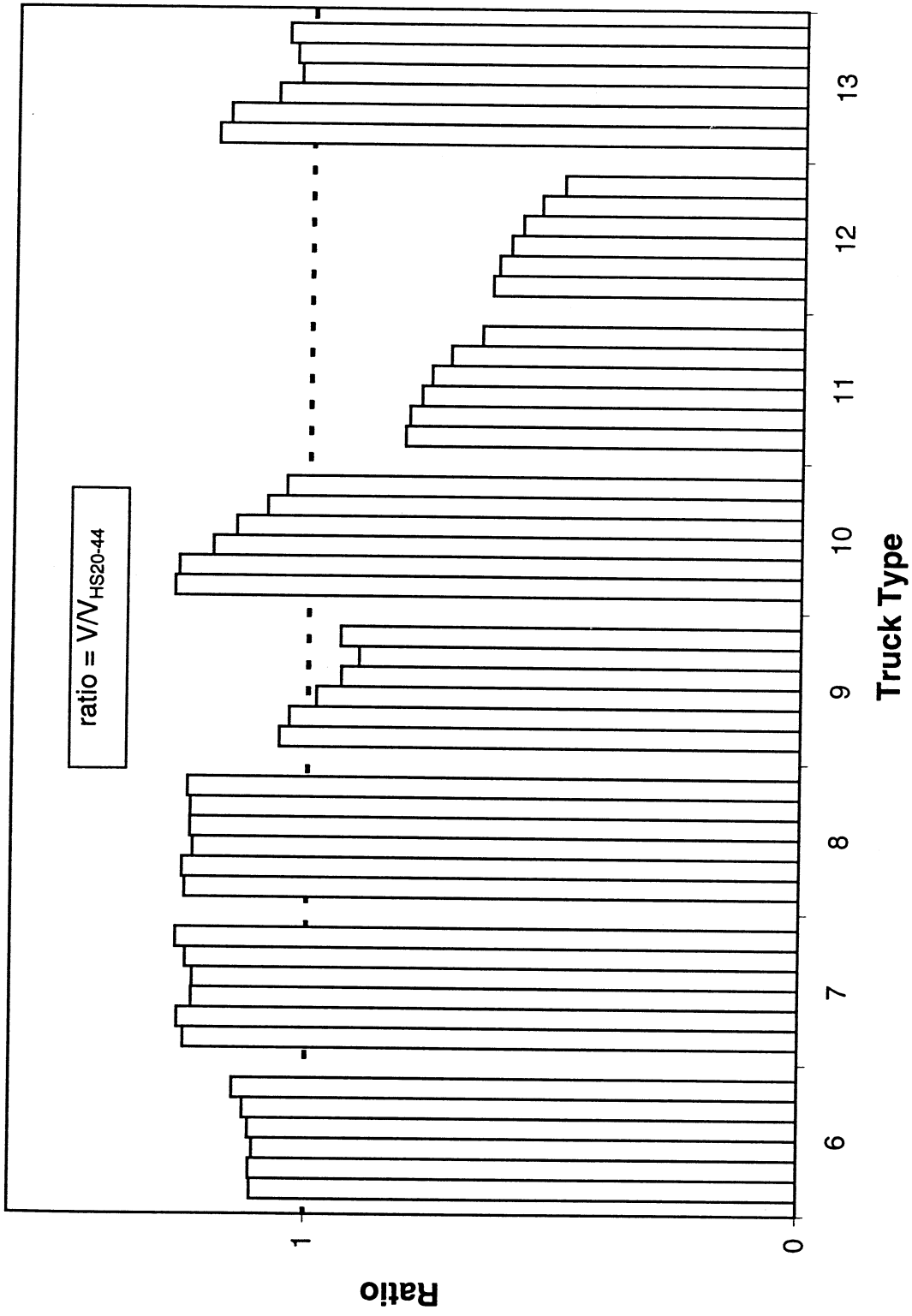
Note: Columns in each truck type denote the longest to the shortest span length.

(b) Shear

Fig. 5-7. Comparisons of Effects between the Heaviest Trucks and HS20-44
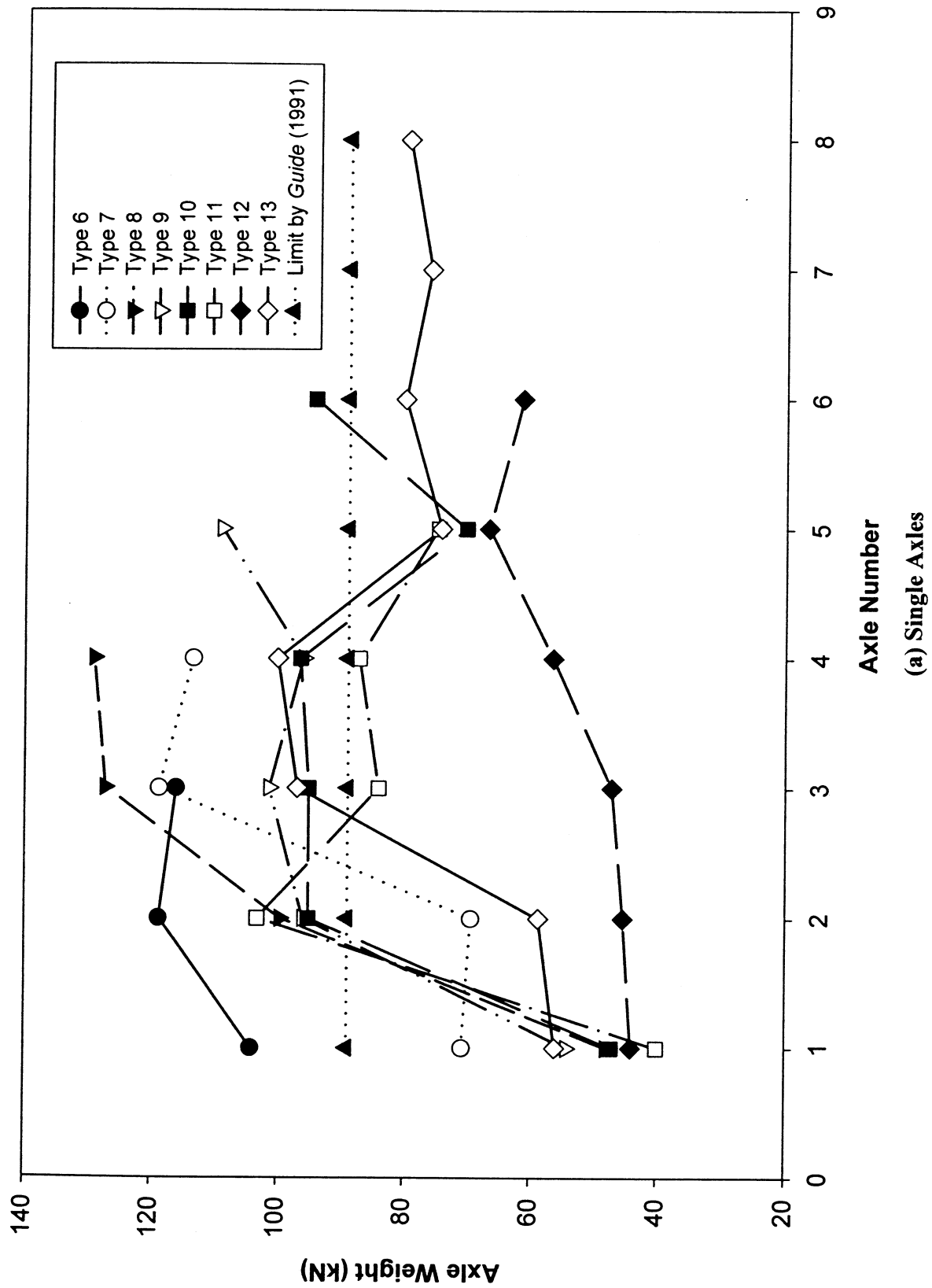
Fig. 5-8. Axle Weight of Various Truck Types

(a) Single Axles
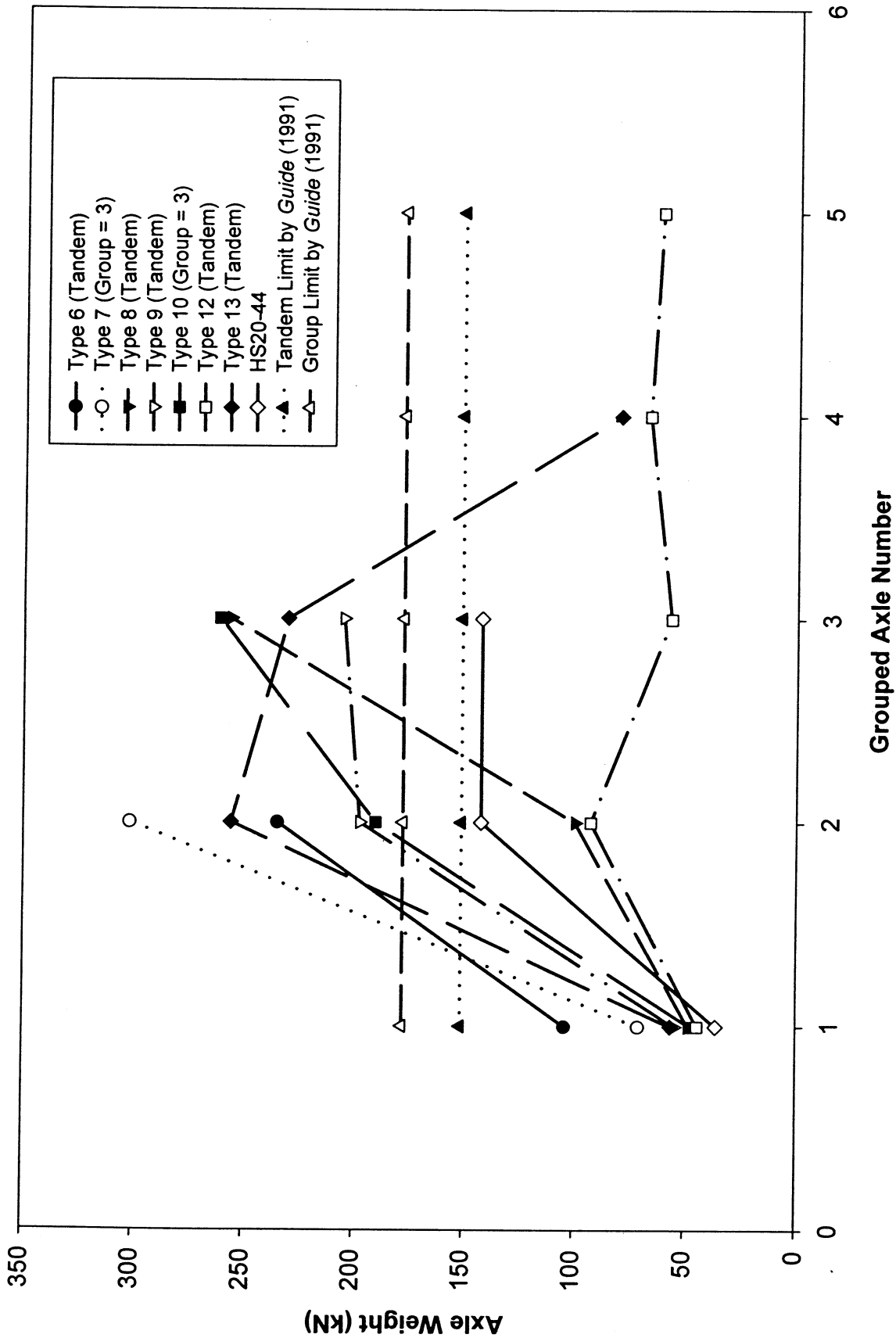
(b) Single, Tandem, and Group Axles

Fig. 5-8. Axle Weight of Various Truck Types

Note: Type 7 truck has a 3-axle group at axle number 2, while Type 10 truck has a 3-axle group at axle number 3.
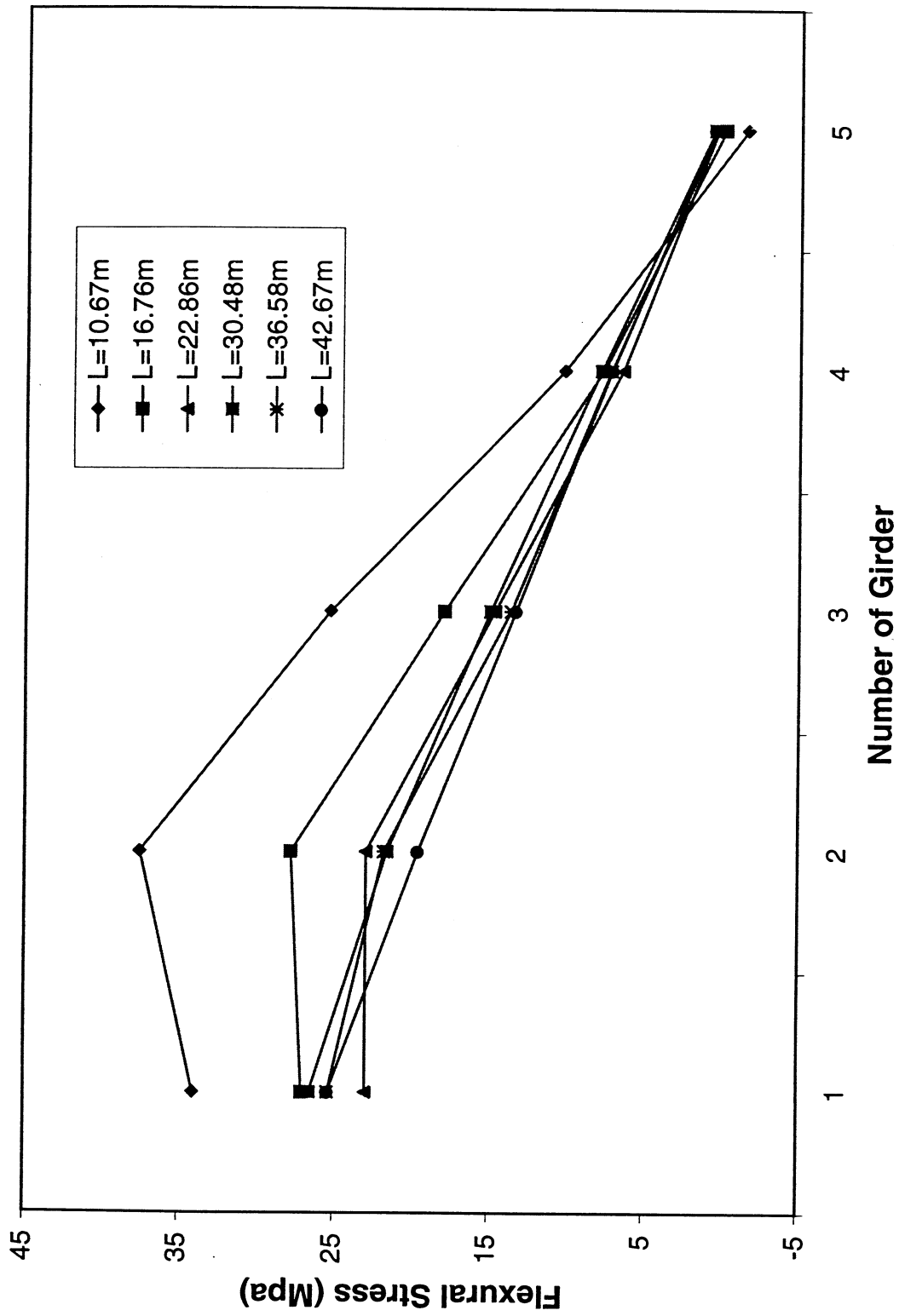
Fig. 5-9. Lateral Distribution of Maximum Flexural Stress and Shear

(a)

Number of Girder

Flexural Stress (Mpa)

L=10.67m
L=16.76m
L=22.86m
L=30.48m
L=36.58m
L=42.67m

Fig. 5-9. Lateral Distribution of Maximum Flexural Stress and Shear

(b)
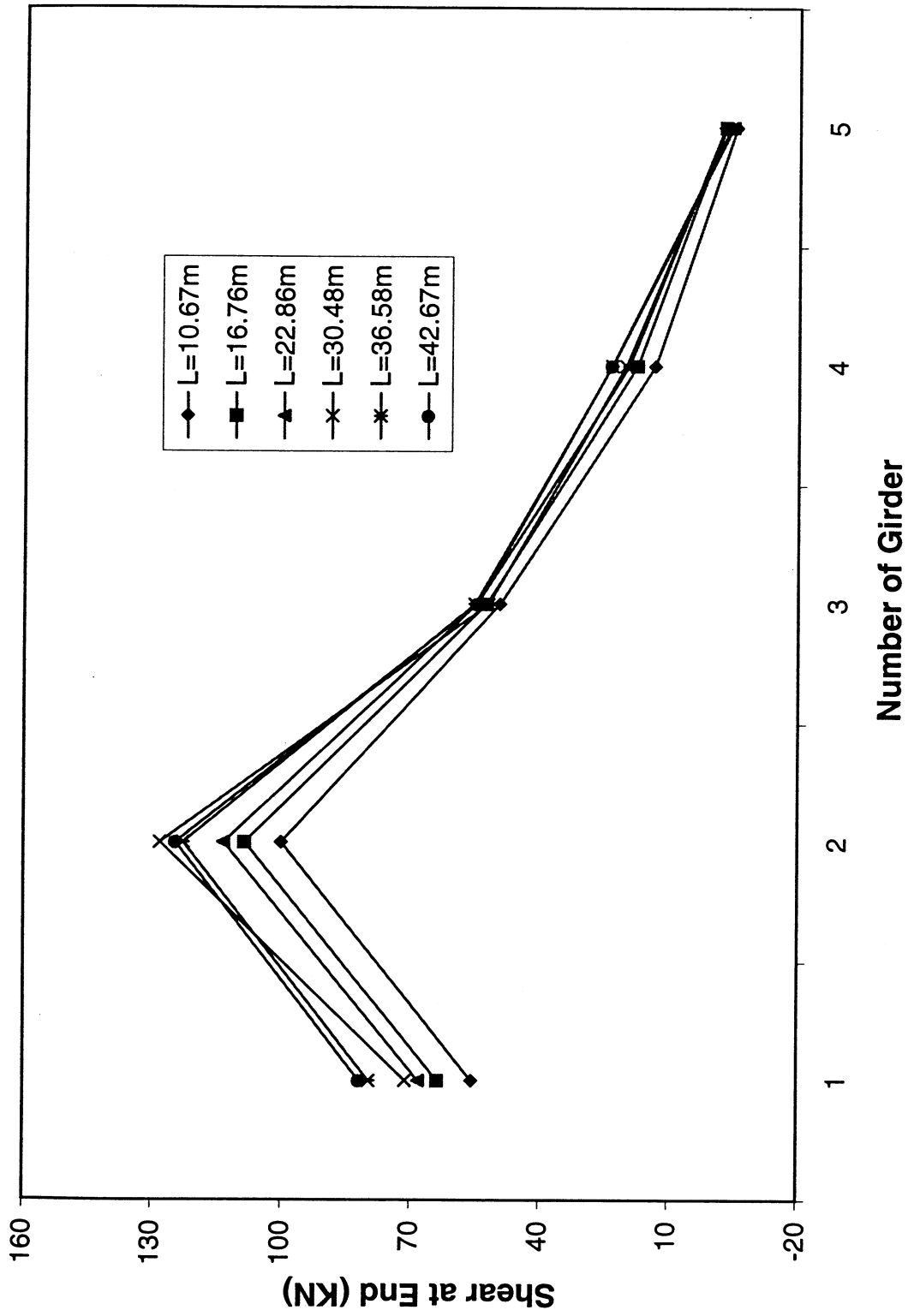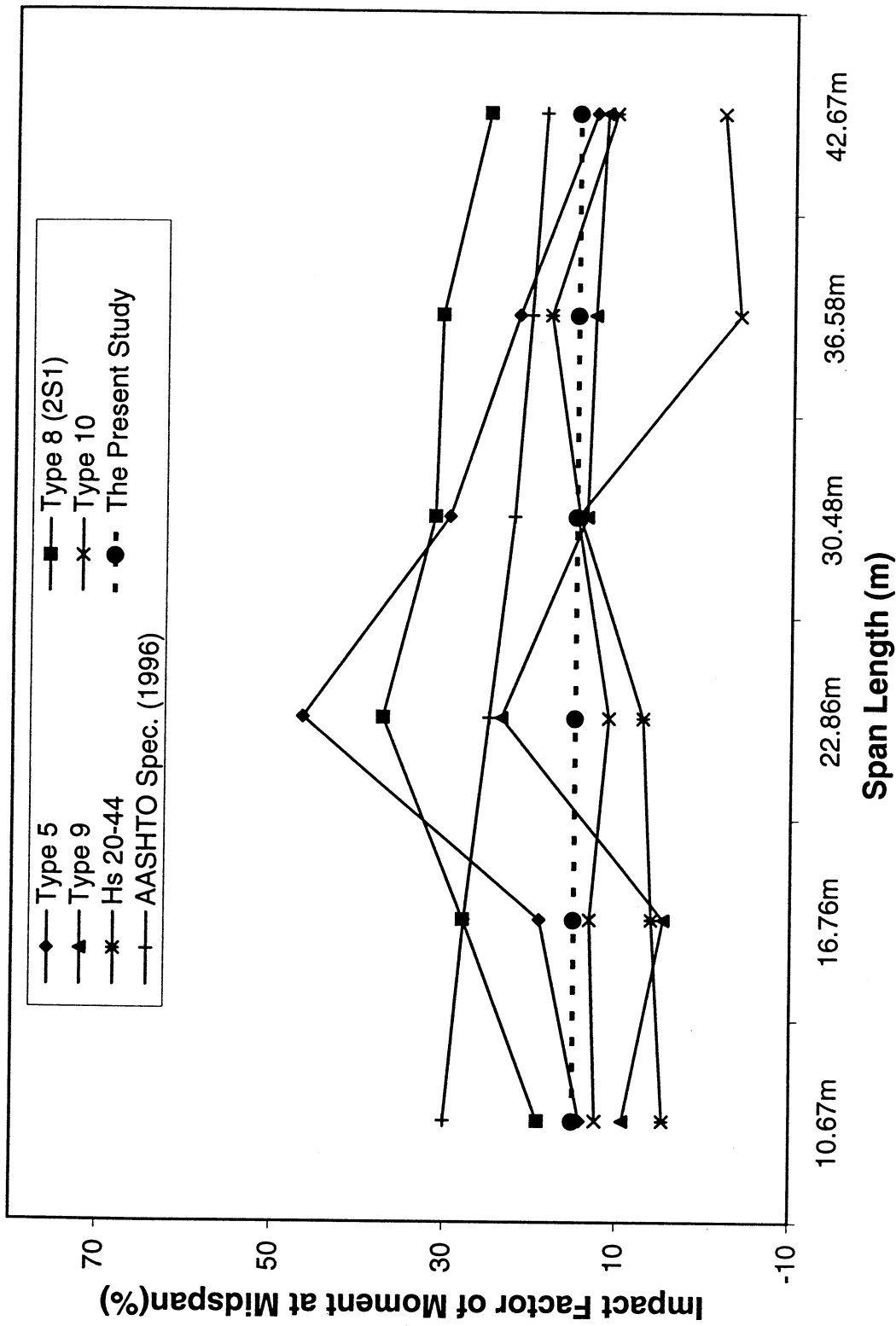
(a) Loaded Truck

Fig. 5-10. Dynamic Impact Factors vs Span Length

103
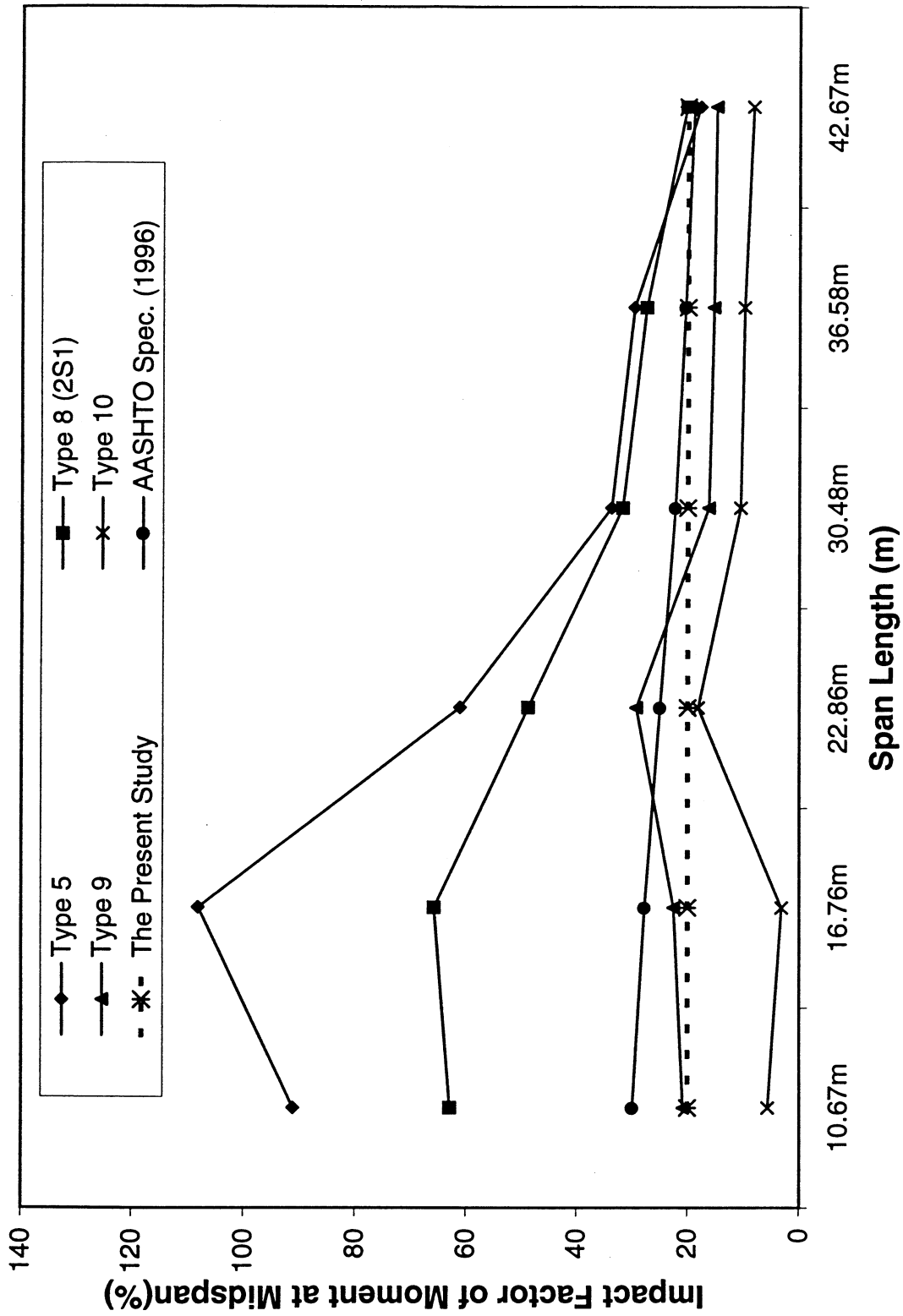
(b) Empty Truck

Fig. 5-10. Dynamic Impact Factors vs Span Length

(c) Loaded Truck

Fig. 5-10. Dynamic Impact Factors vs Span Length

105
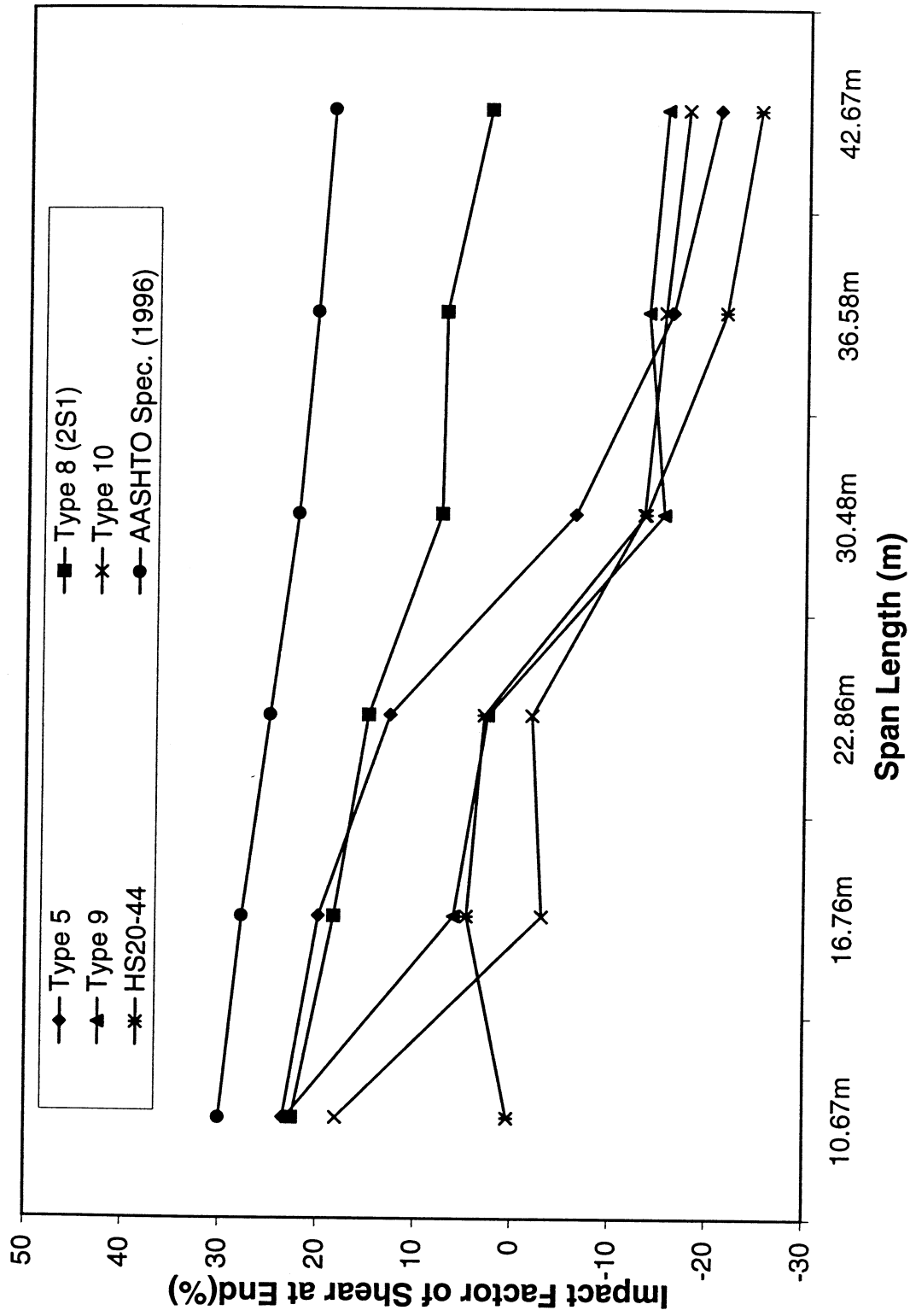
Fig. 5-10. Dynamic Impact Factors vs Span Length

(d) Empty Truck

Y-axis: Impact Factor of Shear at End(%)

X-axis: Span Length (m)

Legend:
- Type 5
- Type 9
- AASHTO Spec. (1996)
- Type 8 (2S1)
- Type 10

Fig. 5-11. Distribution of Moment at Midspan Section

(a) Static

DYNAMIC MOMENT

Legend:
- L = 9.14m
- L = 18.29m
- L = 30.48m
- L = 42.67m

Moment (KN-m) vs Number of Girder

(b)
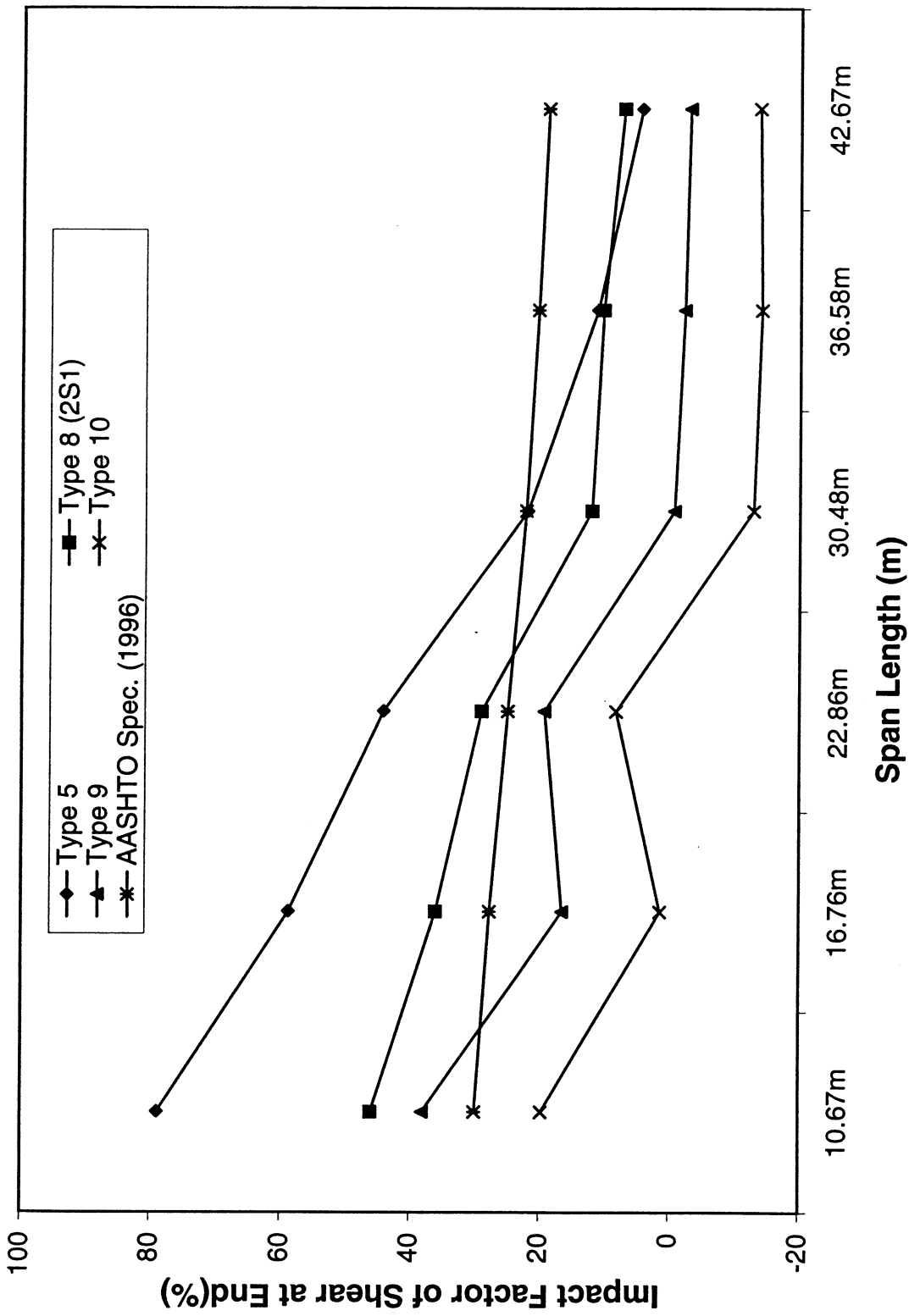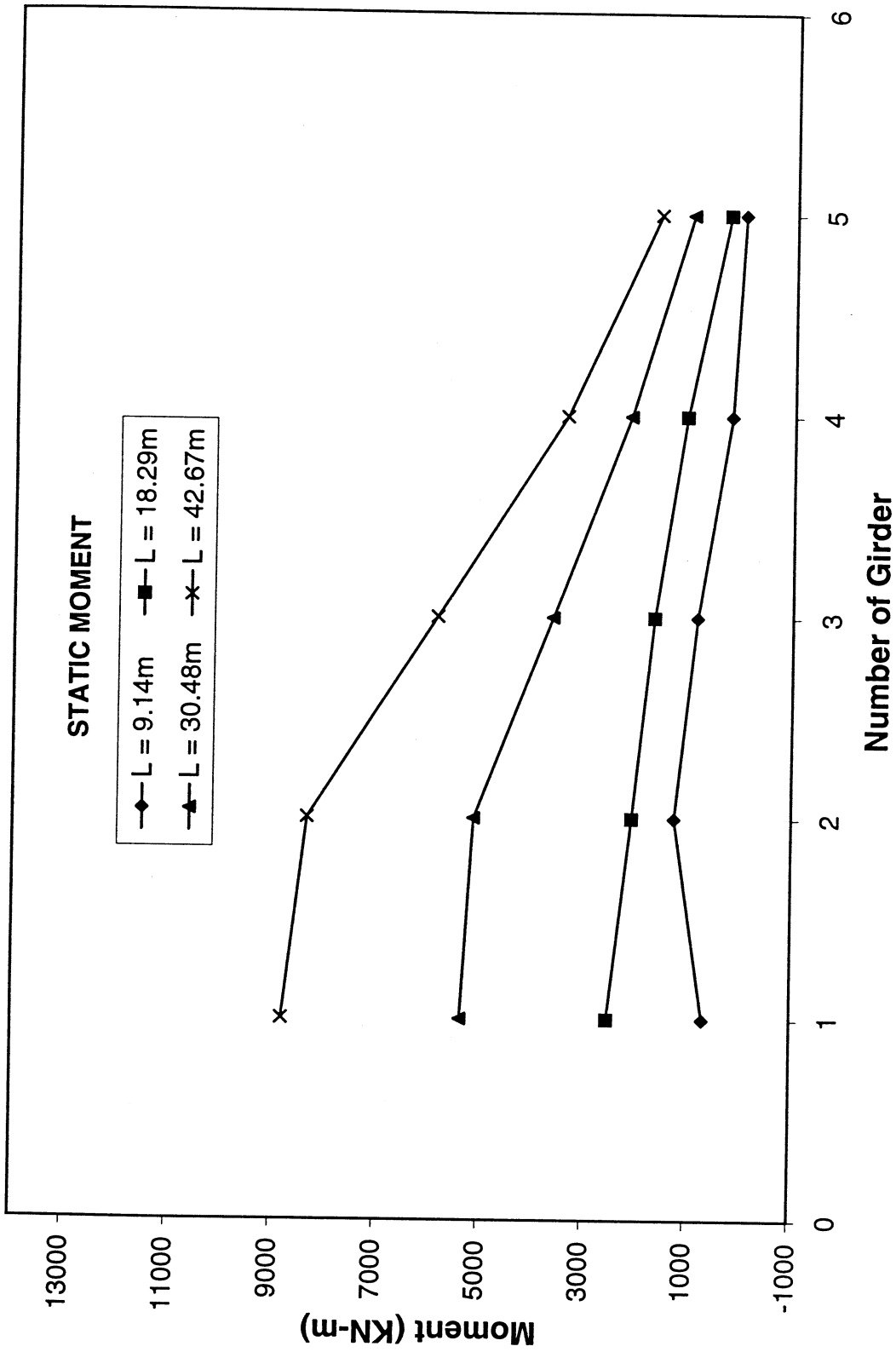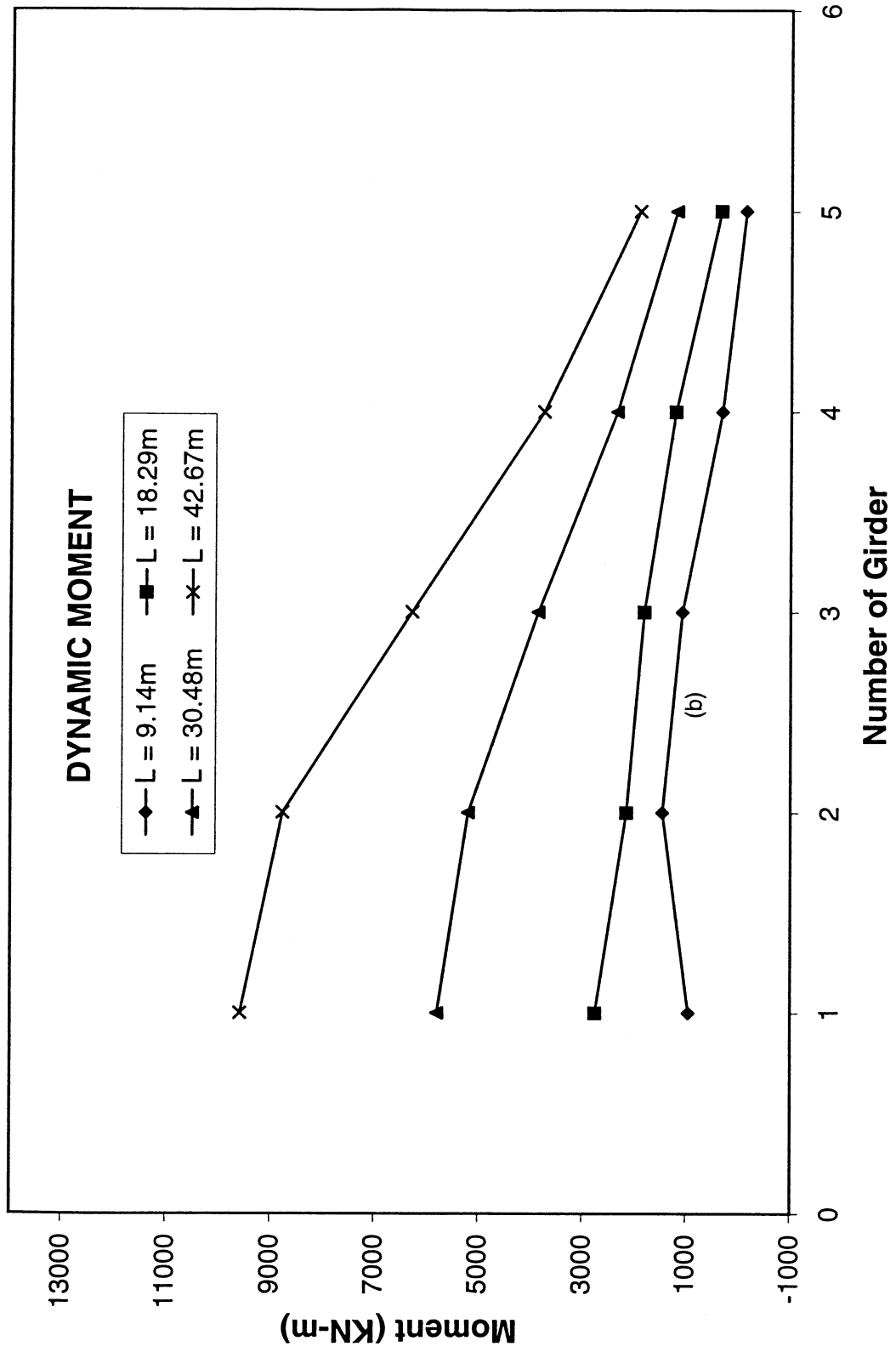
(b) Dynamic

Fig. 5-11. Distribution of Moment at Midspan Section

Fig. 5-12. Dynamic Impact Factors vs Speed

109
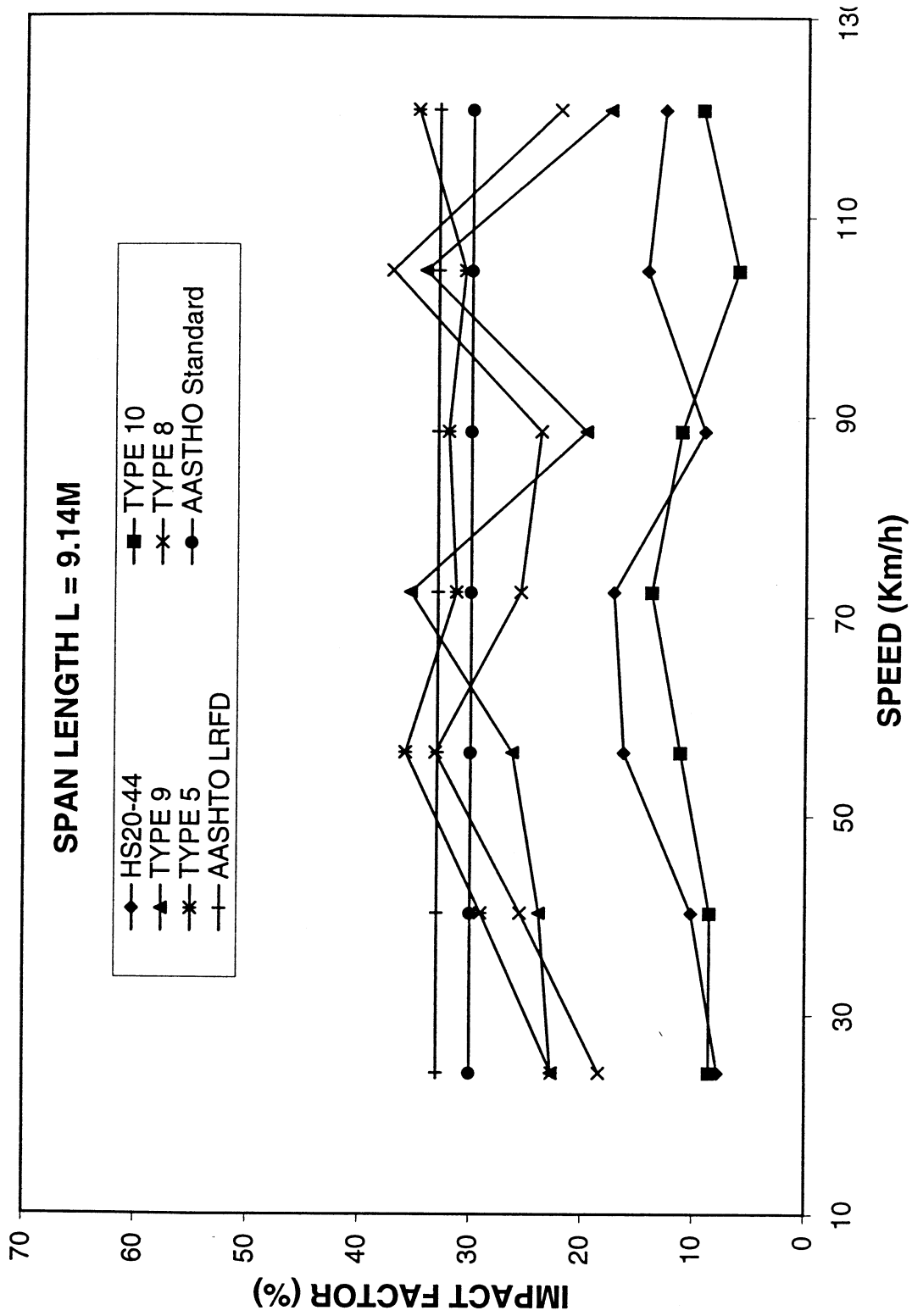
Fig. 5-12. Dynamic Impact Factors vs Speed

(b)

Fig. 5-12. Dynamic Impact Factors vs Speed

(c)

111
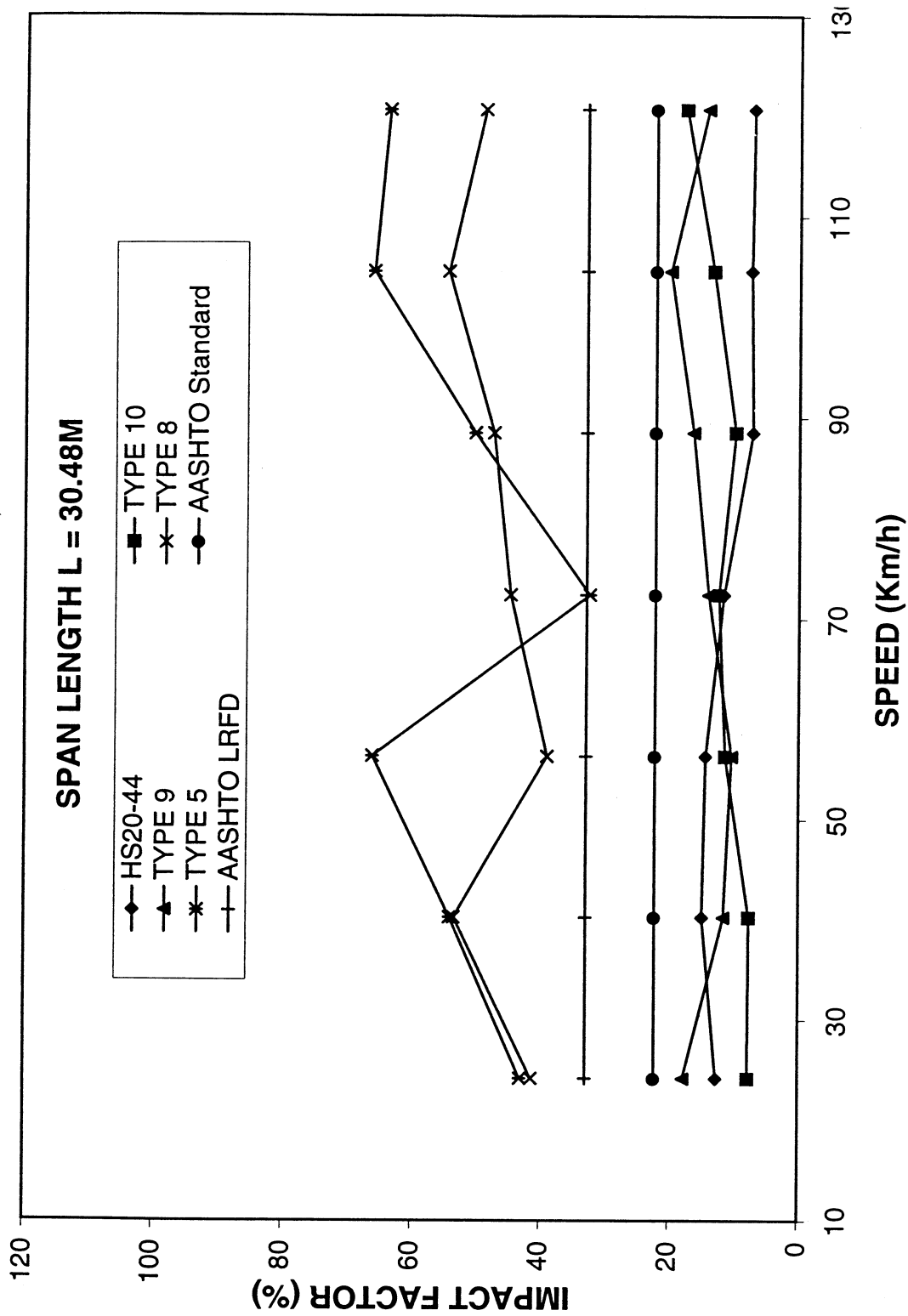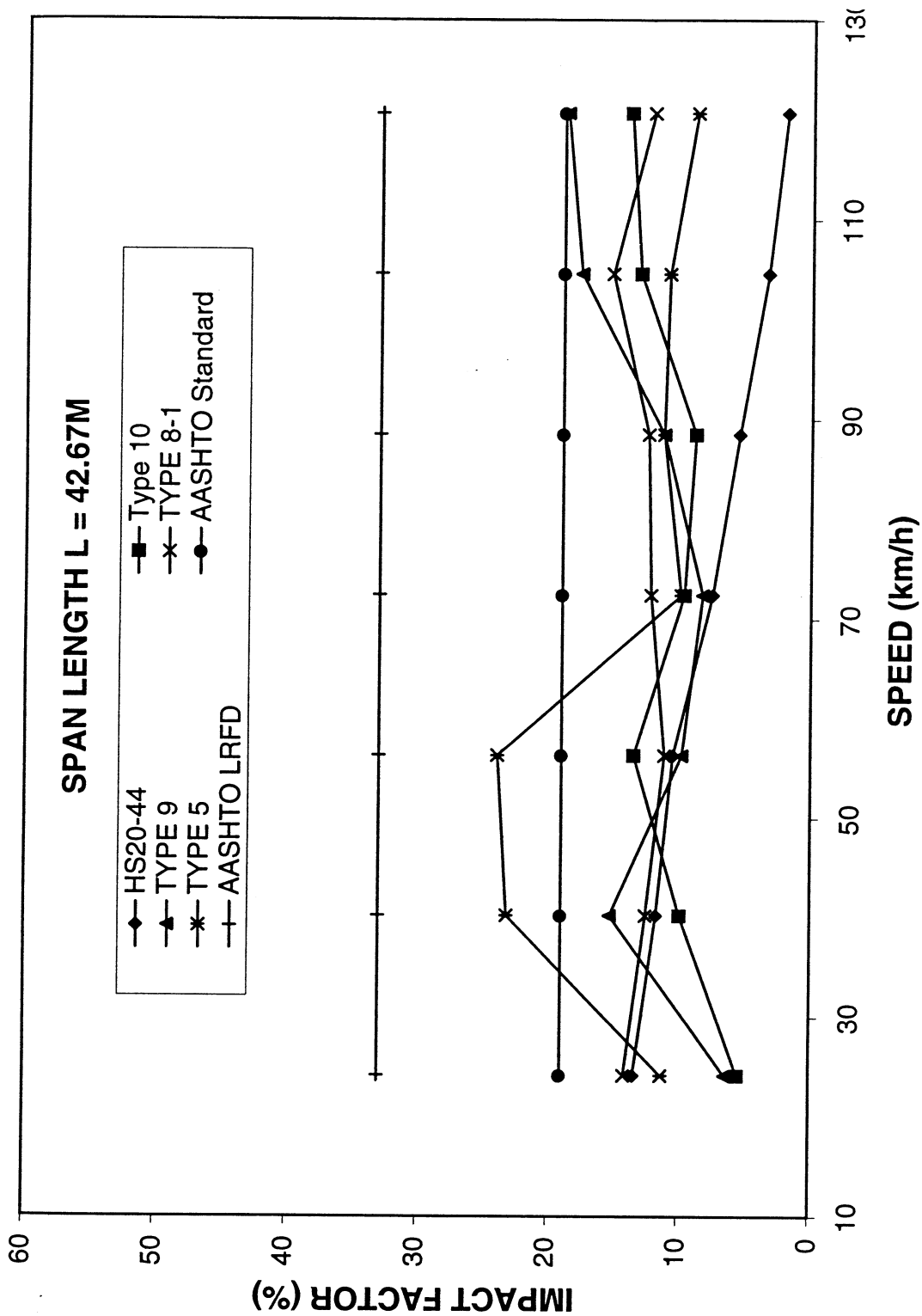
Fig. 5-12. Dynamic Impact Factors vs Speed
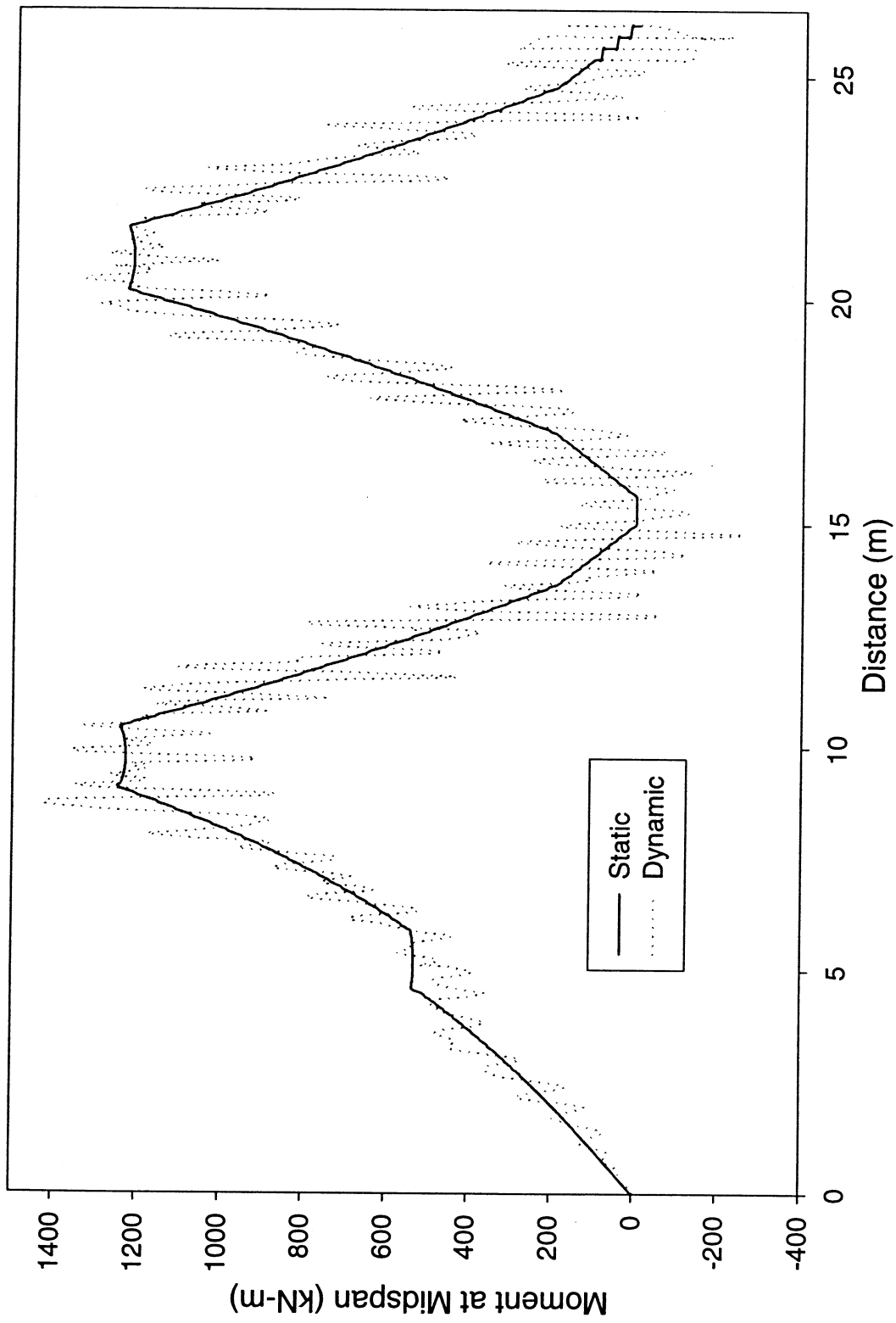
Fig. 5-13. Dynamic History due to Loaded Type 9 (L = 9.14m)

The y-axis is labeled "Moment at Midspan (kN-m)" with values ranging from -400 to 1400. The x-axis is labeled "Distance (m)" with values from 0 to 25. The legend shows "Static" (solid line) and "Dynamic" (dotted line).

SPAN LENGTH = 30 FT

Fig. 5-14. Lateral Distribution under Various Truck Types

(a)

114
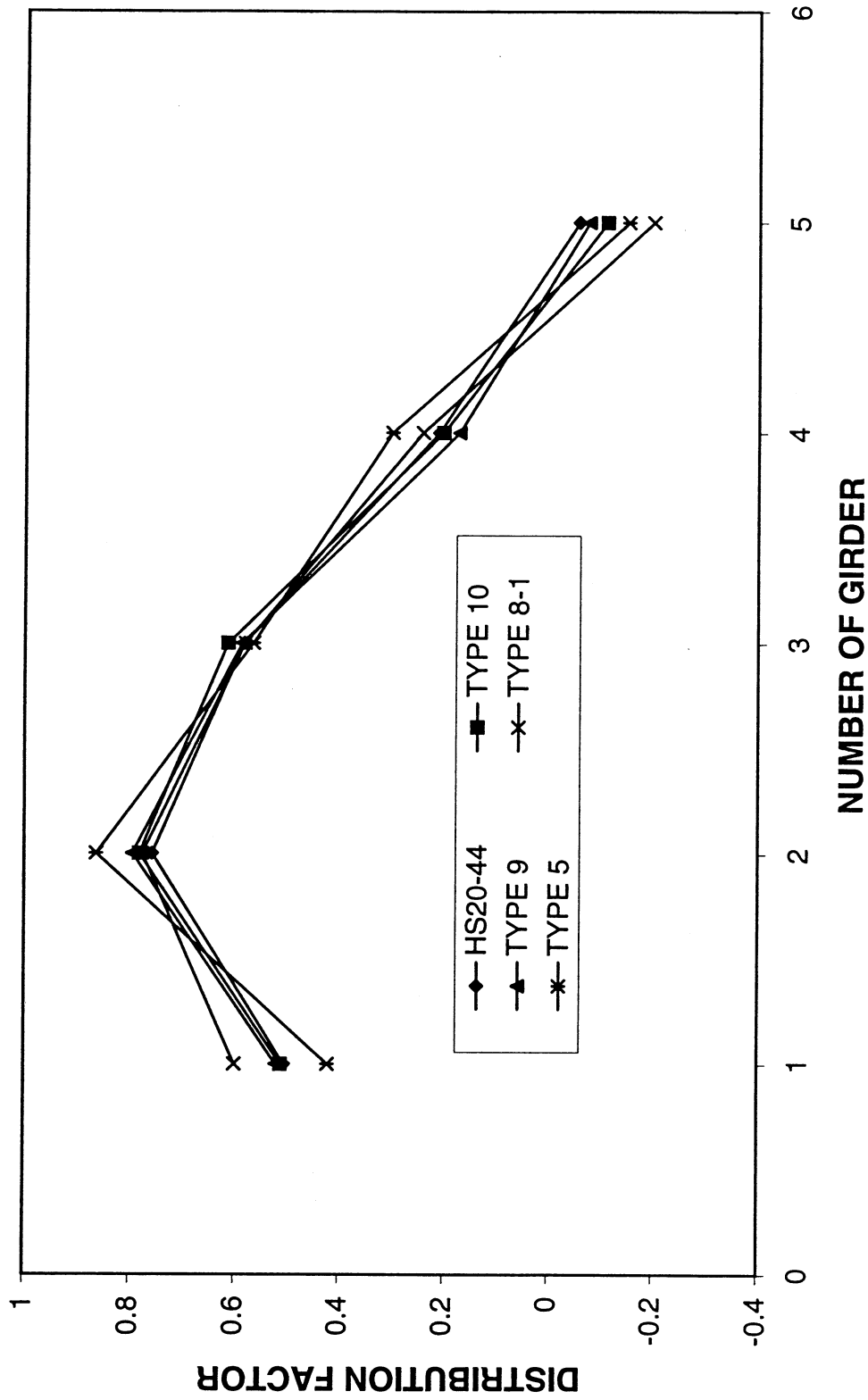
Fig. 5-14. Lateral Distribution under Various Truck Types

(b)

115

SPAN LENGTH = 100 FT

DISTRIBUTION FACTOR

NUMBER OF GIRDER

Legend:
- HS20-44
- TYPE 9
- TYPE 5
- TYPE 10
- TYPE 8-1
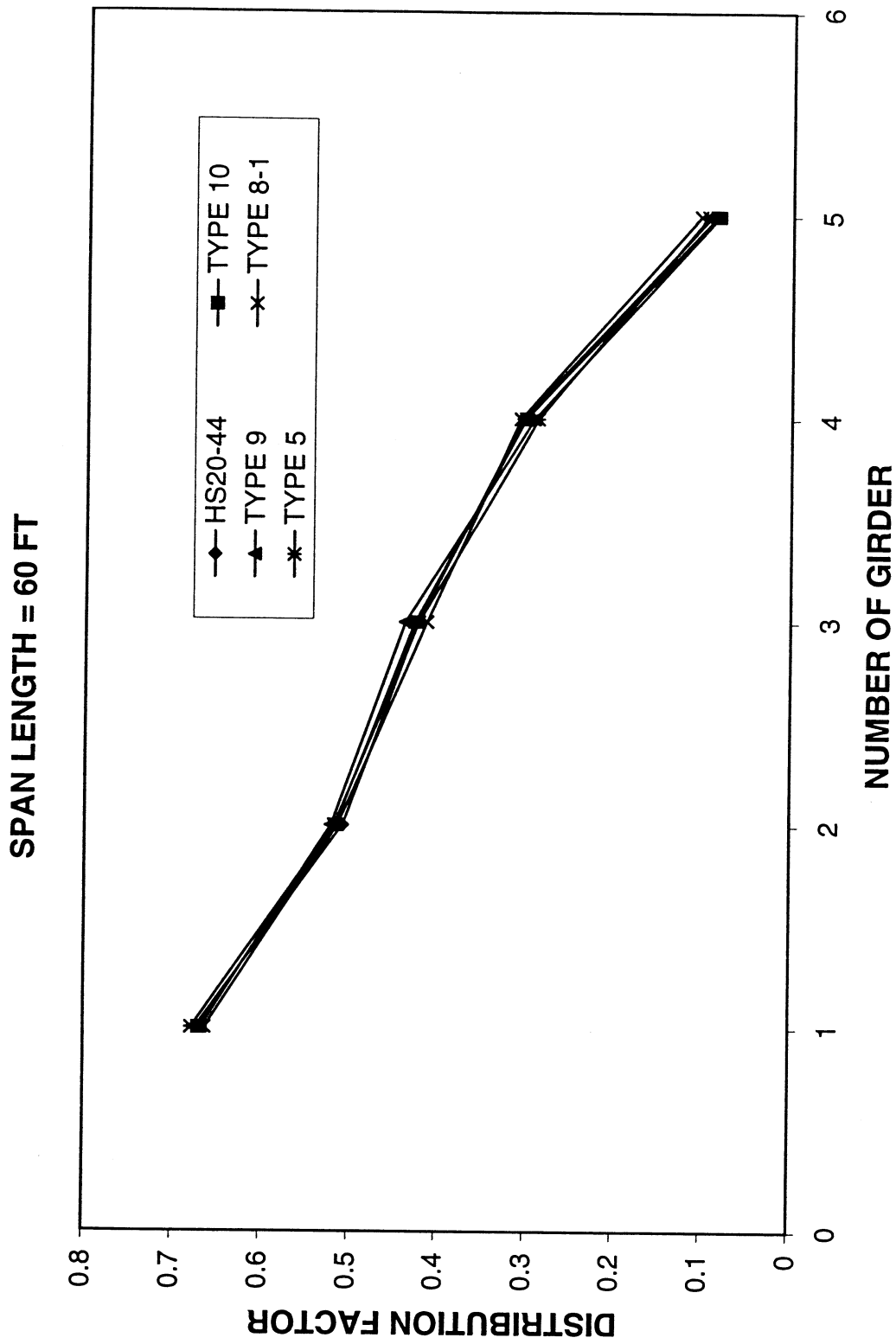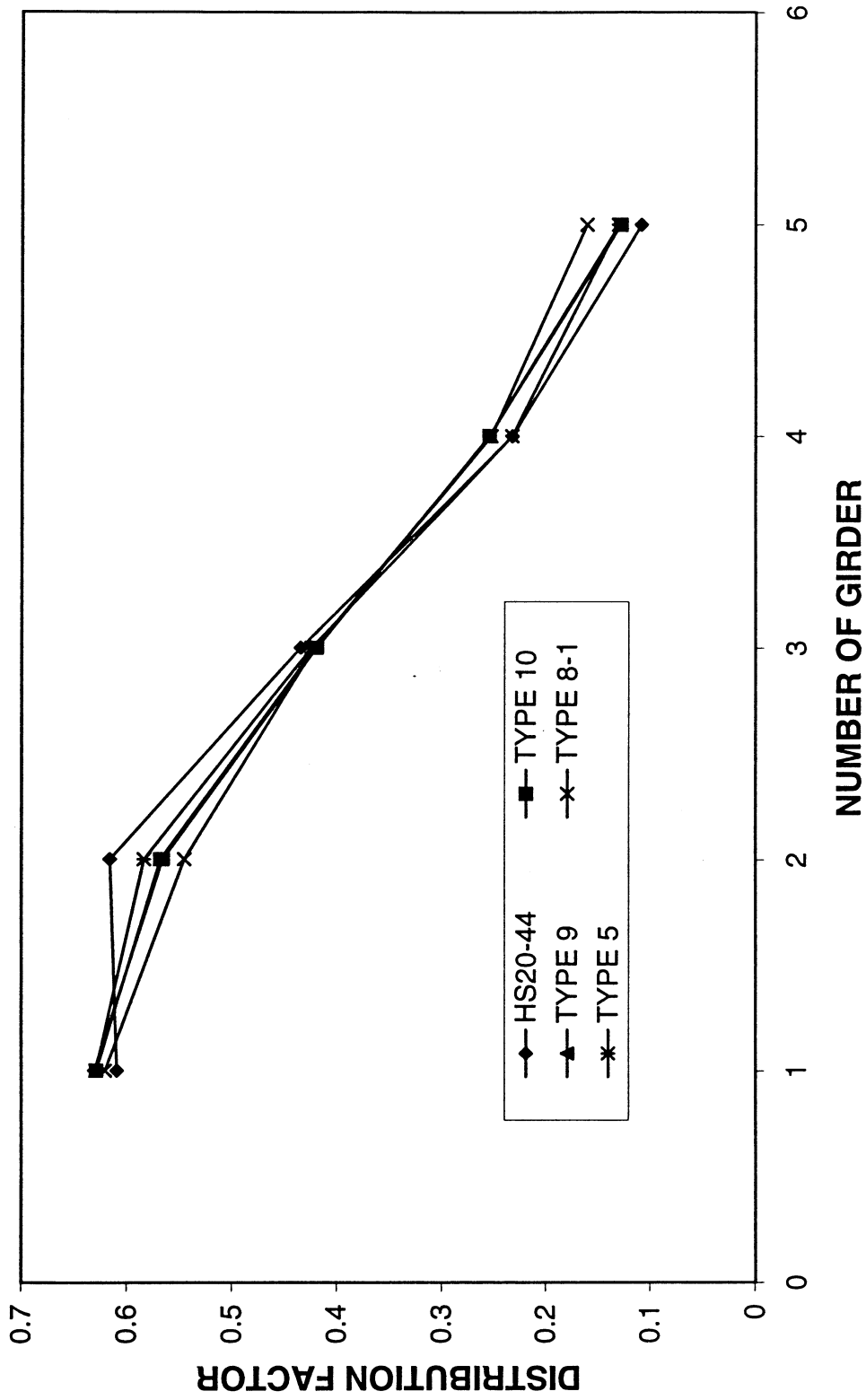
(c)

Fig. 5-14. Lateral Distribution under Various Truck Types

116
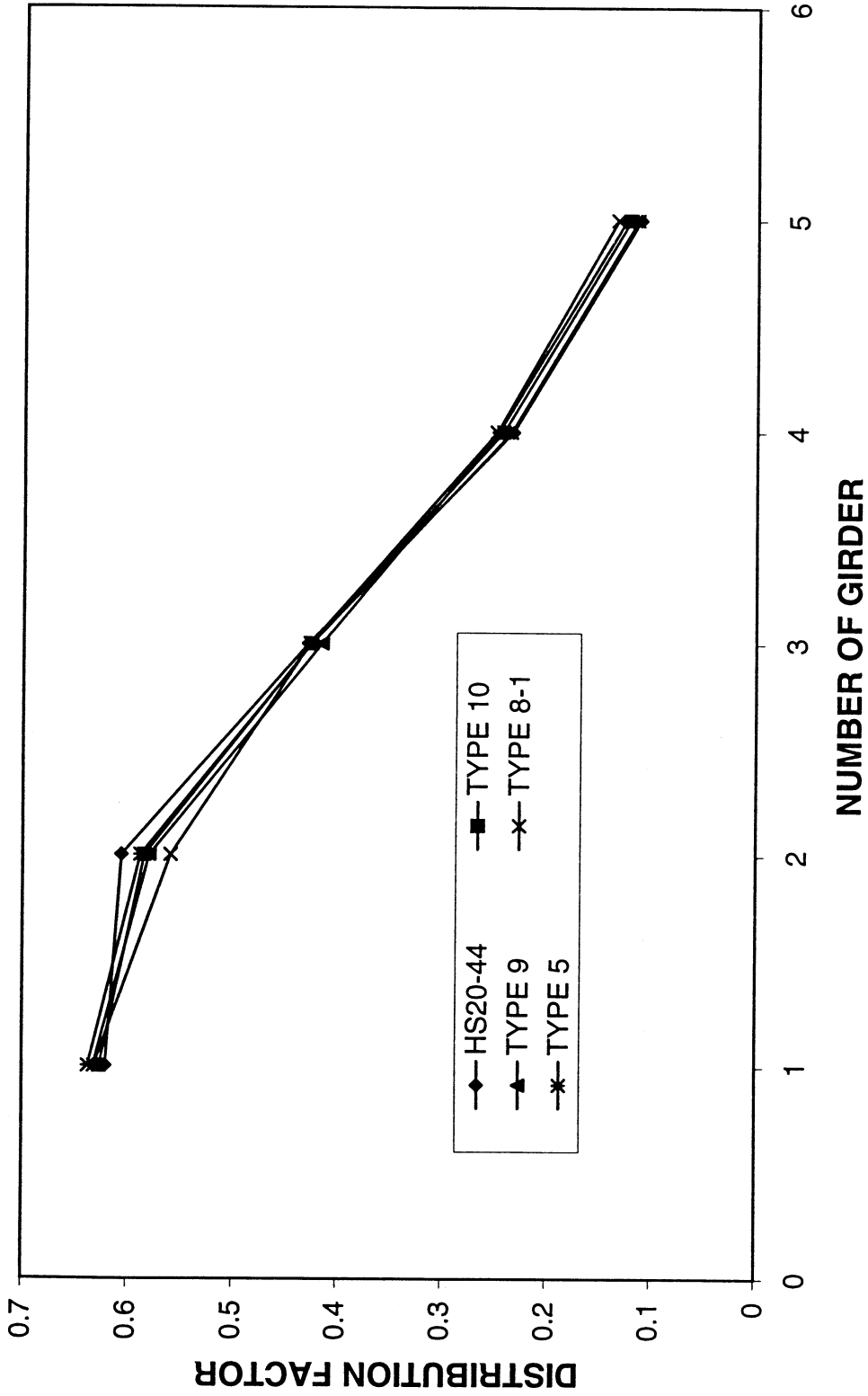
Fig. 5-14. Lateral Distribution under Various Truck Types
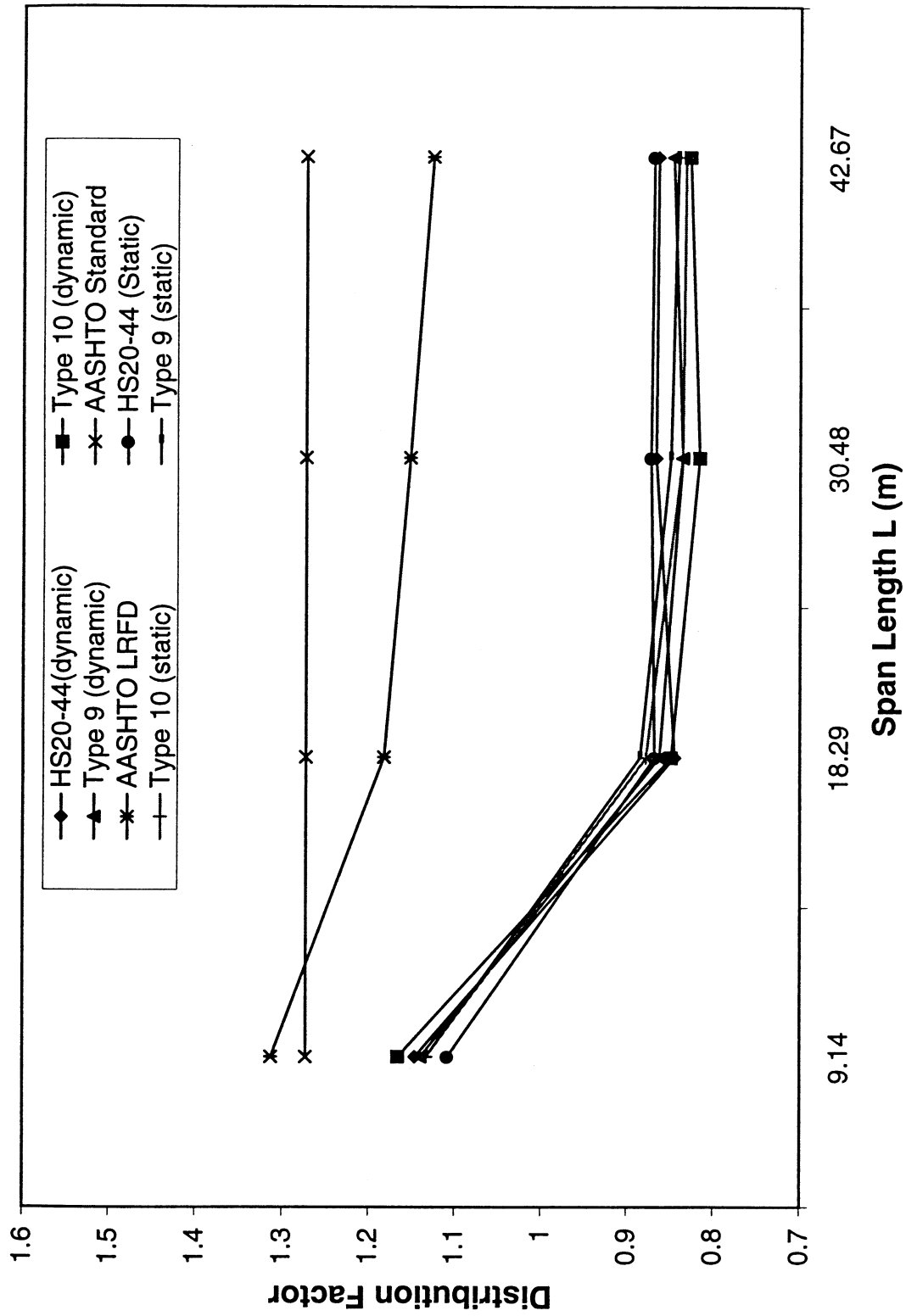
(a) Moment

Fig. 5-15. Comparison of Wheel Load Distribution Factor

118
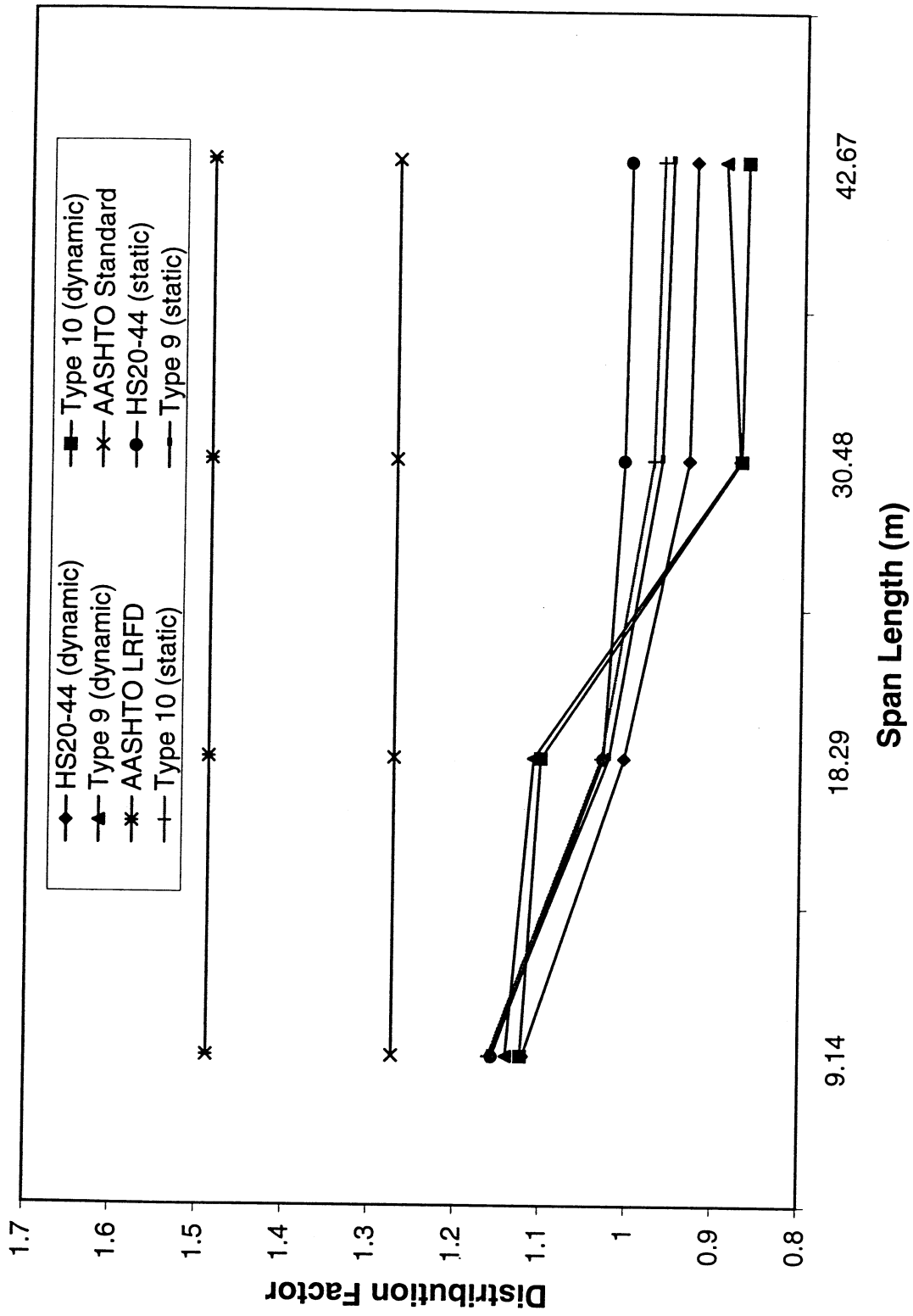
(b) Shear

Fig. 5-15. Comparison of Wheel Load Distribution Factor

Span Length L = 10.67m

Fig. 6-1. Histogram of Dynamic Flexural Stress

(a)
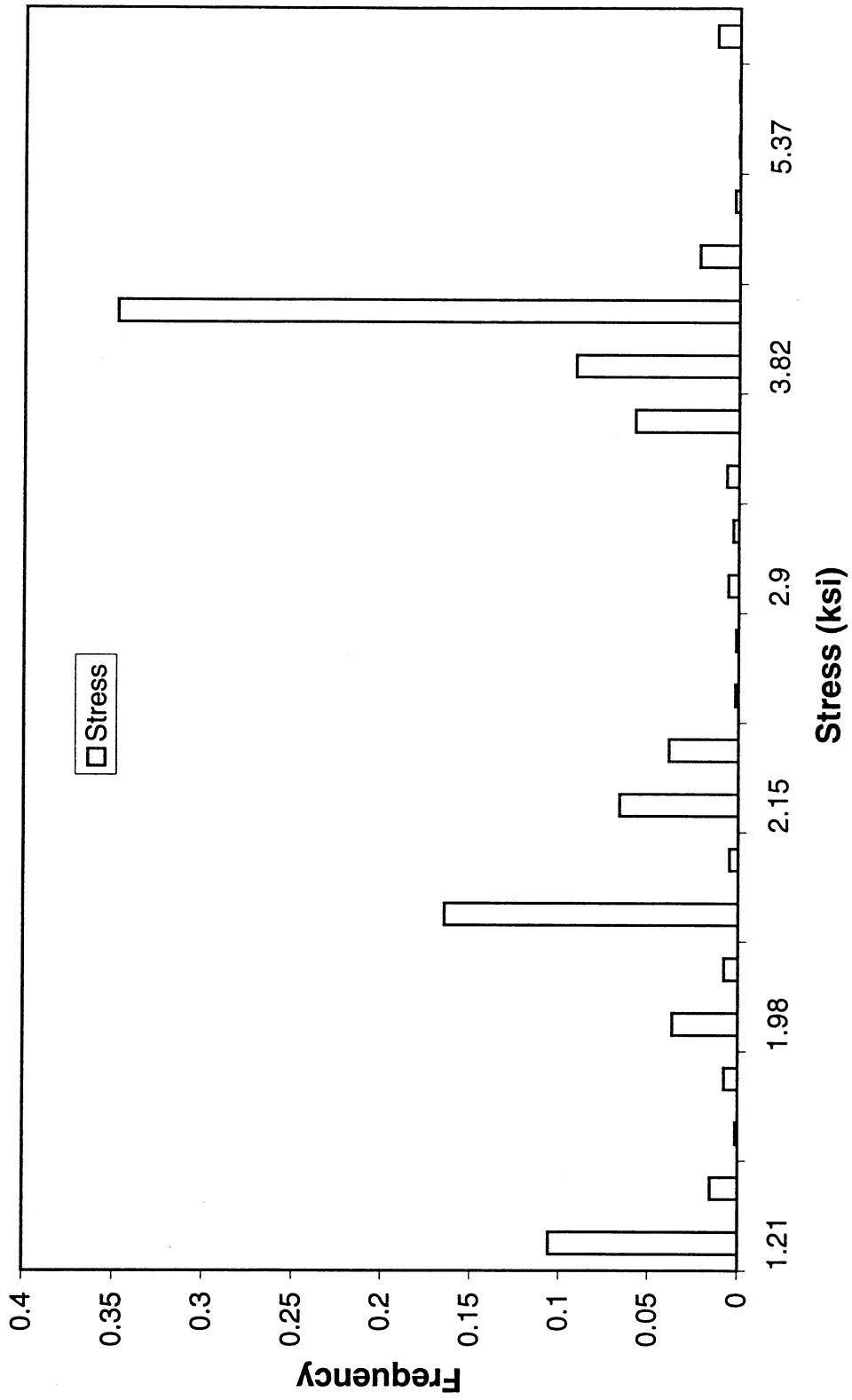
Fig. 6-1. Histogram of Dynamic Flexural Stress
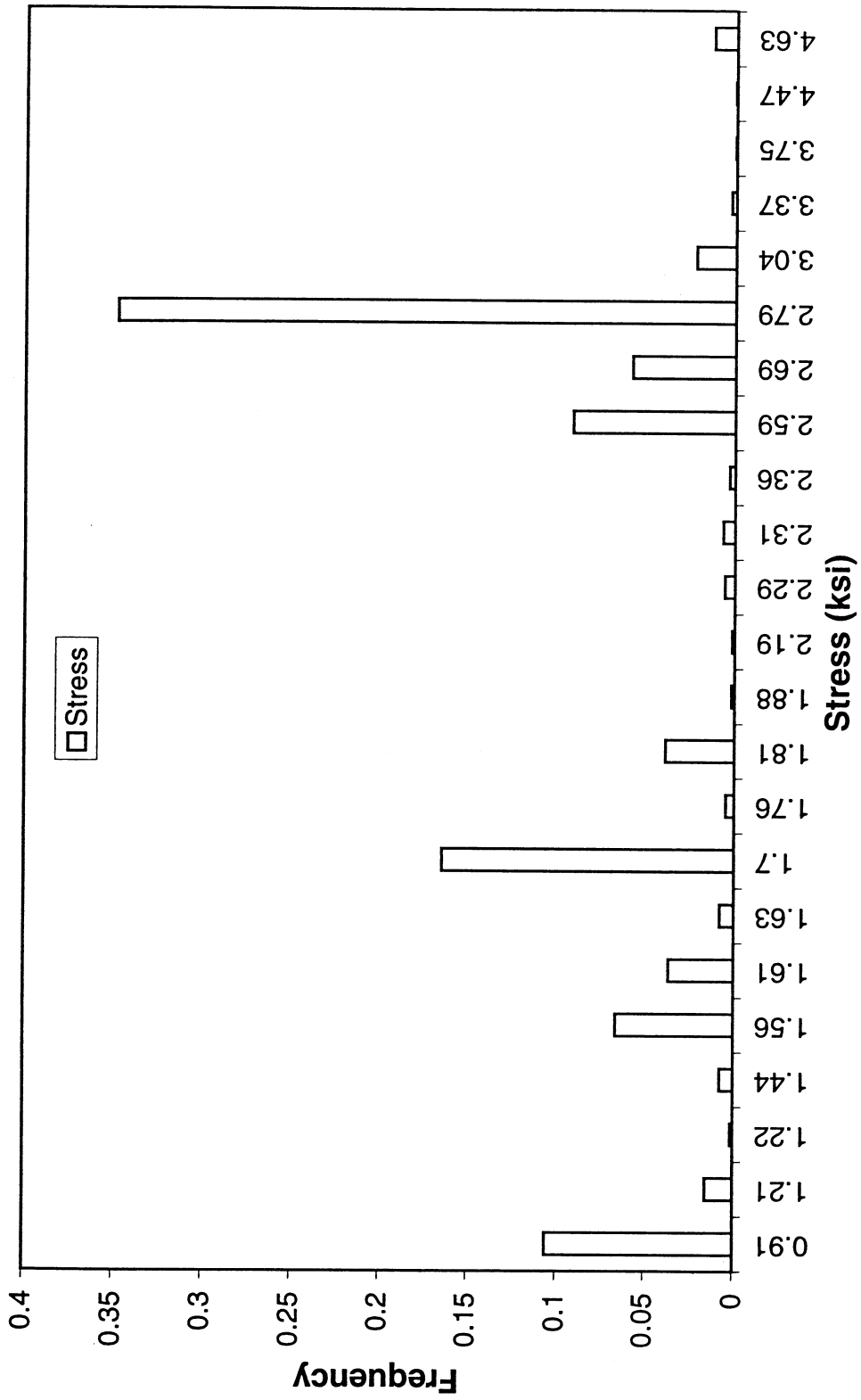
(b)

Fig. 6-1. Histogram of Dynamic Flexural Stress

(c)

Span Length L = 30.48m

Fig. 6-1. Histogram of Dynamic Flexural Stress

(d)

Span Length L = 36.58m

Fig. 6-1. Histogram of Dynamic Flexural Stress

(e)

124

Span Length L = 42.67m

Fig. 6-1. Histogram of Dynamic Flexural Stress

(f)

125
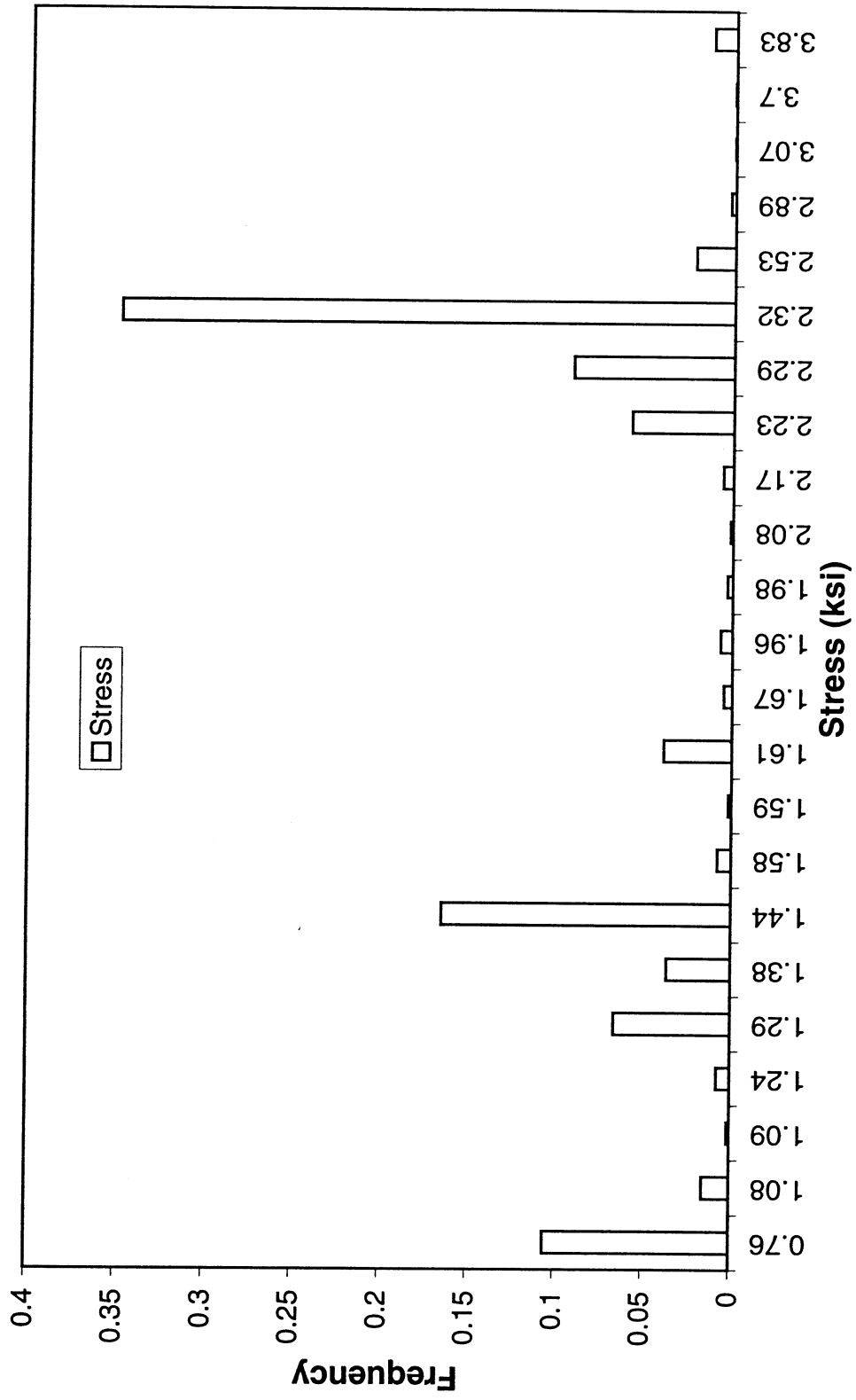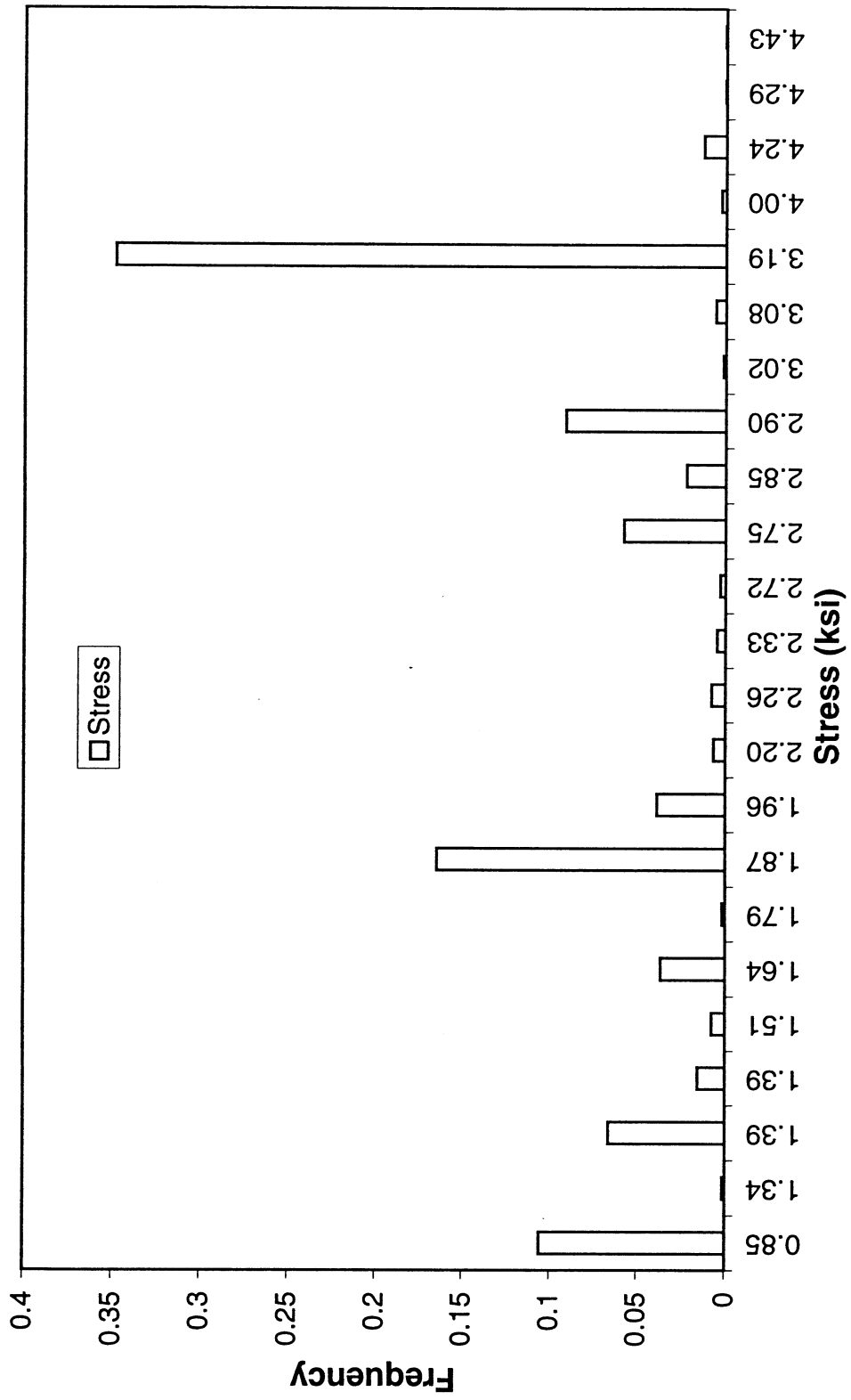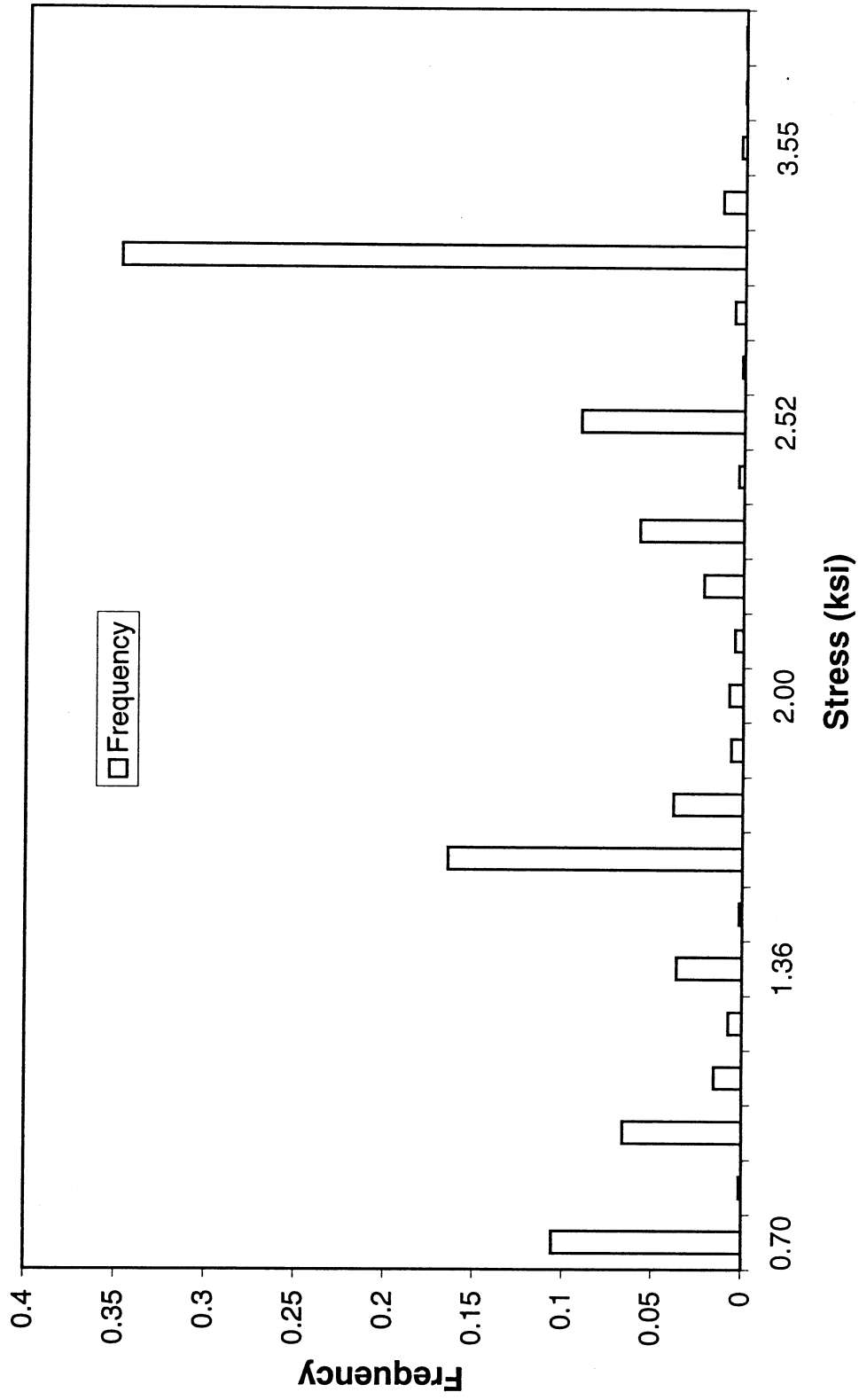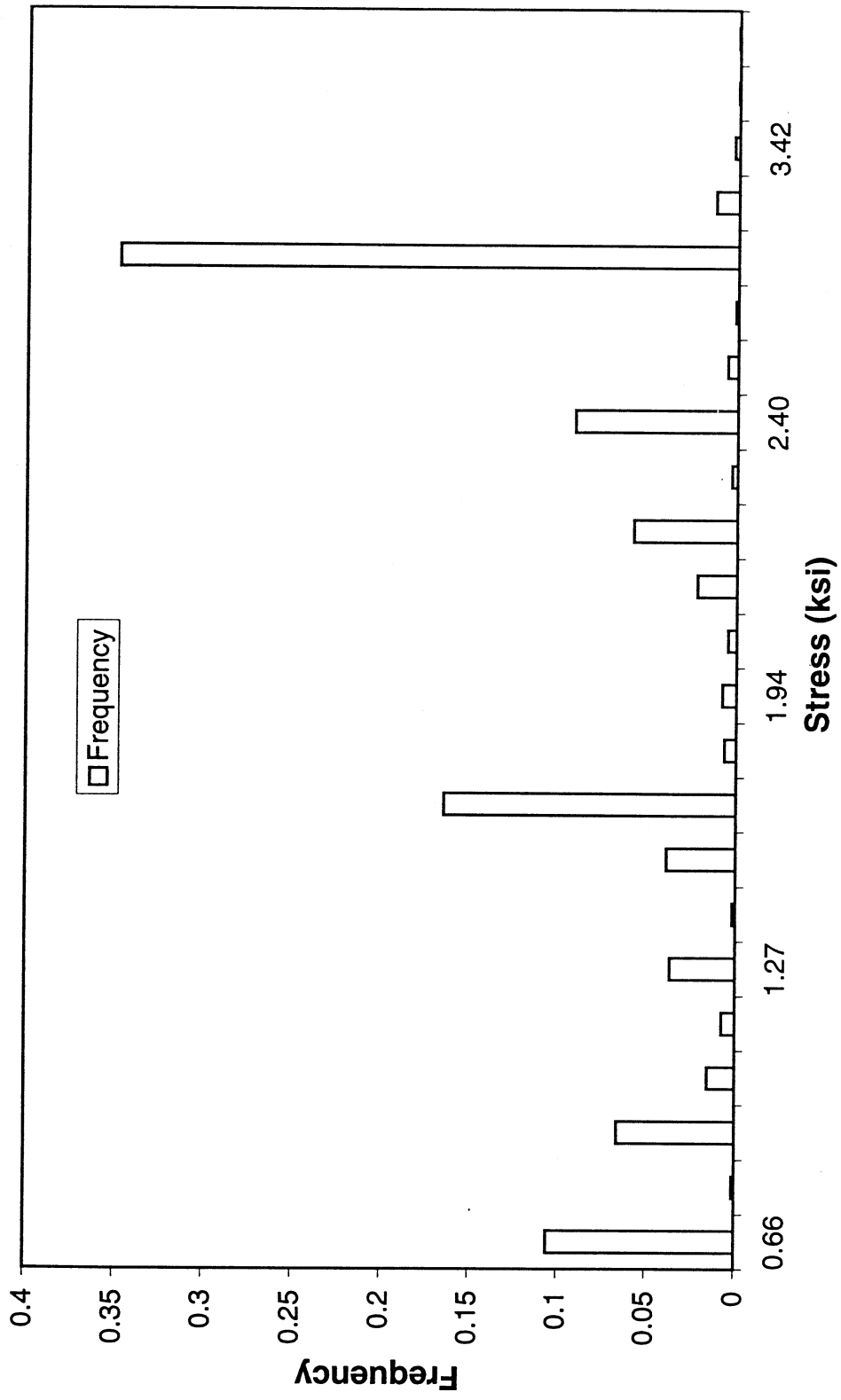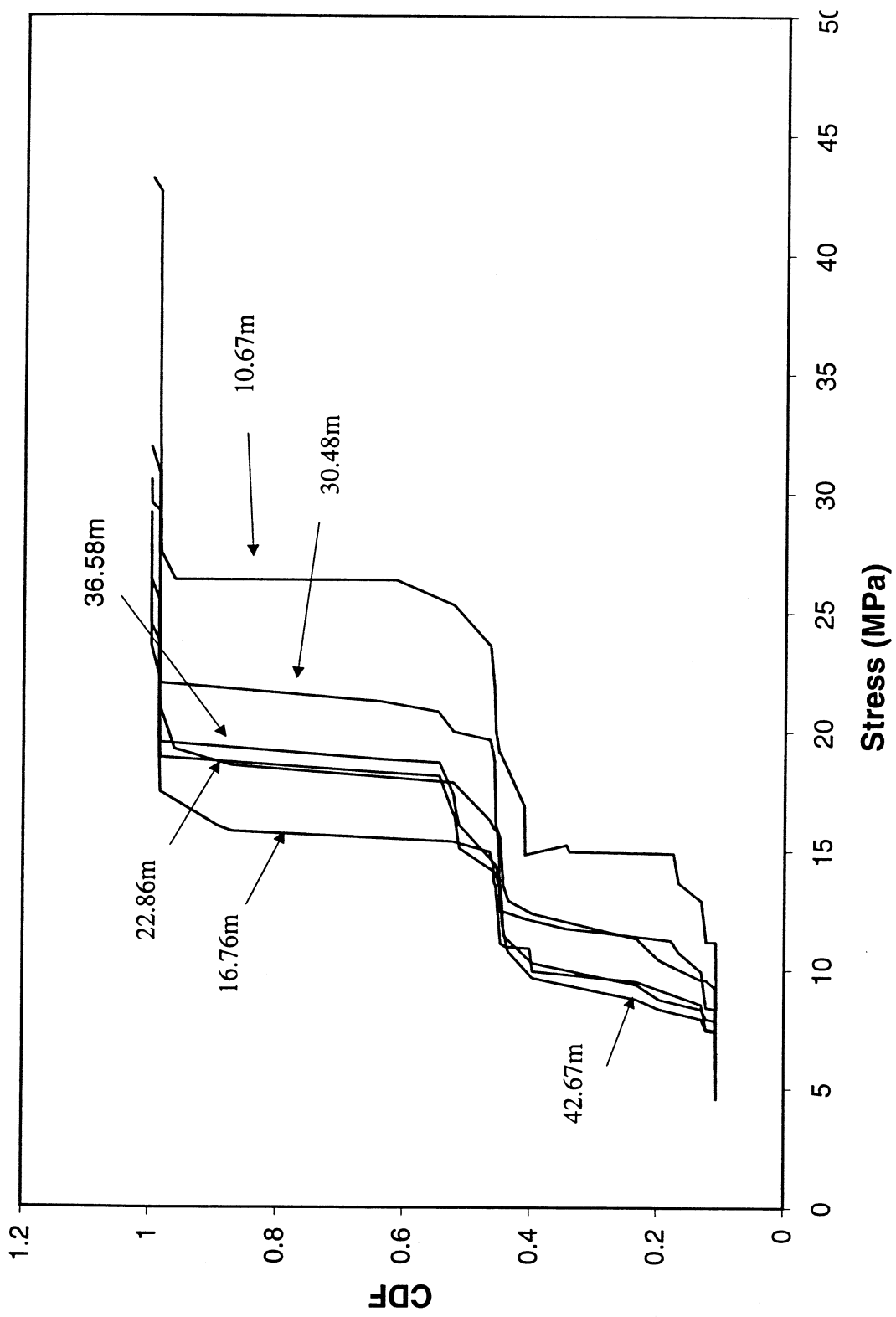
Fig. 6-2. CDF of Calculated Dynamic Stress Range
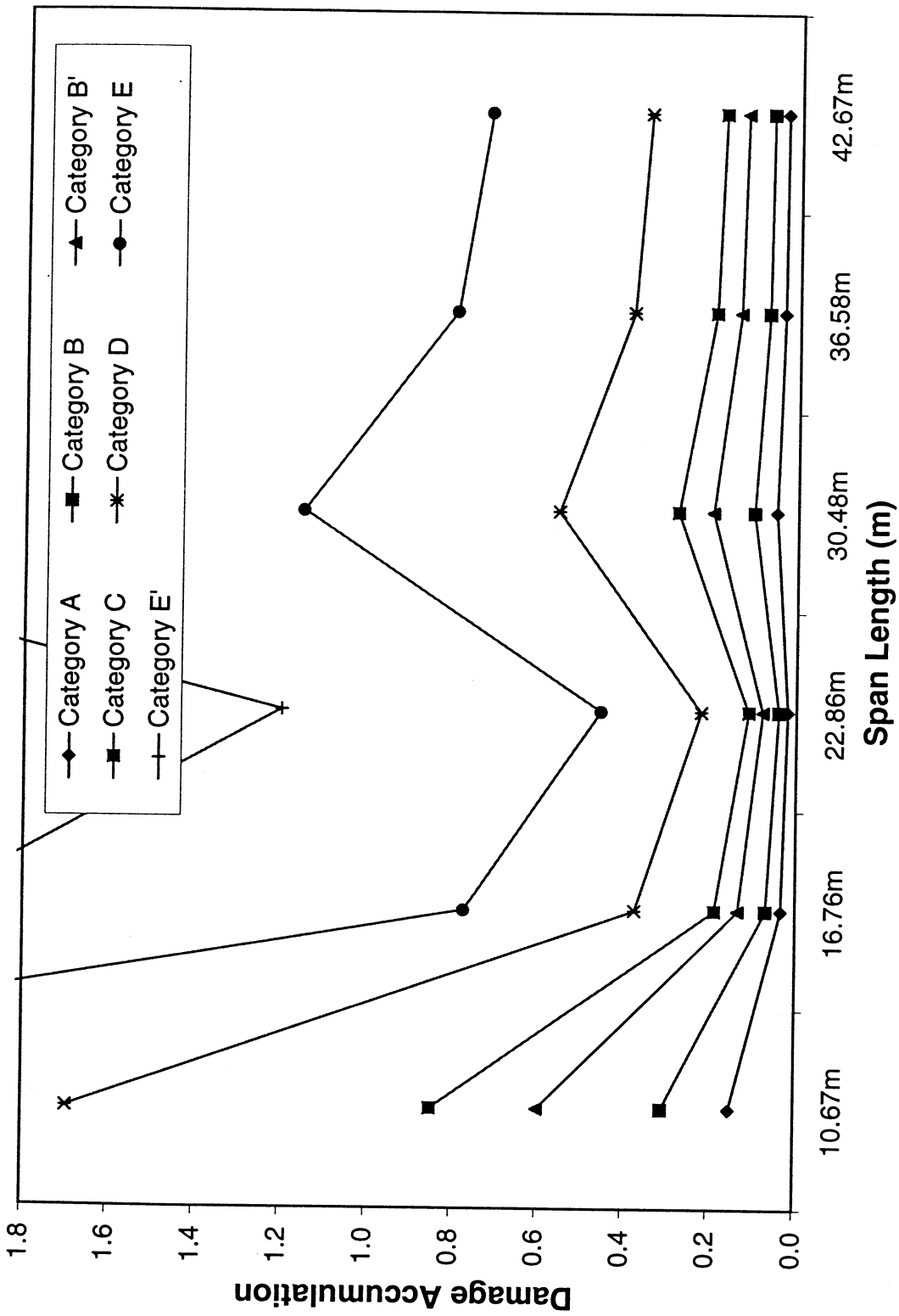
(a) Station #19

Fig. 6-3. Fatigue Damage Accumulation

Fig. 6-3. Fatigue Damage Accumulation

(b) Station #26

128
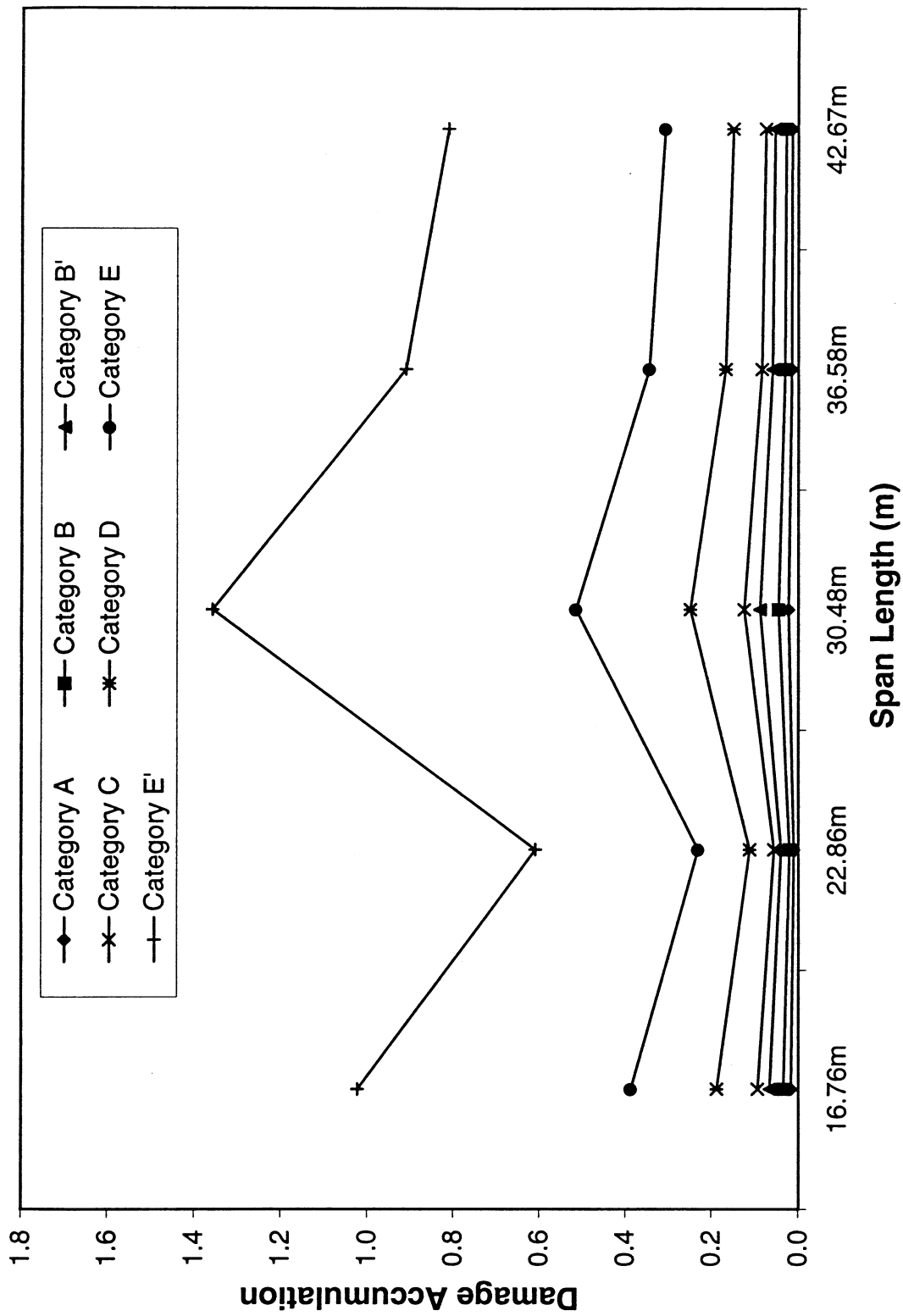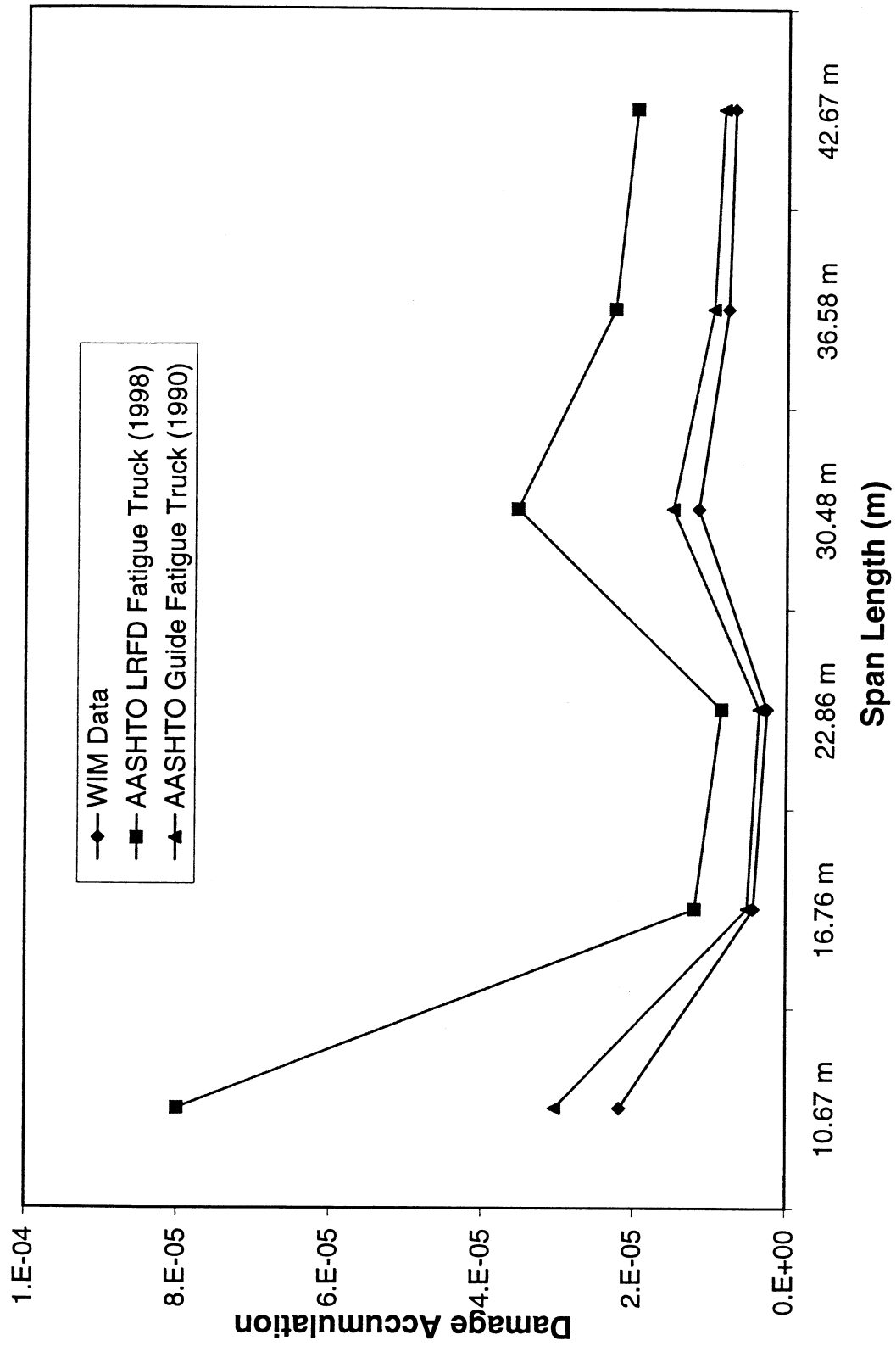
Fig. 6-4. Comparison of Fatigue Damage Accumulation
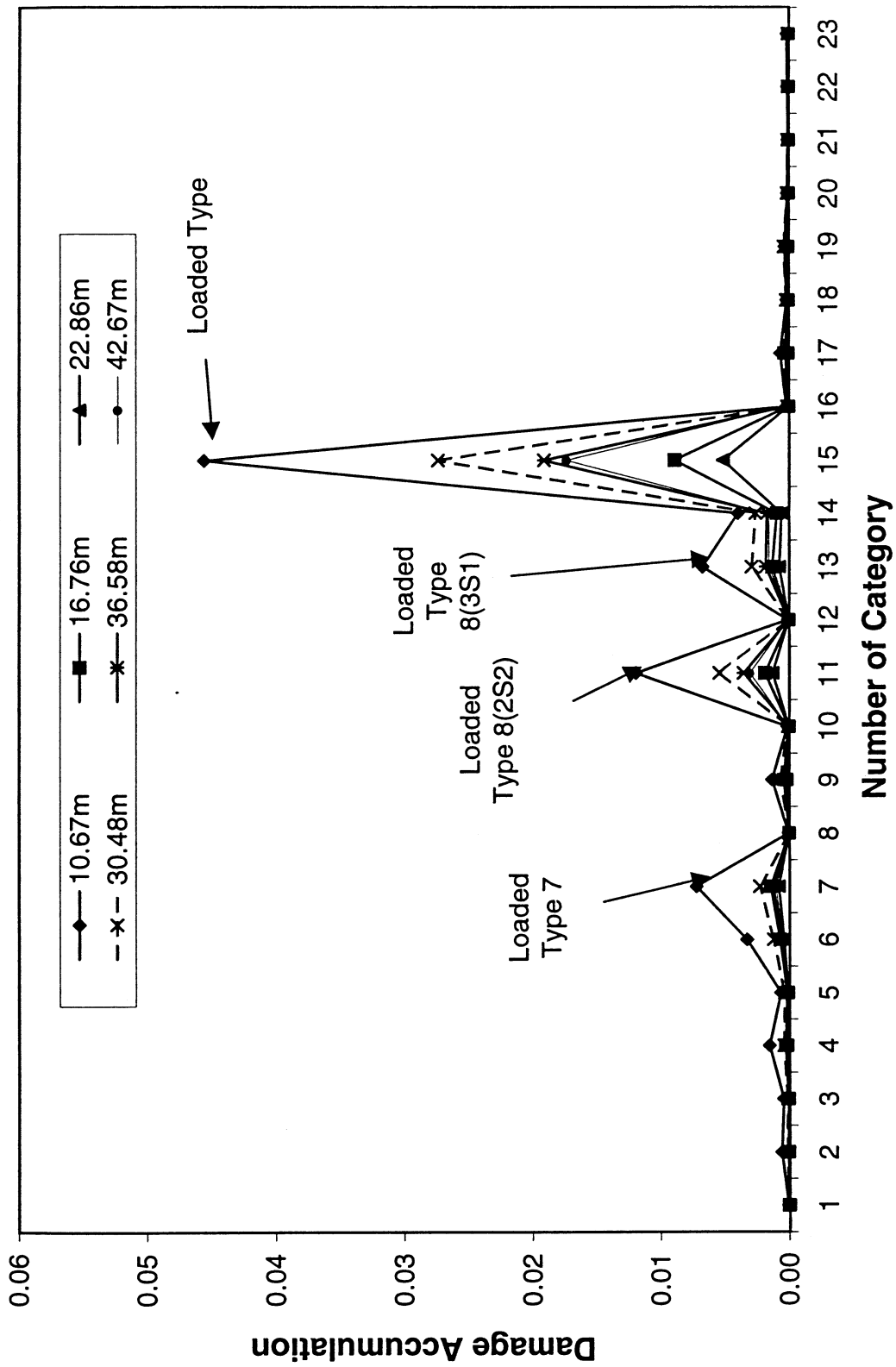
Fig. 6-5. Fatigue Damage Accumulation due to Various Truck Categories

130

Fig. 6-6. Number of Cycles Induced by Various Trucks at Station #19

(a)

Cycles Vs. Span Length

Legend:
- loaded type 6, st#19
- loaded type 7, st#19
- empty type 8-1, st#19
- loaded type 8-1, st#19
- empty type 8-2, st#19
- AASHTO LRFD
- AASHTO Guide

Number of Cycles (y-axis)

Span Length (m) (x-axis)

(b)

Fig. 6-6. Number of Cycles Induced by Various Trucks at Station #19

132

Cycles VS. Span Length

**Fig. 6-6. Number of Cycles Induced by Various Trucks at Station #19**

(c)

133

Fig. 6-6. Number of Cycles Induced by Various Trucks at Station #19

(d)

Cycles Vs. Span Length

Legend:
- loaded type 12, st#19
- empty type 13 (7axle), st#19
- loaded type 13 (7axle), st#19
- empty type 13 (8axle), st#19
- AASHTO LRFD

Span Length (m)

Number of Cycles

(e)

Fig. 6-6. Number of Cycles Induced by Various Trucks at Station #19

Cycles Vs. Span Length
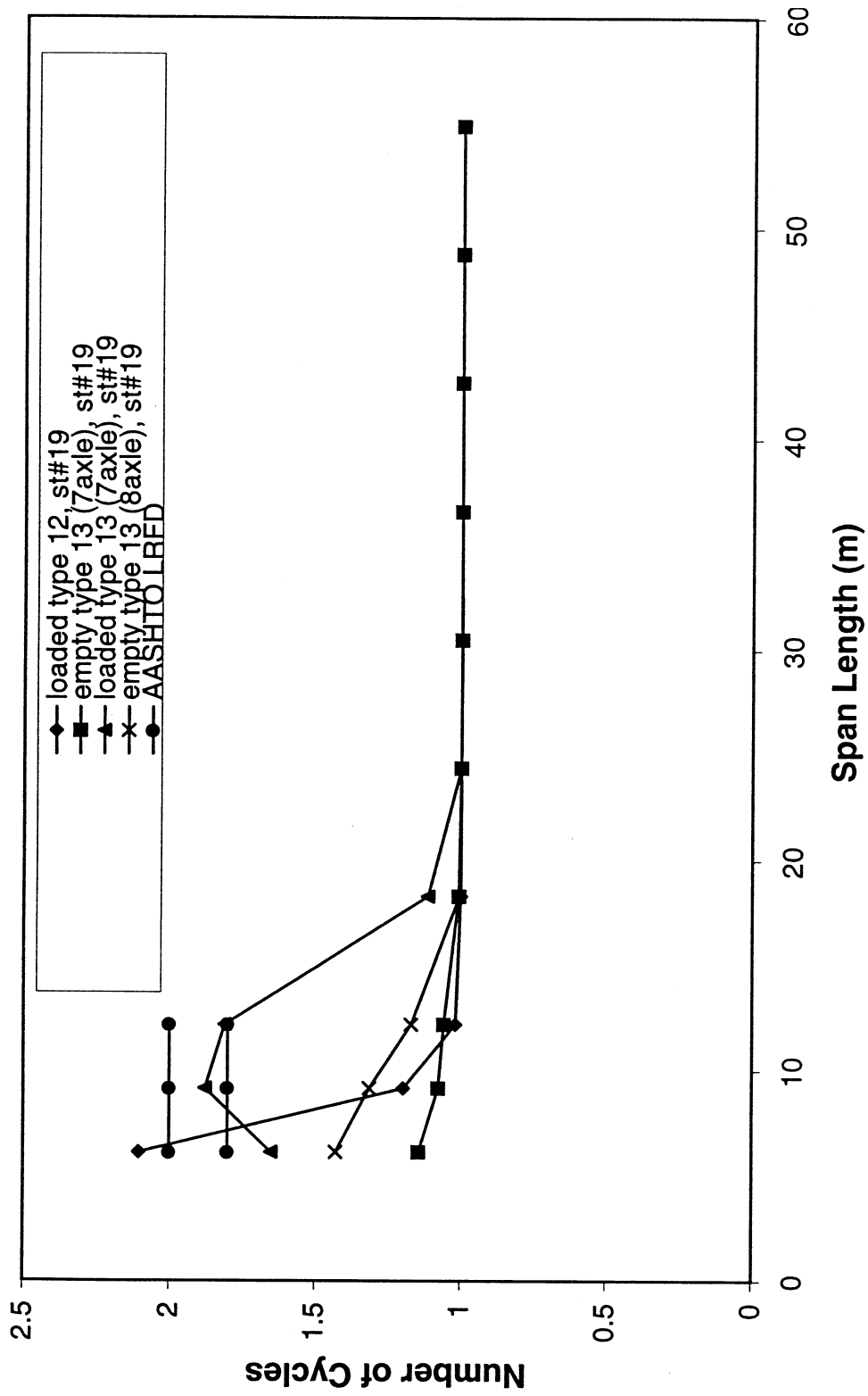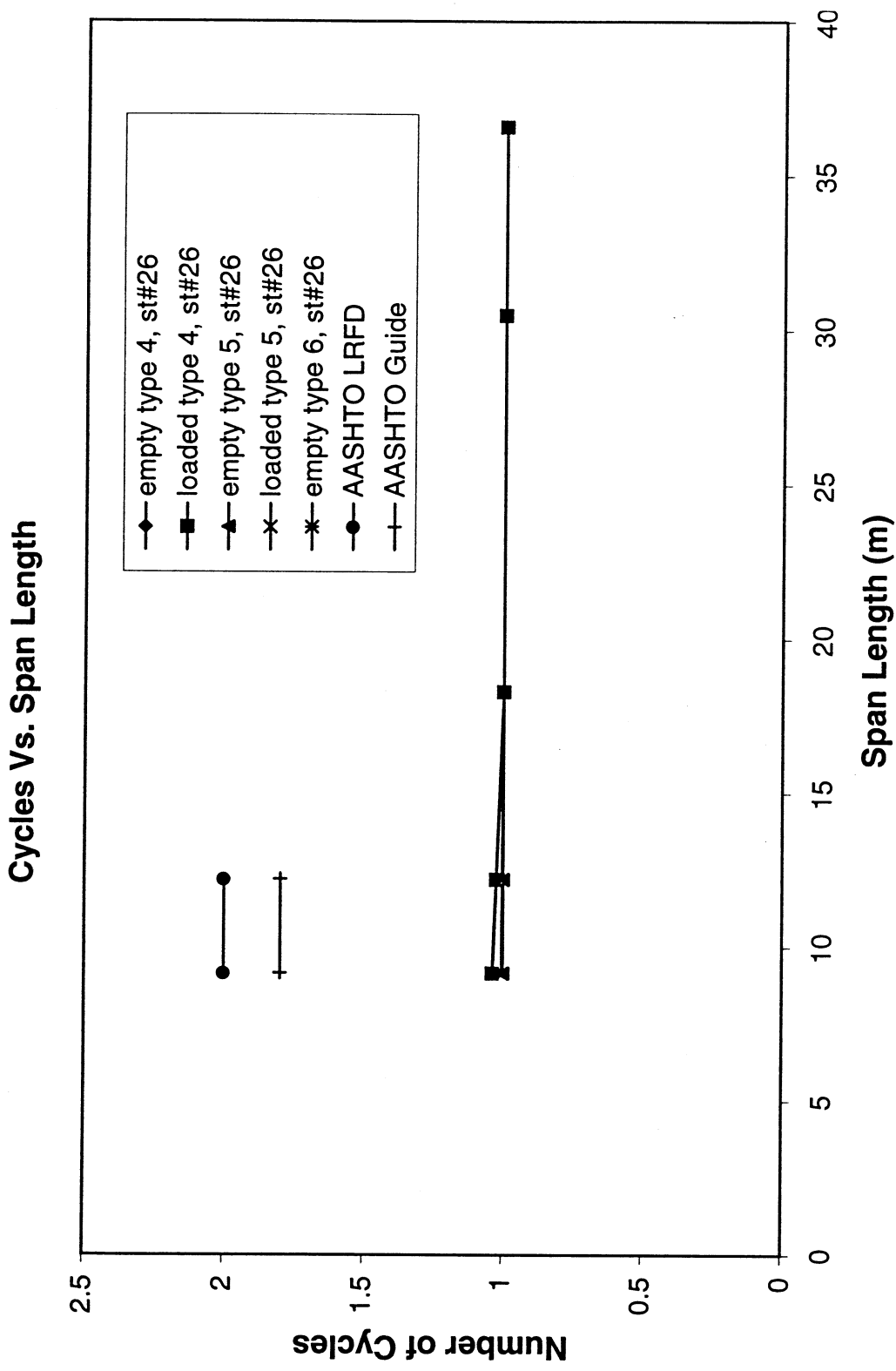
Fig. 6-7. Number of Cycles Induced by Various Trucks at Station #26

(a)

Cycles Vs. Span Length

Fig. 6-7. Number of Cycles Induced by Various Trucks at Station #26

(b)

137

Fig. 6-7. Number of Cycles Induced by Various Trucks at Station #26
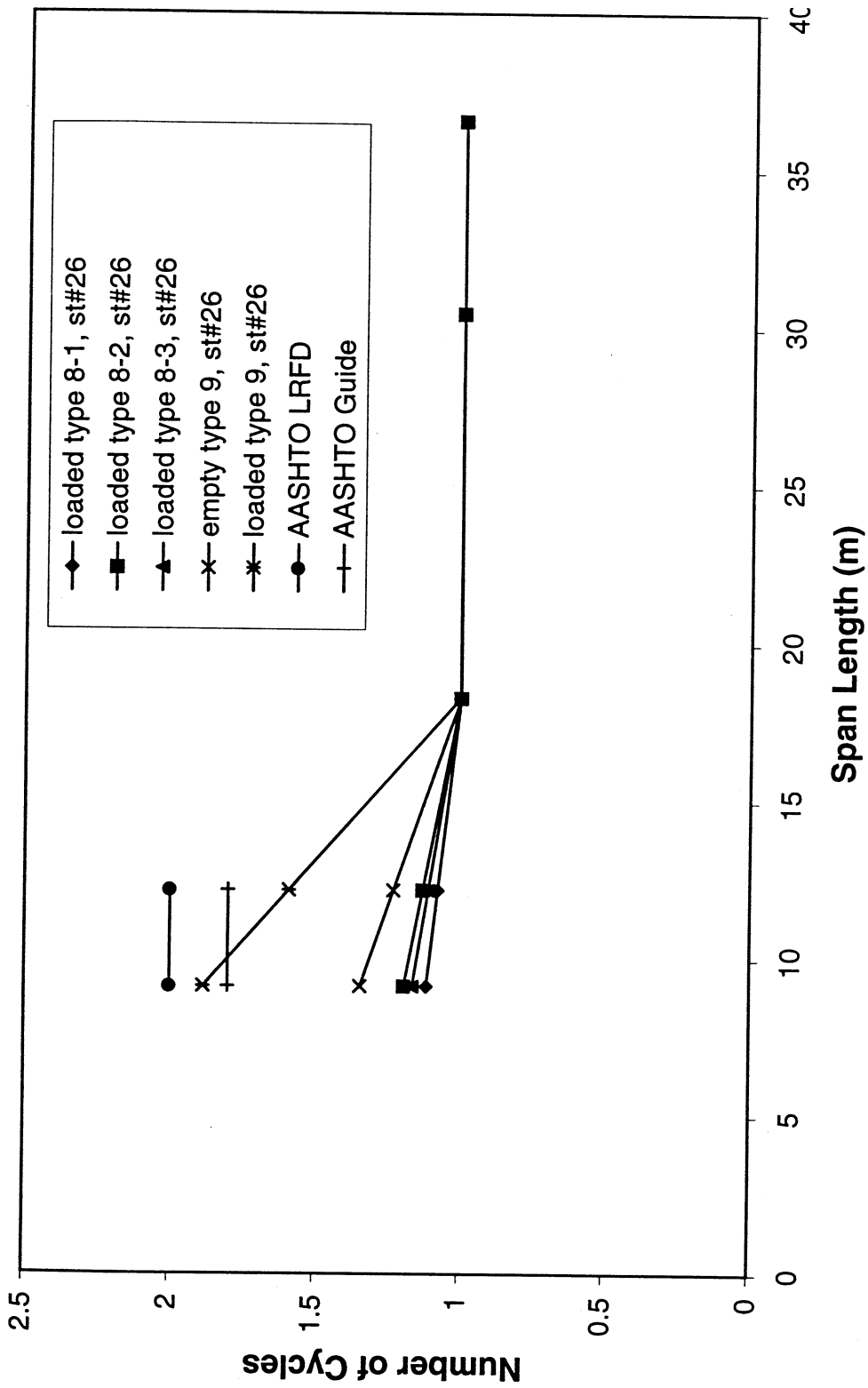
(c)

Fig. 6-7. Number of Cycles Induced by Various Trucks at Station #26
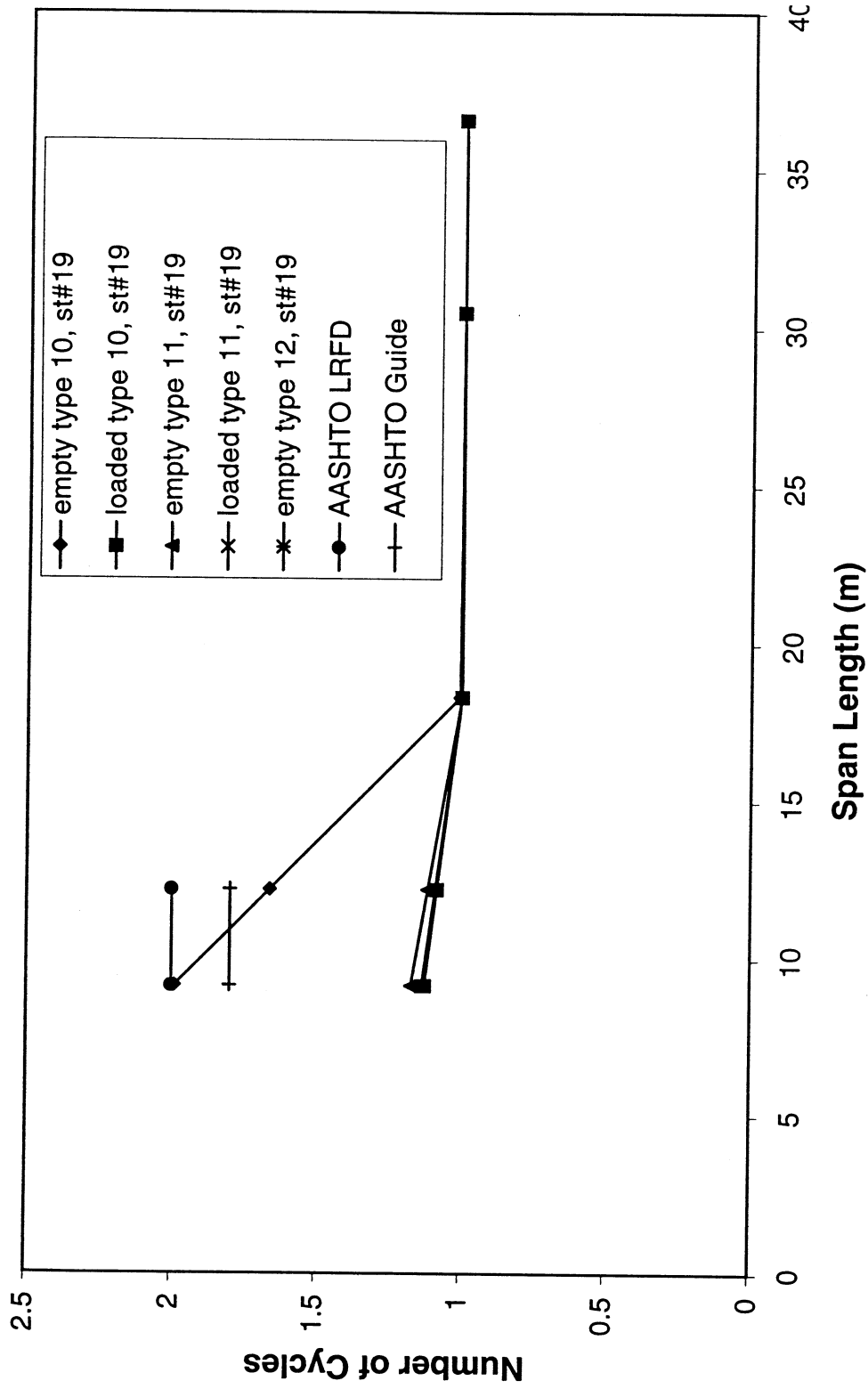
(d)

Cycles Vs. Span Length

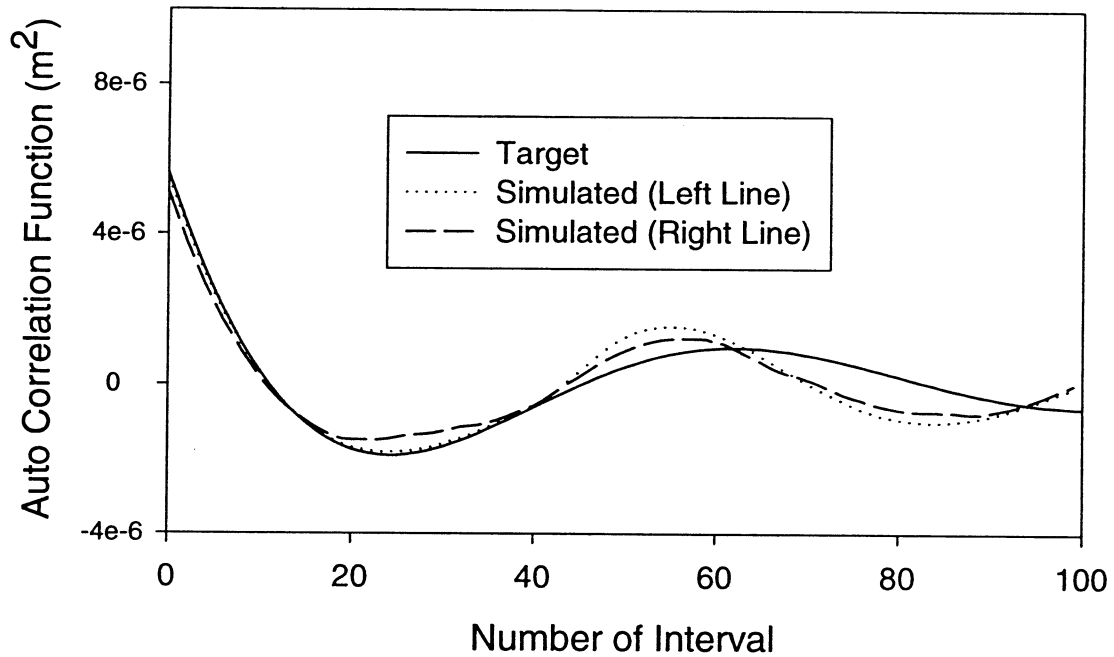Fig. 6-7. Number of Cycles Induced by Various Trucks at Station #26

(e)

140
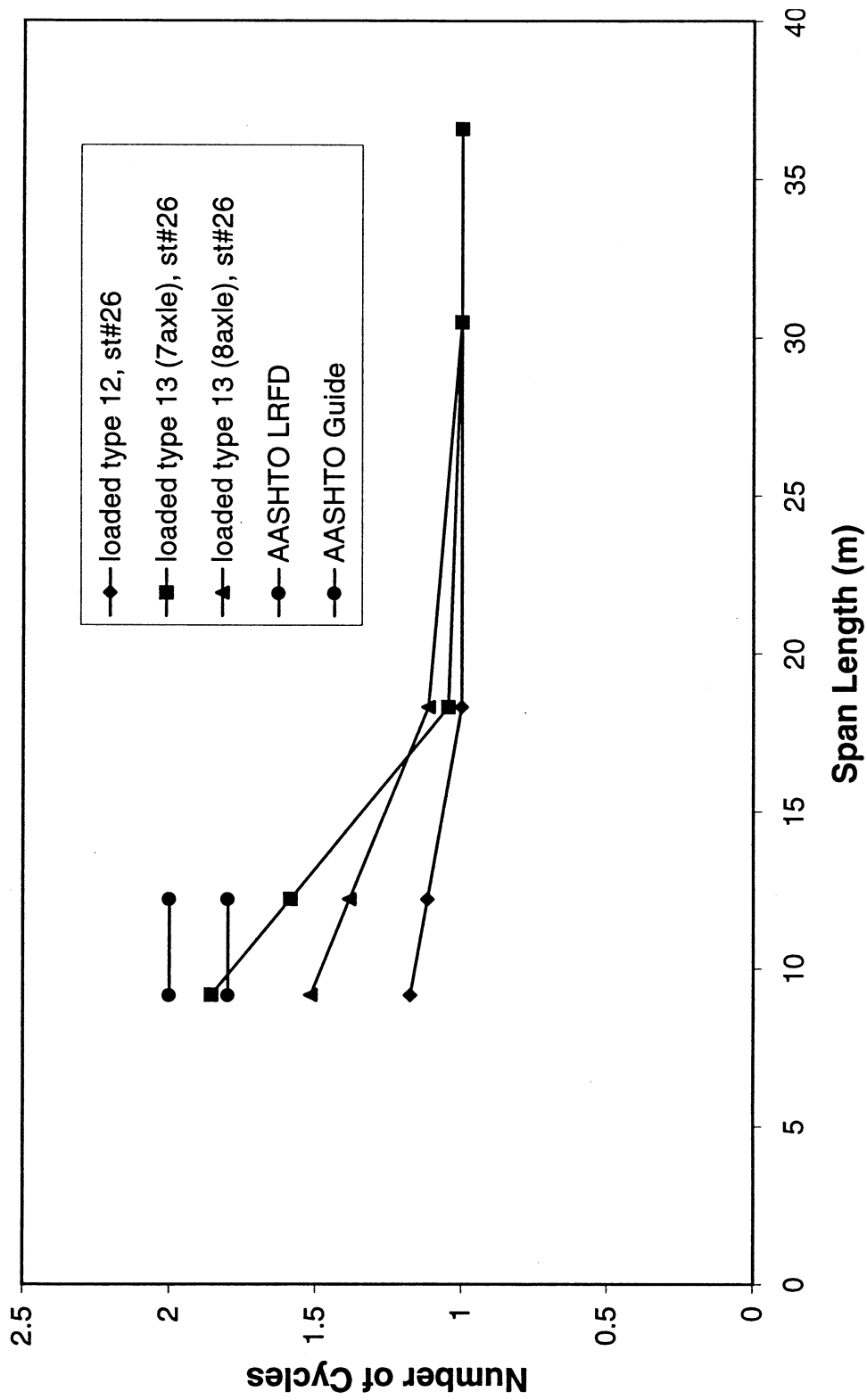
Fig. 7-1. Simulated Road Surface Roughness Profiles
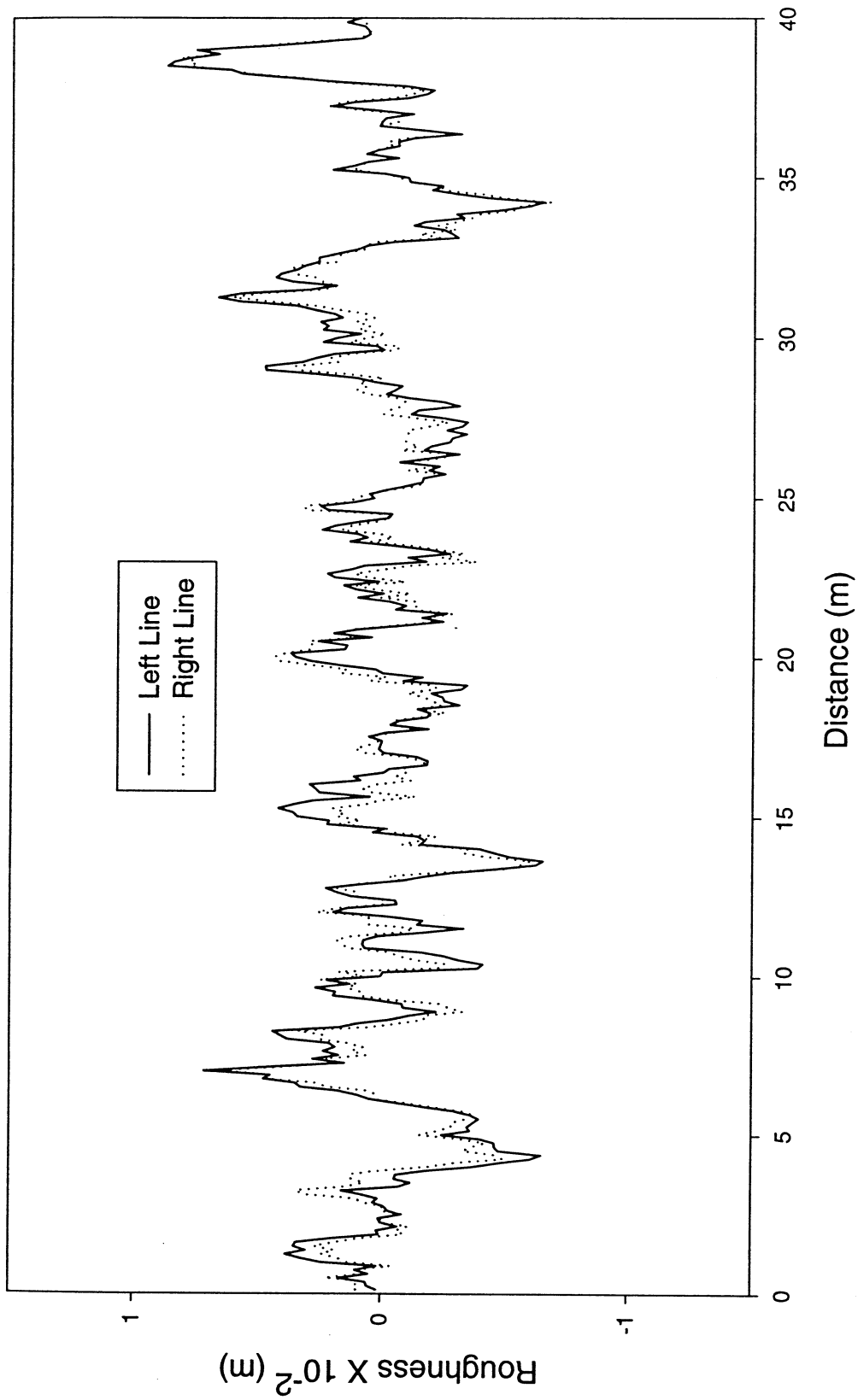
(a) $c = 0.9$

Fig. 7-1. Simulated Road Surface Roughness Profiles
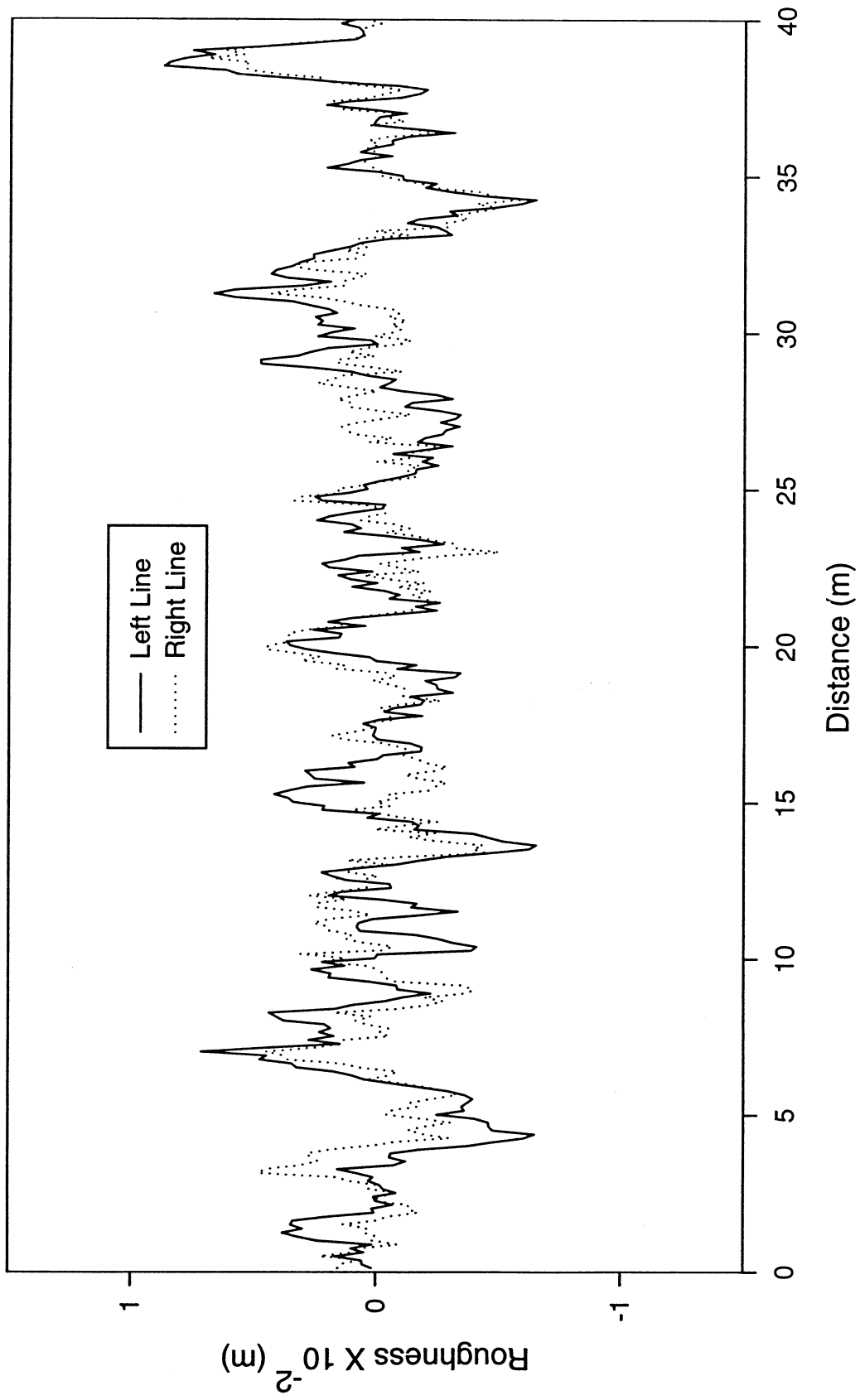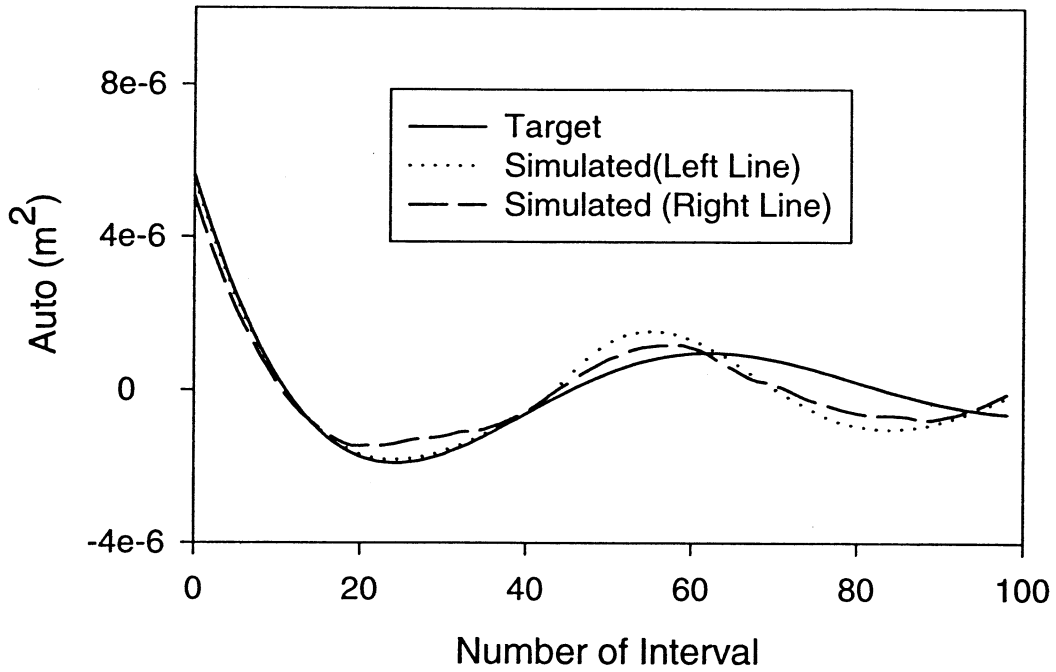
(b) $c = 0.63$

Fig. 7-1. Simulated Road Surface Roughness Profiles
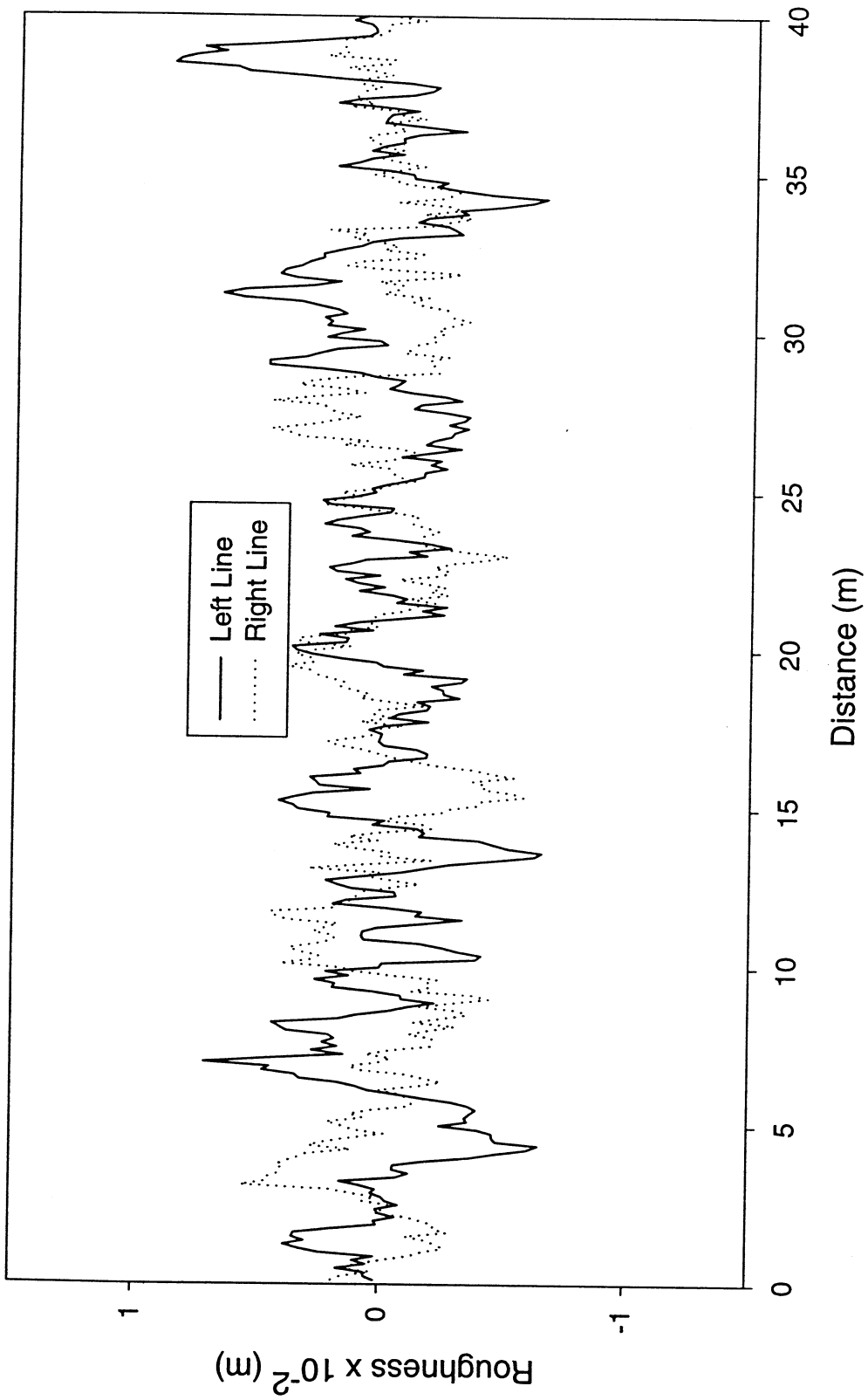
(c) $c = 0.0$

143
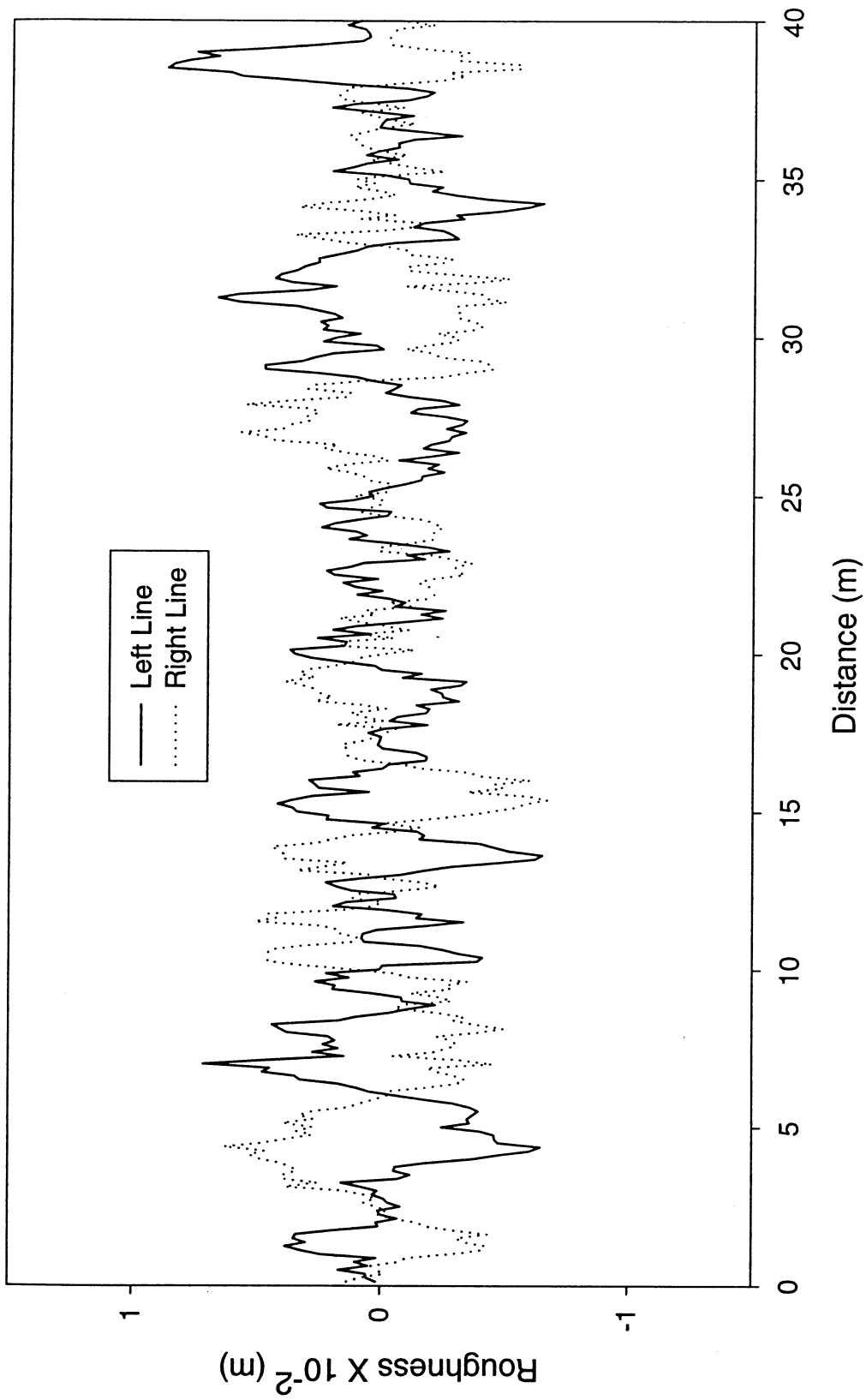
Fig. 7-1. Simulated Road Surface Roughness Profiles

(d) $c = -0.63$
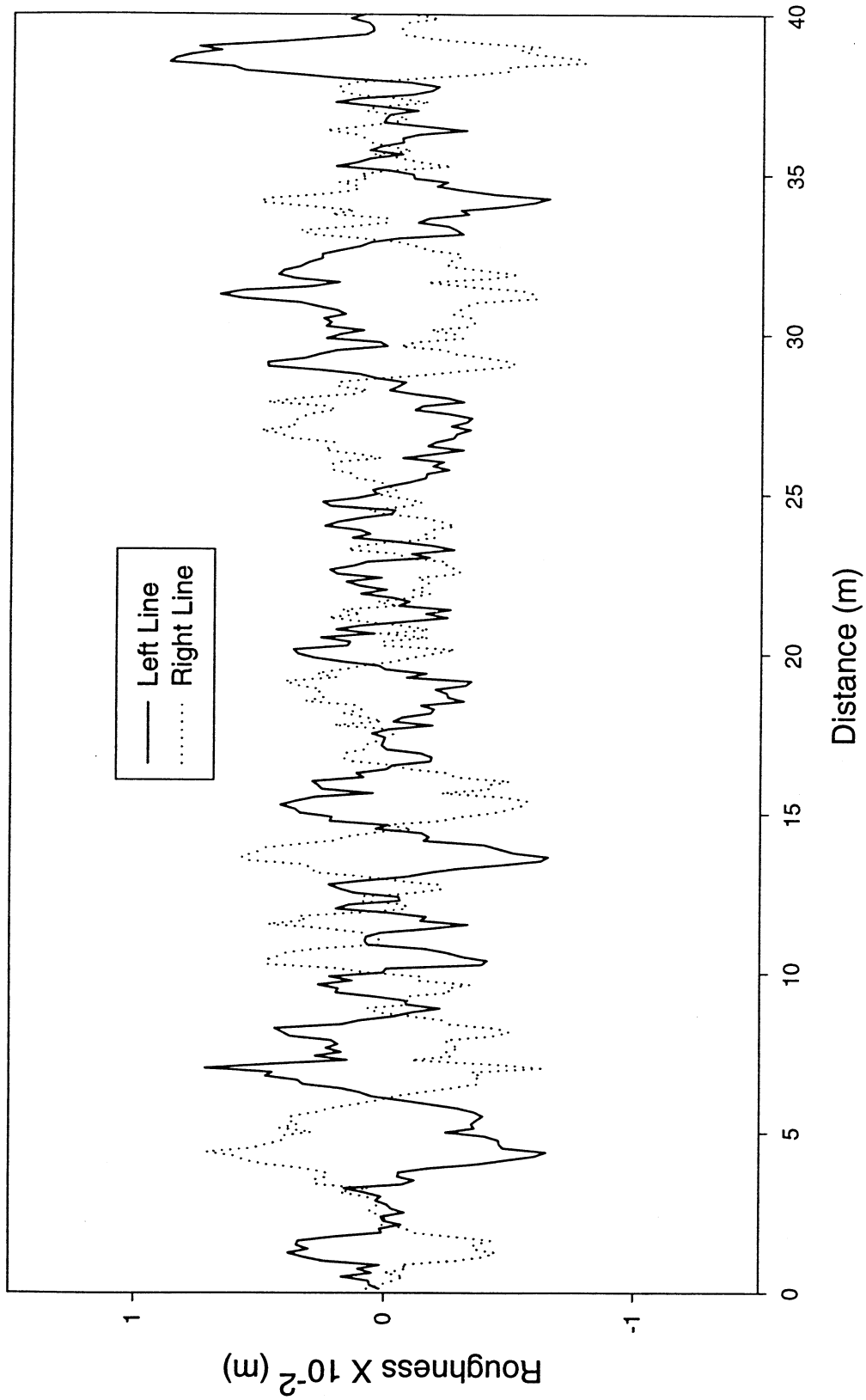
(e) $c = -0.9$

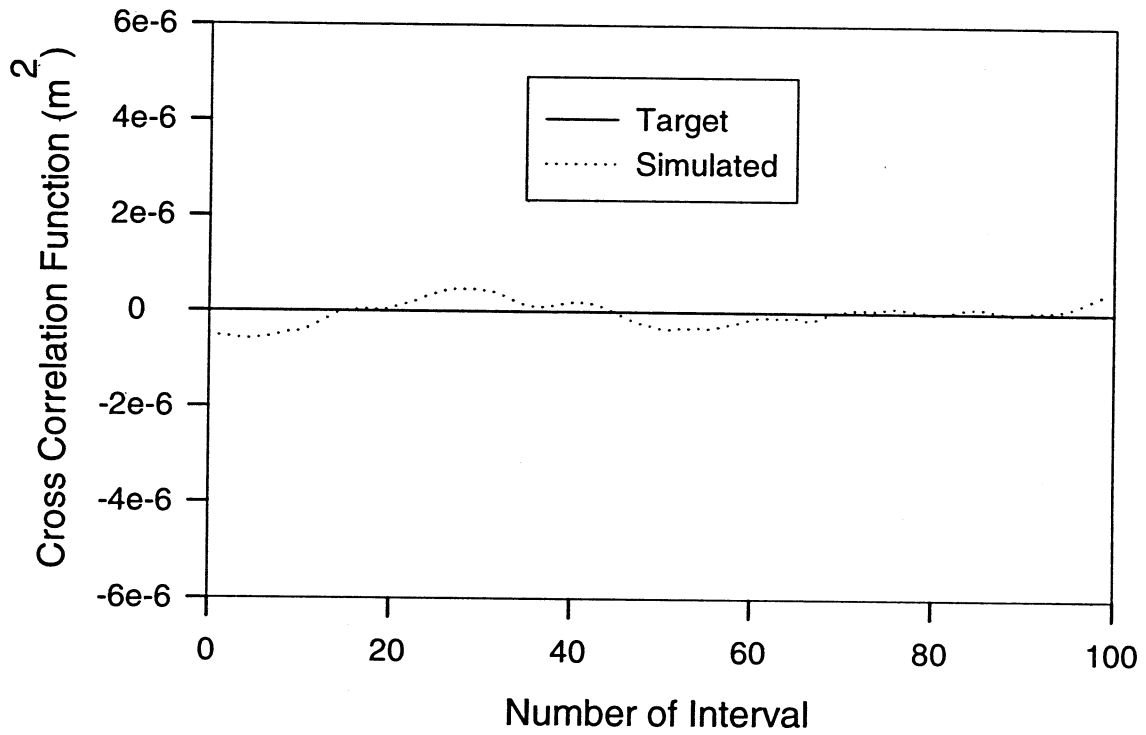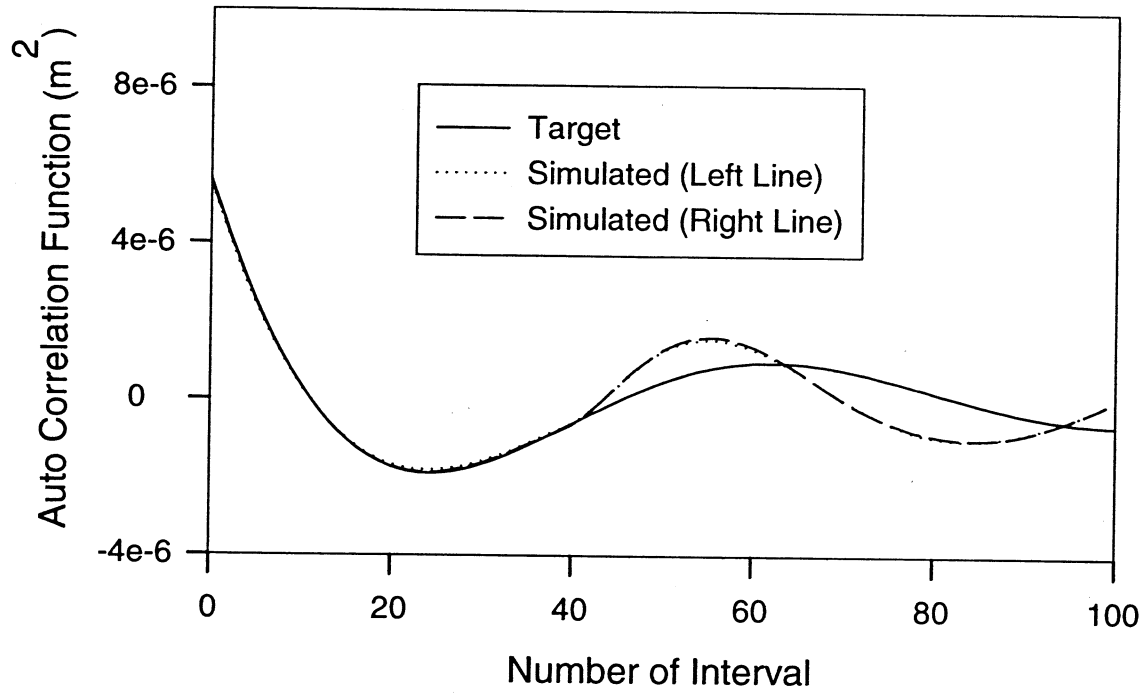**Fig. 7-1. Simulated Road Surface Roughness Profiles**

145
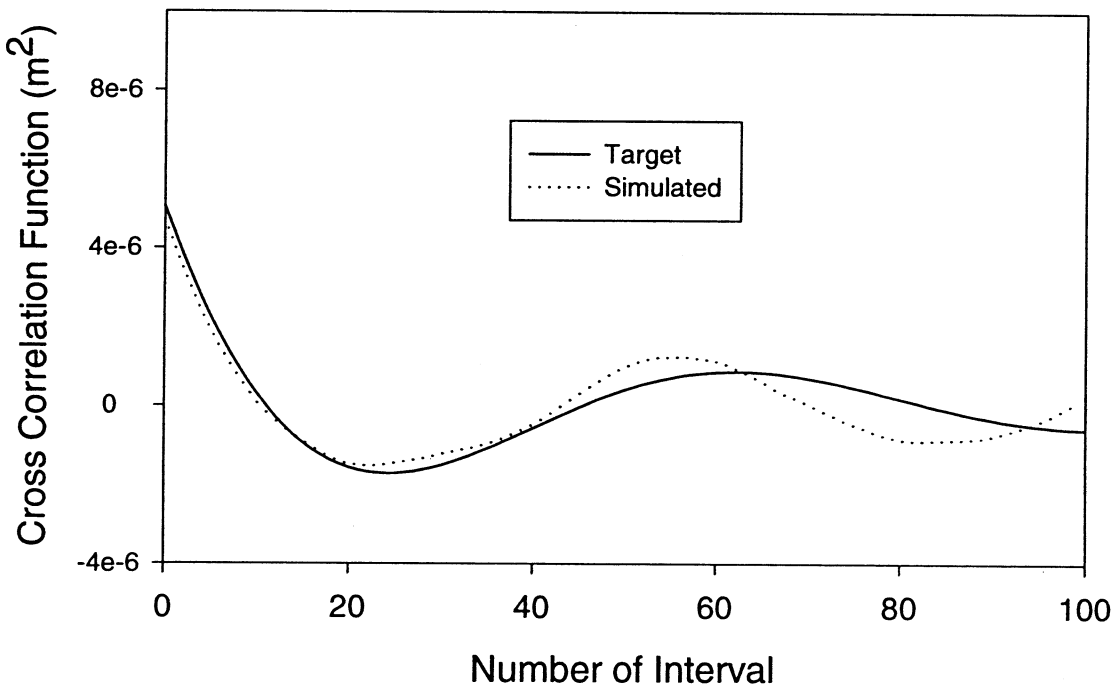
(a) $c = 0.9$

Fig. 7-2. Simulated Auto- and Cross-Correlation Functions and the Targets
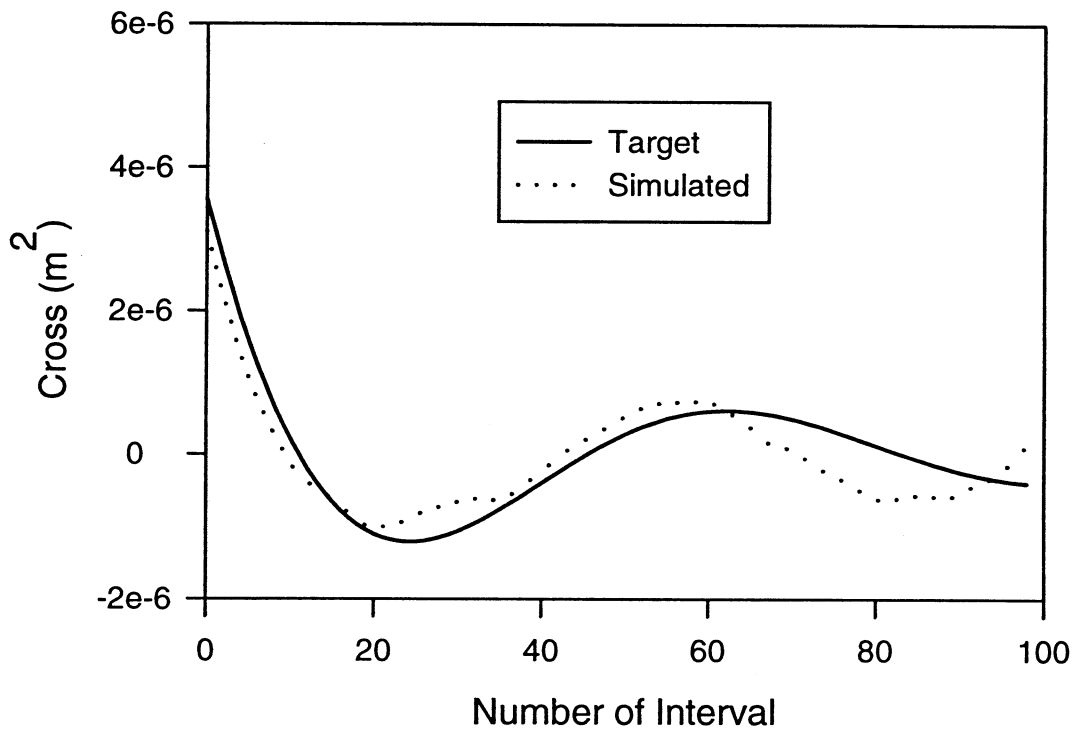
(b) $c = 0.63$

Fig. 7-2. Simulated Auto- and Cross-Correlation Functions and the Targets

(c) $c = 0.0$

Fig. 7-2. Simulated Auto- and Cross-Correlation Functions and the Targets
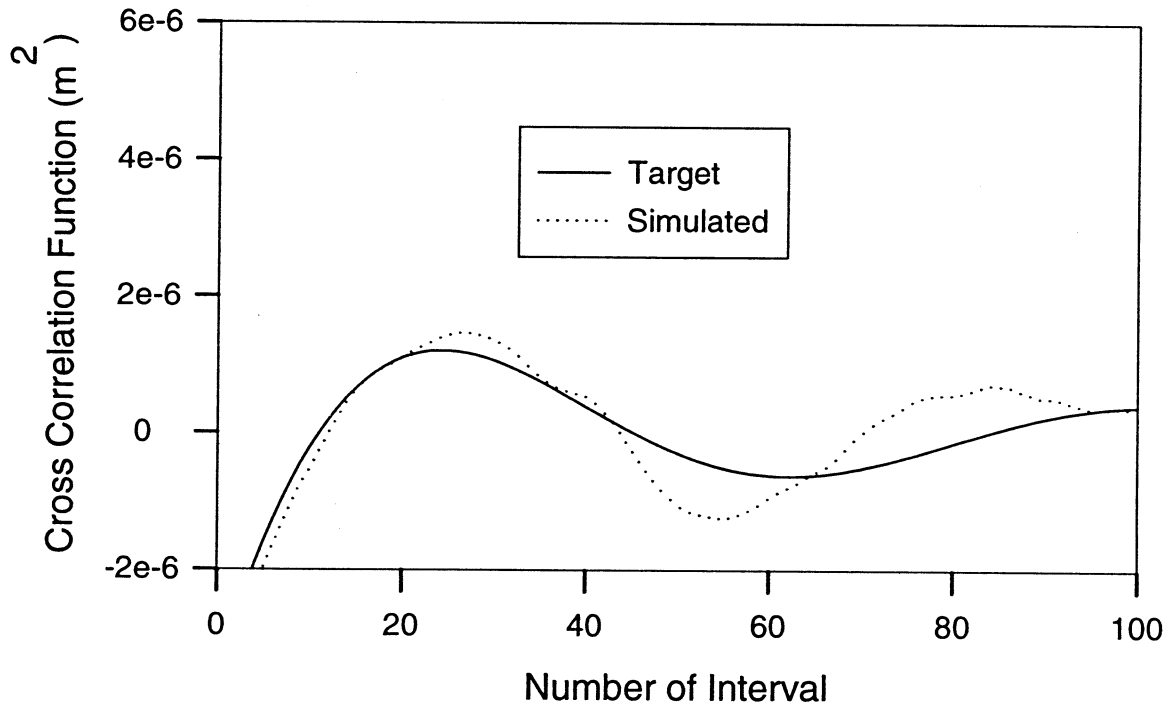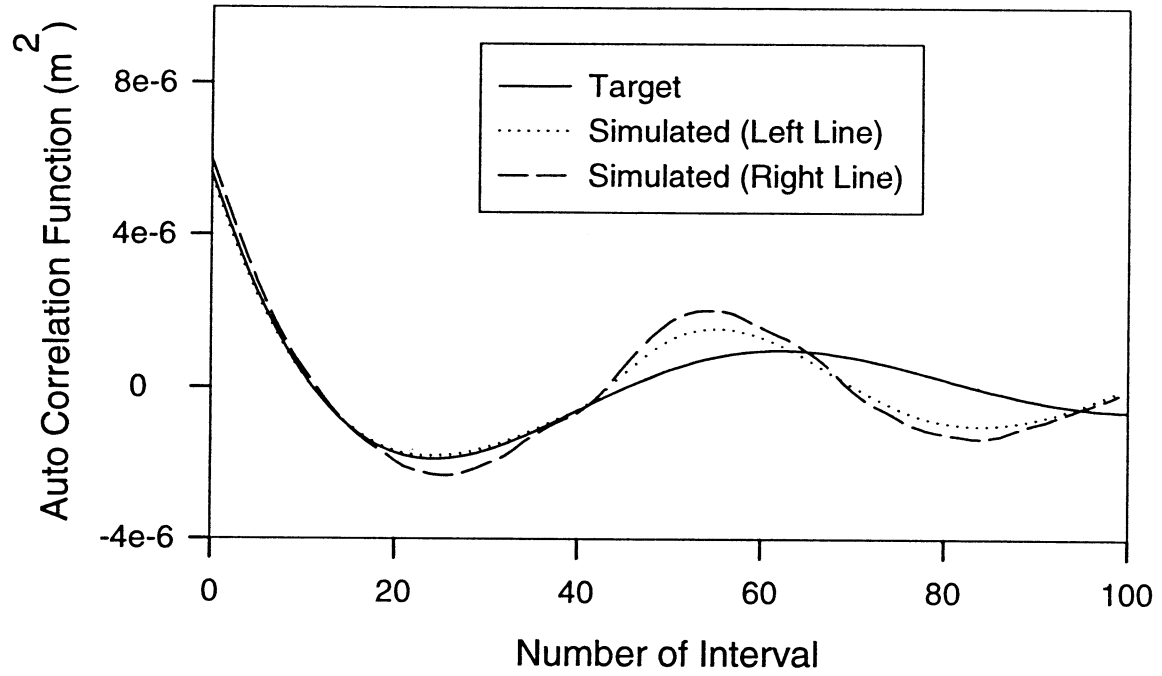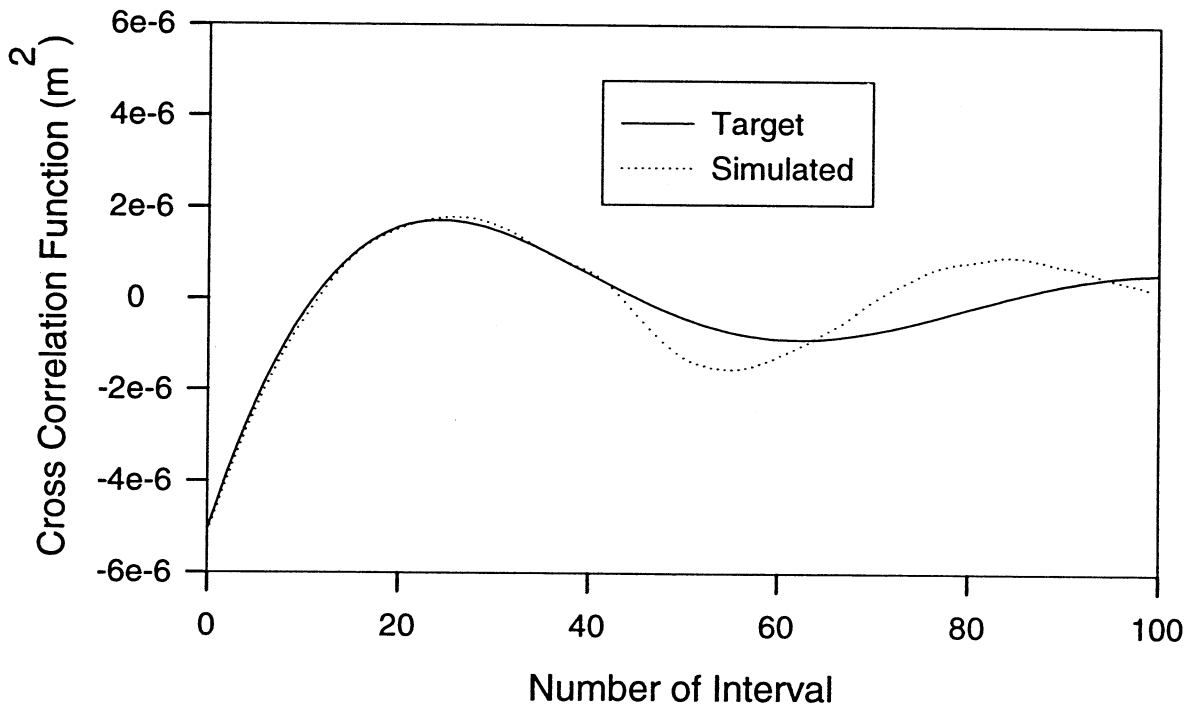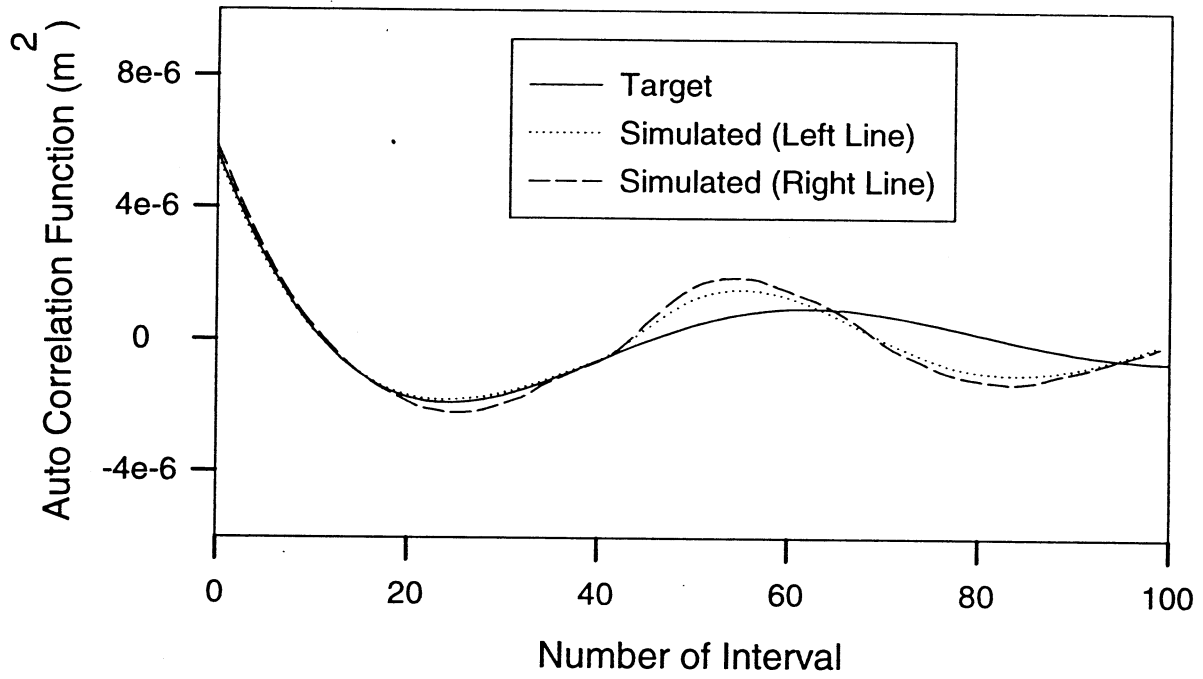
(d) c = -0.63

Fig. 7-2. Simulated Auto- and Cross-Correlation Functions and the Targets

149

Fig. 7-2. Simulated Auto- and Cross-Correlation Functions and the Targets

(e) $c = -0.9$
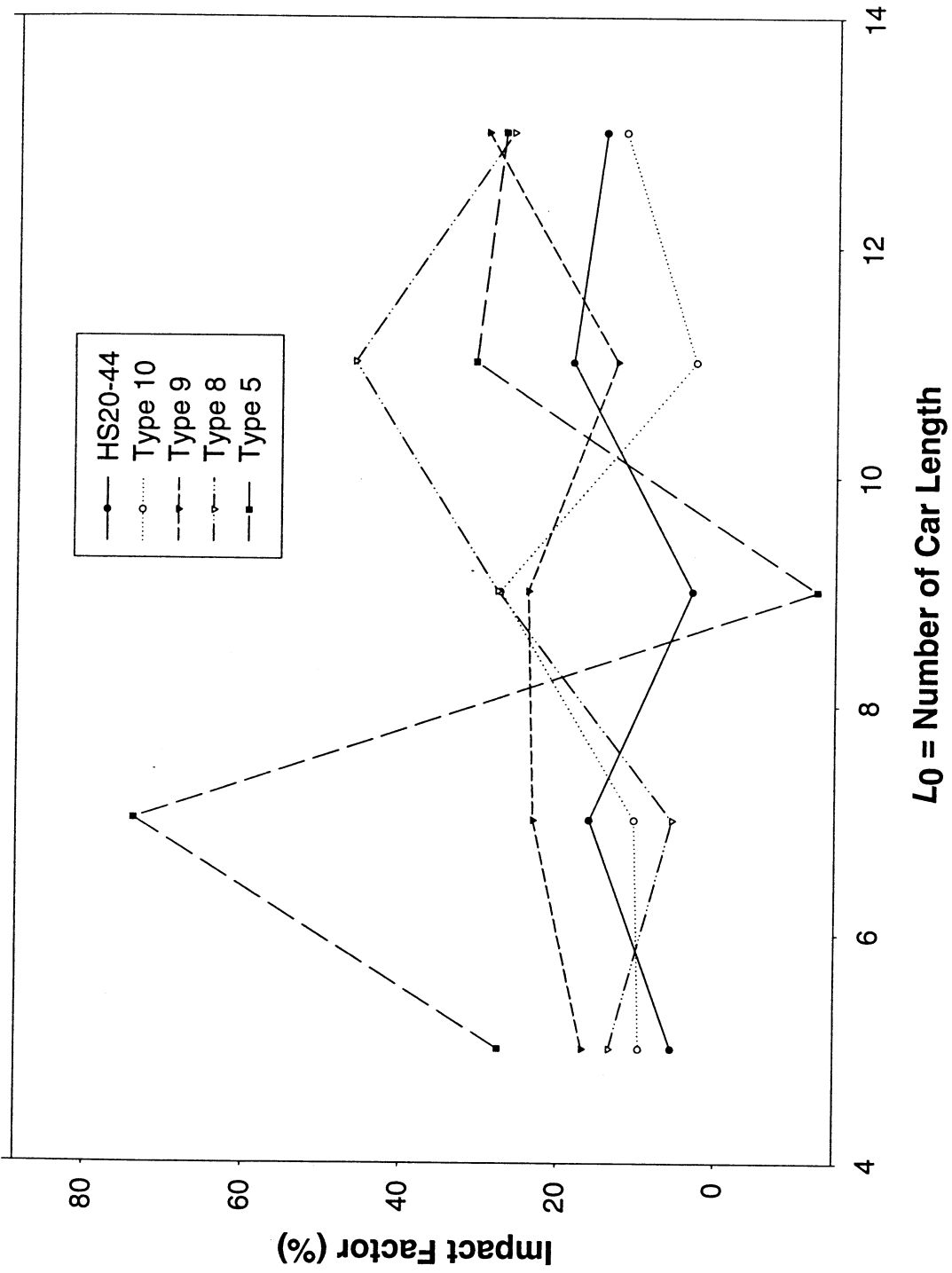
Fig. 7-3. Dynamic Impact Factor vs L_0 (No. Truck Lengths)

L_0 = Number of Car Length

Impact Factor (%)

Legend:
- HS20-44
- Type 10
- Type 9
- Type 8
- Type 5

151

SPAN LENGTH L = 9.14M

Legend:
- c = 0.9
- c = 0.63
- c = 0.0
- c = -0.63
- c = -0.9

IMPACT FACTOR(%)

SPEED (Km/h)

(a)

Fig. 7-4. Impact Factor vs Coefficient of Correlation c

152

SPAN LENGTH L = 18.29M

Legend:
- c = 0.9
- c = 0.63
- c = 0.0
- c = -0.63
- c = -0.9

SPEED (Km/h)

IMPACT FACTOR(%)

(b)

Fig. 7-4. Impact Factor vs Coefficient of Correlation *c*

SPAN LENGTH L = 30.48M

Fig. 7-4. Impact Factor vs Coefficient of Correlation c

(c)

154

SPAN LENGTH L = 42.67M

Legend:
- c = 0.9 (♦)
- c = 0.63 (■)
- c = -0.63 (✳)
- c = 0.0 (▲)
- c = -0.9 (✳)

SPEED (Km/h)

IMPACT FACTOR (%)
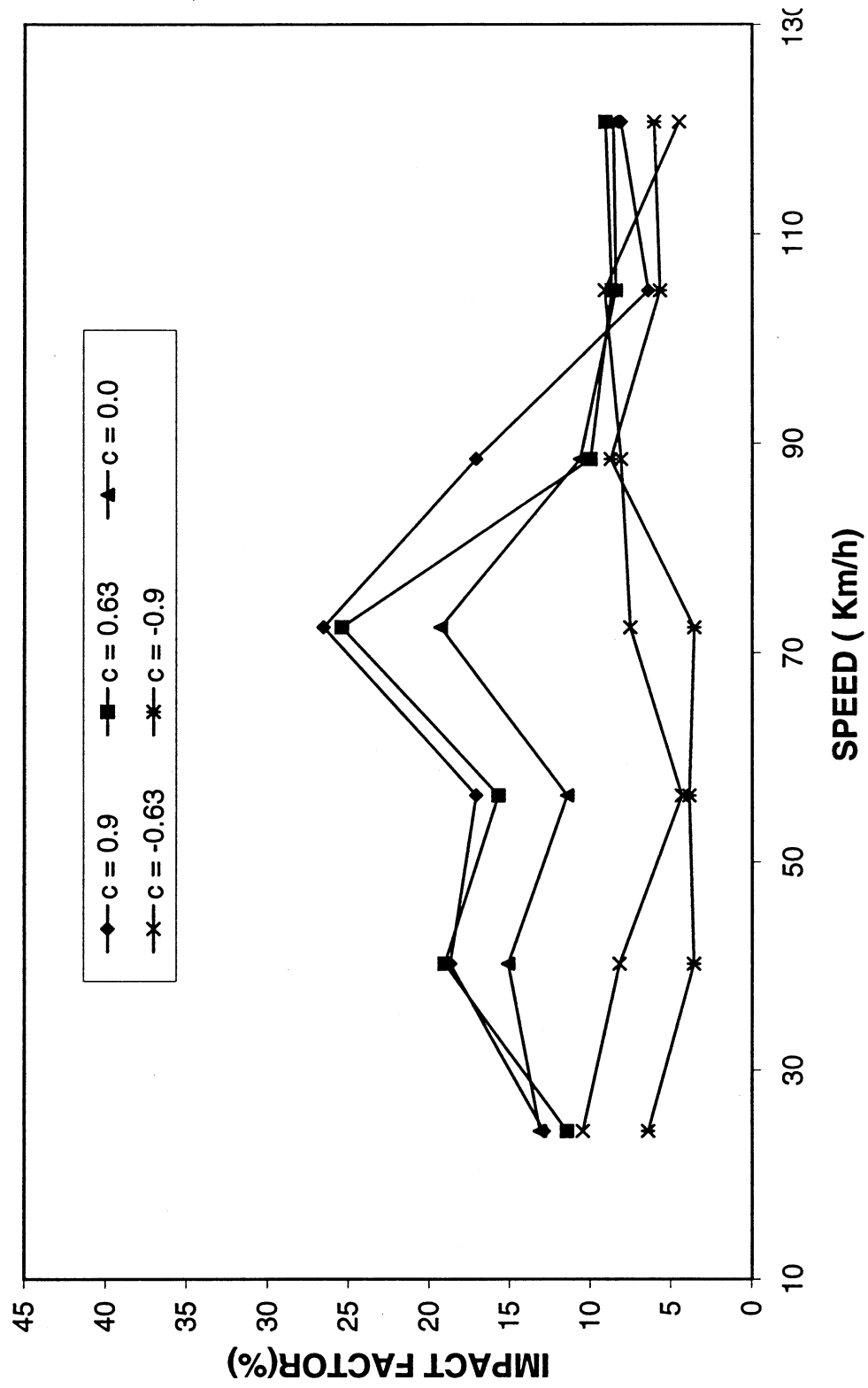
(d)

Fig. 7-4. Impact Factor vs Coefficient of Correlation *c*

155

SPAN LENGTH L = 9.14M

Fig. 7-5. Impact Factor vs Coefficient of Correlation c (Load Case II)

(a)

SPAN LENGTH L = 18.29M

Legend:
- c = 0.9
- c = 0.63
- c = 0.0
- c = -0.63
- c = -0.9
- Smooth Surface

IMPACT FACTOR (%)

SPEED (km/h)

(b)

Fig. 7-5. Impact Factor vs Coefficient of Correlation c (Load Case II)

Fig. 7-5. Impact Factor vs Coefficient of Correlation c (Load Case II)

(c)

158

SPAN LENGTH L = 42.67M

Fig. 7-5. Impact Factor vs Coefficient of Correlation *c* (Load Case II)

(d)

159

One-Truck Loading

Legend:
- $\blacklozenge$ L = 9.14m
- $\blacktriangleleft$ L = 18.29m
- $\blacksquare$ L = 30.48m
- $\ast$ L = 42.67m

Impactor Factor (%)

Coefficient of Correlation

(a)

Fig. 7-6. Maximum Impact Factor vs Span Length and c

160

Two-Truck Loading

Fig. 7-6. Maximum Impact Factor vs Span Length and c

(b)

161

Fig. 7-7. Impact Factors at the Midspan Section (Load Case I)

(a) L = 9.14m

(b) L = 18.29m

Fig. 7-7. Impact Factors at the Midspan Section (Load Case I)
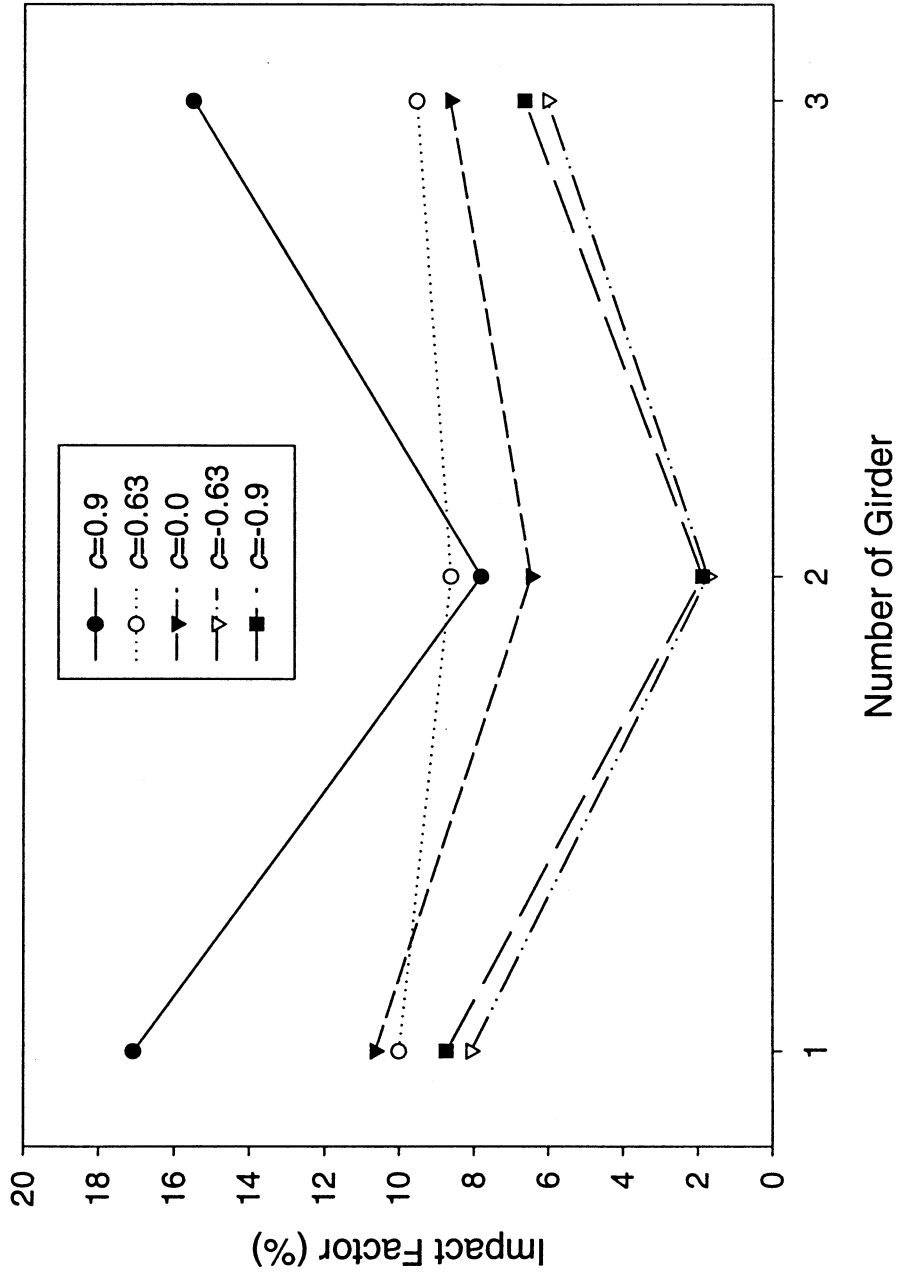
(c) L = 30.48m

Fig. 7-7. Impact Factors at the Midspan Section (Load Case I)
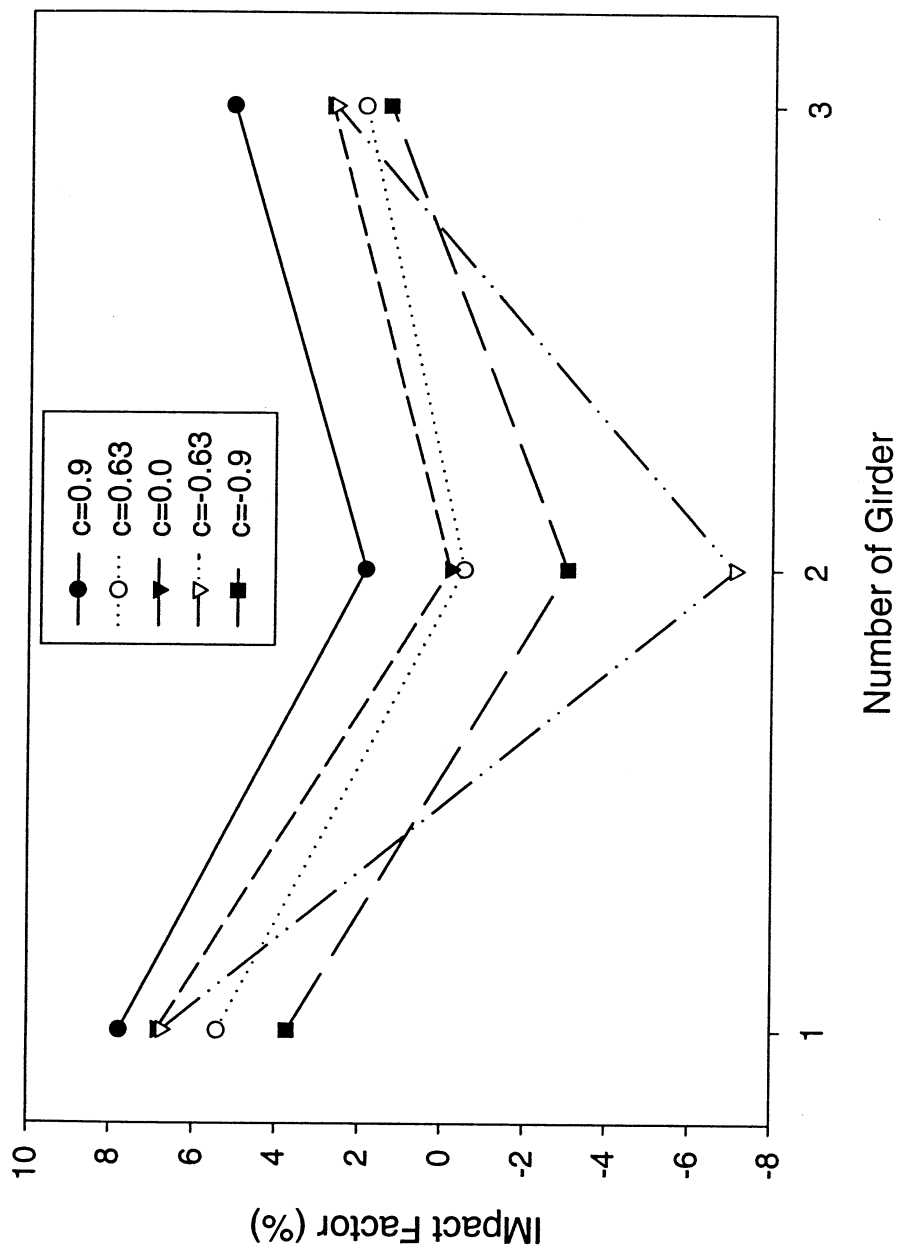
Fig. 7-7. Impact Factors at the Midspan Section (Load Case I)

(d) L = 42.67m

SPAN LENGTH L = 9.14m

Fig. 7-8. Impact Factors at the Midspan Section (Load Case II)

(a)

166

SPAN LENGTH L = 18.29m

Legend:
- ◆ c=0.9
- ▲ c=0.0
- ✳ c=-0.9
- ■ c=0.63
- ✕ c=-0.63

(b)
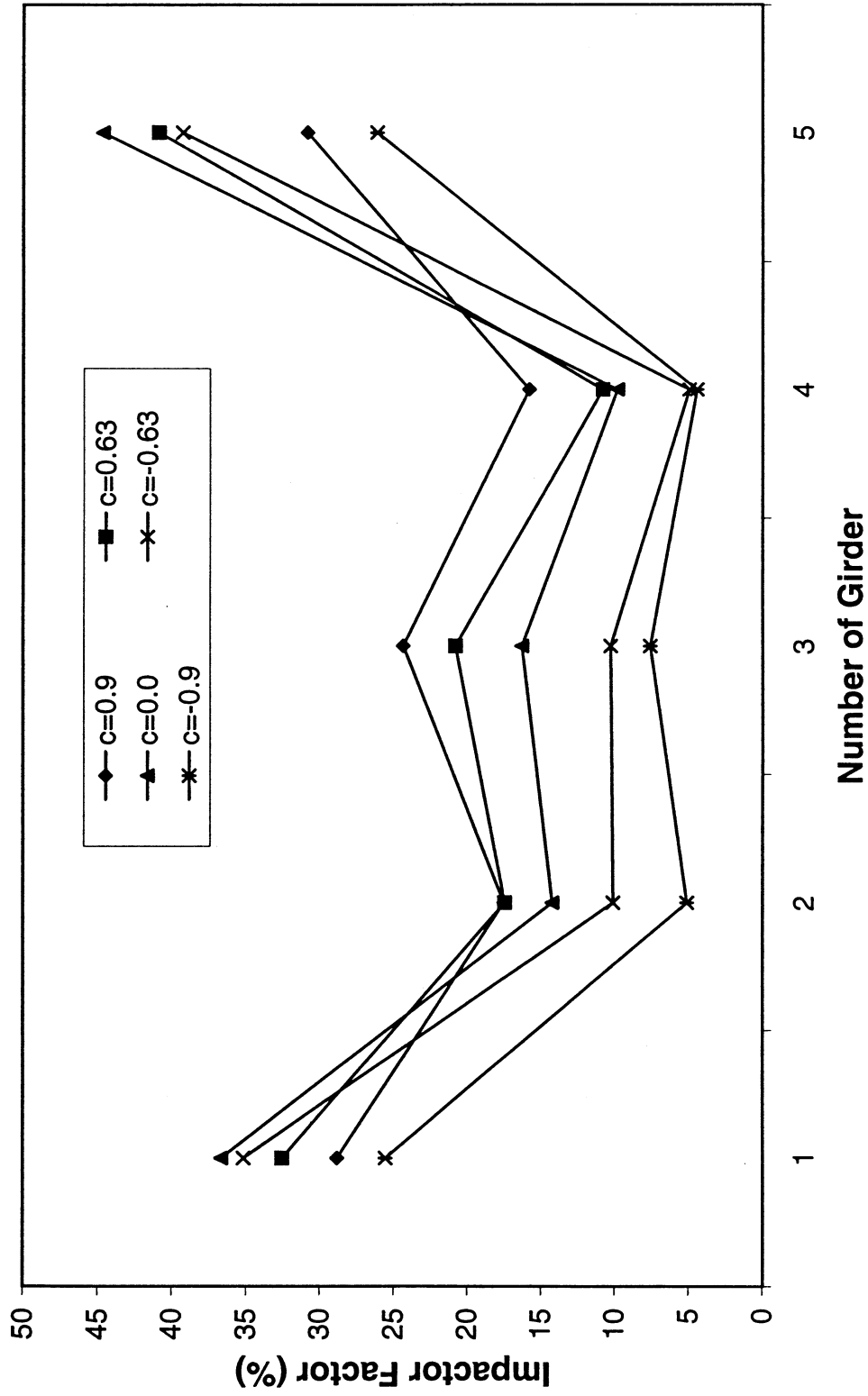
Fig. 7-8. Impact Factors at the Midspan Section (Load Case II)

SPAN LENGTH L = 30.48m

Legend:
- c=0.9
- c=0.0
- c=-0.9
- c=0.63
- c=-0.63

Number of Girder

Impactor Factor (%)

Fig. 7-8. Impact Factors at the Midspan Section (Load Case II)

(c)

Fig. 7-8. Impact Factors at the Midspan Section (Load Case II)

(d)

169
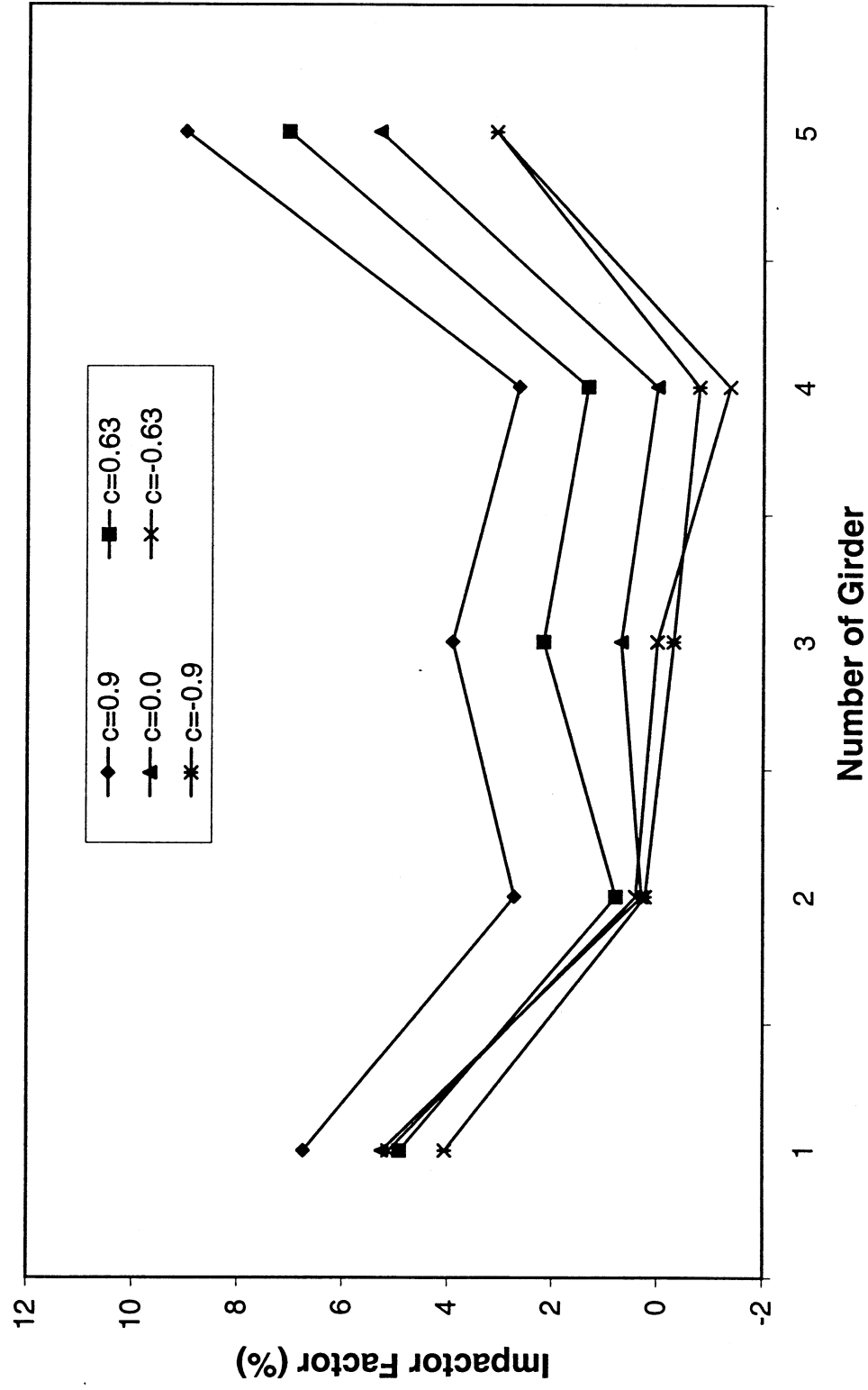
A.1 Type 5

| Item	Empty Truck	Loaded Truck
l_1	198.06 in	214.70 in
l_2	128.65 in	150.69 in
l_3	69.42 in	63.98 in
s_1	44.0 in	44.0 in
s_2	36.0 in	36.0 in
d_1	68.0 in	68.0 in
d_2	72.0 in	72.0 in
K_{sy1}, K_{sy2}	1.385 k/in	1.385 k/in
K_{sy3}, K_{sy4}	10.865 k/in	10.865 k/in
K_{ty1}, K_{ty2}	4.996 k/in	4.996 k/in
K_{ty3}, K_{ty4}	20.000 k/in	20.000 k/in
D_{sy1}, D_{sy2}	0.0075 k-sec/in	0.0075 k-sec/in
D_{sy3}, D_{sy4}	0.0425 k-sec/in	0.0425 k-sec/in
D_{tyi} ($i = 1$ to 4)	0.0000 k-sec/in	0.0000 k-sec/in
F_{y1}, F_{y2}	0.3 kips	0.3 kips
F_{y3}, F_{y4}	3.2 kips	3.2 kips
m_{t1}	0.016615 k-sec^2/in	0.039855 k-sec^2/in
I_{xt1}	32.698 k-in-sec^2	78.434 k-sec^2/in
I_{zt1}	97.5395 k-in-sec^2	233.972 k-sec^2/in
m_{ai} ($i = 1$ to 2)	0.00828 k-sec^2/in	0.00828 k-sec^2/in
I_{xai} ($i = 1$ to 2)	6.45972 k-in-sec^2	6.45972 k-in-sec^2

A.2 Type 8

Item	Empty Truck	Loaded Truck
l_1	163.56 in	174.24
l_2	293.76 in	301.92
l_3	65.424 in	69.696
l_4	98.136 in	104.544
L_5	98.136 in	104.544
L_6	293.76 in	301.92
L_7	146.88 in	150.96
l_8	146.88 in	150.96
s_1	44.0 in	44.0 in
$s_{2,}s_3$	36.0 in	36.0 in
d_1	68.0 in	68.0 in
$d_{2,}d_3$	72.0 in	72.0 in
K_{sy1}, K_{sy2}	1.385 k/in	1.385 k/in
K_{sy3}, K_{sy4}	10.865 k/in	10.865 k/in
K_{sy5}, K_{sy6}	11.241 k/in	11.241 k/in
K_{ty1}, K_{ty2}	4.996 k/in	4.996 k/in
K_{ty3}, K_{ty4}	20.000 k/in	20.000 k/in
K_{ty5}, K_{ty6}	20.024 k/in	20.024 k/in
D_{sy1}, D_{sy2}	0.0075 k-sec/in	0.0075 k-sec/in
D_{sy3}, D_{sy4}	0.0425 k-sec/in	0.0425 k-sec/in
D_{sy5}, D_{sy6}	0.0410 k-sec/in	0.0410 k-sec/in
D_{tyi} (i = 1 to 6)	0.0000 k-sec/in	0.0000 k-sec/in
F_{y1}, F_{y2}	0.3 kips	0.3 kips
F_{y3}, F_{y4}	3.2 kips	3.2 kips
F_{y5}, F_{y6}	3.2 kips	3.2 kips
m_{t1}	0.02505 k-sec^2/in	0.02568 k-sec^2/in
I_{xt1}	30.0533 k-in-sec^2	30.809 k-sec^2/in
I_{zt1}	127.0193 k-in-sec^2	130.214 k-sec^2/in
m_{t2}	0.009486 k-sec^2/in	0.04005 k-sec^2/in
I_{xt2}	43.71 k-in-sec^2	61.5168 k-sec^2/in
I_{zt2}	300.0 k-in-sec^2	439.415 k-sec^2/in
m_{a1}	0.00559 k-sec^2/in	0.00559 k-sec^2/in
I_{xa1}	4.36020 k-in-sec^2	4.36020 k-in-sec^2
m_{a2}	0.00923 k-sec^2/in	0.00923 k-sec^2/in
I_{xa2}	7.26696 k-in-sec^2	7.26696 k-in-sec^2
m_{a3}	0.00745 k-sec^2/in	0.00745 k-sec^2/in
I_{xa3}	5.81364 k-in-sec^2	5.81364 k-in-sec^2

A.3 Type 9

Item	Empty Truck	Loaded Truck
l_1	186.6 in	177.12 in
l_2	54.0 In	54.0 in
l_3	383.64 In	384.36 in
l_4	54.5 In	55.85 in
l_5	6.121 in	45.78 in
l_6	180.479 in	131.34 in
l_7	207.479 in	158.34 in
l_8	183.662 in	228.764 in
l_9	226.978	182.611 in
s_1	44.0 in	44.0 in
s_i (i = 2 to 5)	36.0 in	36.0 in
d_1	68.0 in	68.0 in
d_i (i = 2 to 5)	72.0 in	72.0 in
K_{sy1}, K_{sy2}	2.77 k/in	2.77 k/in
K_{syi} (i = 3 to 10)	3.985 k/in	3.985 k/in
K_{syi} (i = 7 to 10)	3.881 k/in	3.881 k/in
K_{ty1}, K_{ty2}	8.008 k/in	8.008 k/in
K_{tyi} (i = 3 to 10)	16.015 k/in	16.015 k/in
D_{sy1}, D_{sy2}	0.01370 k-sec/in	0.01370 k-sec/in
D_{syi} (i = 3 to 10)	0.02059 k-sec/in	0.02059 k-sec/in
D_{syi} (i = 7 to 10)	0.02162 k-sec/in	0.02162 k-sec/in
D_{tyi} (i = 1 to 10)	0.0000 k-sec/in	0.0000 k-sec/in
F_{y1}, F_{y2}	0.375 kips	0.375 kips
F_{yi}, (i = 3 to 10)	1.55 kips	1.55 kips
m_{t1}	0.01852 k-sec^2/in	0.02829 k-sec^2/in
I_{xt1}	22.224 k-in-sec^2	33.944 k-sec^2/in
I_{zt1}	71.2135 k-in-sec^2	108.763 k-sec^2/in
m_{t2}	0.04762 k-sec^2/in	0.1169 k-sec^2/in
I_{xt2}	73.1443 k-in-sec^2	179.60 k-sec^2/in
I_{zt2}	1194.338 k-in-sec^2	2954.40 k-sec^2/in
m_{a1}	0.00339 k-sec^2/in	0.00339 k-sec^2/in
I_{xa1}	2.6442 k-in-sec^2	2.6442 k-in-sec^2
m_{ai} (i = 2 to 3)	0.00532 k-sec^2/in	0.00532 k-sec^2/in
I_{xai} (i = 2 to 3)	4.1496 k-in-sec^2	4.1496 k-in-sec^2
m_{ai} (i = 4 to 5)	0.00602 k-sec^2/in	0.00602 k-sec^2/in
I_{xai} (i = 4 to 5)	4.6956 k-in-sec^2	4.6956 k-in-sec^2

A.4 Type 10

Item	Empty Truck	Loaded Truck
l_1	185.3 in	195.12 in
l_2	53.8 in	55.2 in
l_3	377.04 in	319.92 in
l_4	51.66 in	53.2 in
l_5	49.8 in	53.3 in
l_6	74.12 in	78.048 in
l_7	111.18 in	117.072 in
l_8	188.52 in	159.96 in
l_9	138.08 in	144.672 in
l_{10}	215.42 in	187.56 in
l_{11}	240.18 in	213.16 in
s_1	44.0 in	44.0 in
$s_i\,(i = 2\text{ to }6)$	36.0 in	36.0 in
d_1	68.0 in	68.0 in
$d_i\,(i = 2\text{ to }6)$	72.0 in	72.0 in
K_{sy1}, K_{sy2}	2.77 k/in	2.77 k/in
$K_{syi}\,(i = 3\text{ to }6)$	3.278 k/in	3.278 k/in
$K_{syi}\,(i = 7\text{ to }8)$	4.507 k/in	4.507 k/in
$K_{syi}\,(i = 9\text{ to }12)$	3.848 k/in	3.848 k/in
K_{ty1}, K_{ty2}	8.008 k/in	8.008 k/in
$K_{tyi}\,(i = 3\text{ to }6)$	12.014 k/in	12.014 k/in
$K_{tyi}\,(i = 7\text{ to }8)$	16.015 k/in	16.015 k/in
$K_{tyi}\,(i = 9\text{ to }12)$	14.021 k/in	14.021 k/in
D_{sy1}, D_{sy2}	0.01370 k-sec/in	0.01370 k-sec/in
$D_{syi}\,(i = 3\text{ to }6)$	0.01868 k-sec/in	0.01868 k-sec/in
$D_{syi}\,(i = 7\text{ to }8)$	0.02330 k-sec/in	0.02330 k-sec/in
$D_{syi}\,(i = 9\text{ to }12)$	0.02153 k-sec/in	0.02153 k-sec/in
$D_{tyi}\,(i = 1\text{ to }12)$	0.0000 k-sec/in	0.0000 k-sec/in
F_{y1}, F_{y2}	0.45 kips	0.45 kips
$F_{yi},\,(i = 3\text{ to }6)$	1.2 kips	1.2 kips
$F_{yi},\,(i = 7\text{ to }8)$	1.6 kips	1.6 kips
$F_{yi},\,(i = 9\text{ to }12)$	1.4 kips	1.4 kips

To be continued

Continued

m_{t1}	0.0336 k-sec^2/in	0.031842 k-sec^2/in
I_{xt1}	40.32 k-in-sec^2	38.2104 k-sec^2/in
I_{zt1}	166.16 k-in-sec^2	157.466 k-sec^2/in
m_{t2}	0.0798 k-sec^2/in	0.14733 k-sec^2/in
I_{xt2}	122.5728 k-in-sec^2	226.299 k-sec^2/in
I_{zt2}	2300.66 k-in-sec^2	3556.96 k-sec^2/in
m_{a1}	0.00339 k-sec^2/in	0.00339 k-sec^2/in
I_{xa1}	2.6442 k-in-sec^2	2.6442 k-in-sec^2
m_{ai} ($i = 2$ to 3)	0.00532 k-sec^2/in	0.00532 k-sec^2/in
I_{xai} ($i = 2$ to 3)	4.1496 k-in-sec^2	4.1496 k-in-sec^2
m_{ai} ($i = 4$ to 6)	0.00602 k-sec^2/in	0.00602 k-sec^2/in
I_{xai} ($i = 4$ to 6)	4.6956 k-in-sec^2	4.6956 k-in-sec^2